Fog Collection on Plant Surfaces and Biomimetic Applications

Dissertation

Zur

Erlangung des Doktorgrades (Dr. rer. nat.)

der

Mathematisch-Naturwissenschaftlichen Fakultät

der

Rheinischen Friedrich-Wilhelms-Universität Bonn

vorgelegt von

Md. Abul Kalam Azad

aus

Satkhira, Bangladesh

Bonn, Januar 2016

Angefertigt mit Genehmigung der Mathematisch-Naturwissenschaftlichen Fakultät der Rheinischen Friedrich-Wilhelms-Universität Bonn.

1. Gutachter: Prof. Dr. Wilhelm Barthlott
2. Gutachter: Prof. Dr. Kerstin Koch

Tag der Promotion: 18.04.2016

Erscheinungsjahr: 2016

Dedicated to

the martyrs of the liberation war of Bangladesh,1971

and

the people living in the water stressed regions of the world

Contents

1. General introduction

1.1. Fog in arid regions: a neglected source of water

According to 'The United Nations World Water Development Report 4' (UNESCO 2012) and JMP (Joint Monitoring Program) update 2013 (WHO and UNICEF 2013) about one billion people in the world lack access to adequate quantities of water. The United Nations Conventions to Combat Desertification (UNCCD) reports that by 2025 around 2.4 billion people will be living in the areas with absolute water scarcity (UNCCD 2014) if necessary measures are not taken. The report also indicates the shortages of water as the triggers for conflicts as well as population displacement. However, there is hope; there is plenty of fog in certain arid regions, e.g., the Namib and the Atacama fog Desert. Dry regions of the world, i.e., semiarid, arid and perarid regions, and the flow of the cold ocean currents are shown in **Figure 1.1**. Fog is formed by the movement of air mass over the ocean currents with different temperature (Taylor 1917). This kind of fog is called advection fog. It can be cold sea fog, i.e., generated by the action of warm air movement over the cold ocean currents or warm sea fog, i.e., generated by the action of cold air movement over relatively warm ocean currents (Petterssen 1936). There are other mechanisms for other kinds of fog formation which were first investigated by G. I. Taylor in 1917 (Taylor 1917) and were collectively described in a review (Koračin *et al* 2014).

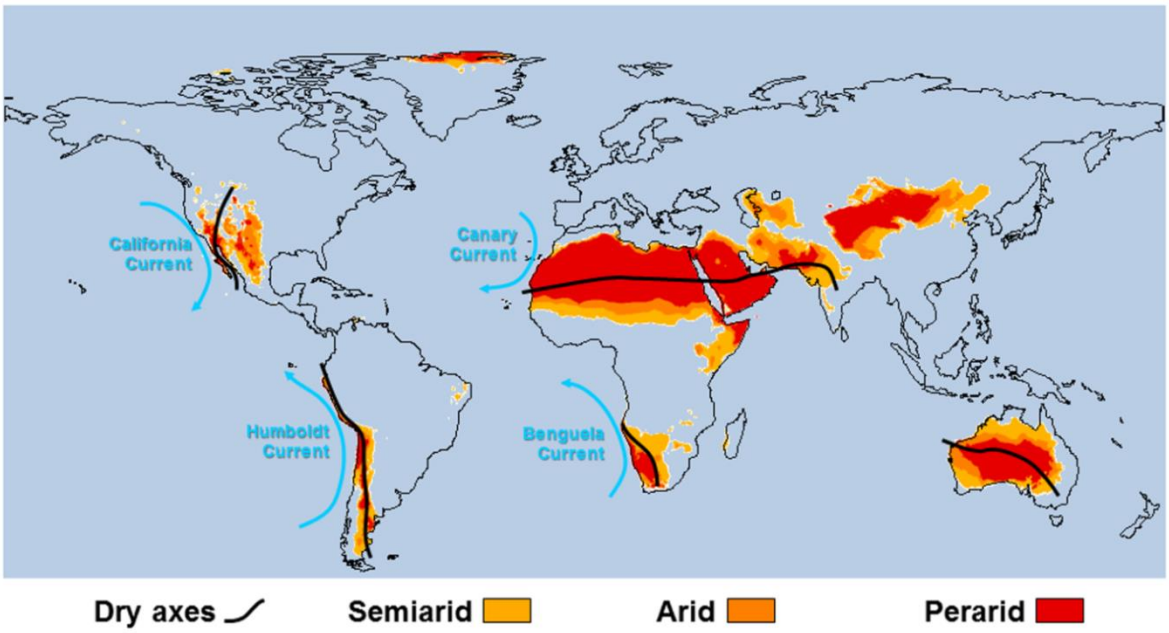

Figure 1.1: Dry regions of the world and cold ocean coasts with fog. The flow of cold currents is shown. (adapted with permission from Rafiqpoor, M.D. & Breckle, S.-W. (2016): Climate and Vegetation Zones of the Earth. A Dari Textbook (in preparation))

Fog, coming off the ocean, enters into the inland (**Figure 1.2a–b**) and can be an alternative source of fresh water for the people living in this climatic condition with a little access to water. According to an estimate by CDA (Centro del Desierto de Atacama-Atacama Desert Centre), there is about 10^8 m^3 of fog water content available in Chile (Chhatre 2012). Currently the water consumption in Northern Chile is around 4% of the total fog water content in Chile (Chhatre 2012; Park *et al* 2014). There are fog-collection opportunities in many regions of the world (Klemm *et al* 2012; Fessehaye *et al* 2014) that will be discussed later in **section 1.2**. The United Nations water crisis report by Food & Agricultural Organization (FAO) considers the fog-collection technology important and cost effective "for drinking water, crop irrigation, livestock beverage and forest restoration in dryland mountains" (FAO 2011). Fog-collection projects in different countries around the world have been studied and proved to be feasible and effective where enough fog events are available (Klemm *et al* 2012; Holmes *et al* 2015).

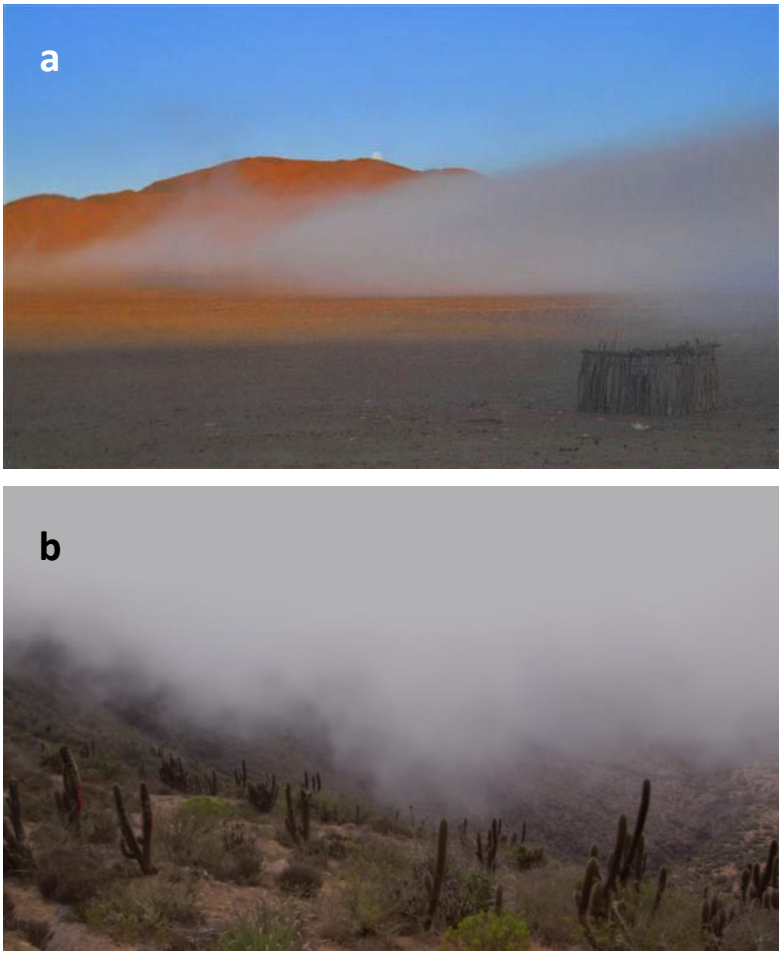

Figure 1.2: (a) Fog, coming off the Atlantic, enters into the in-land in the Namib Desert, (b) Fog from the Pacific flows along the mountain in the Atacama in Chile; typical fog vegetation in the rainless desert is seen. (Source:(a)*http://www.africa-adventure.com/bushtails/8-southern-africa-bush-tails/140-namibia-camps-news*; downloaded on 02.09.2013), (b) photo credit: John Freidah, MIT Department of Mechanical Engineering (2014).

1.2. History of fog collection

More than 400 years ago, in the Canary Islands, the existence of a tree with miraculous power to supply the inhabitants with sufficient water was reported in *Histoire Admirable* by Duret in 1605 (**Figure 1.3a**), and in *Historia Plantarum Generalis* by Bauhin and Cherler in 1610 (**Figure 1.3b**). Duret also reported that there was no other water source in the islands. This wonder tree was called 'Rain tree' (mentioned in Hutchinson 1919)

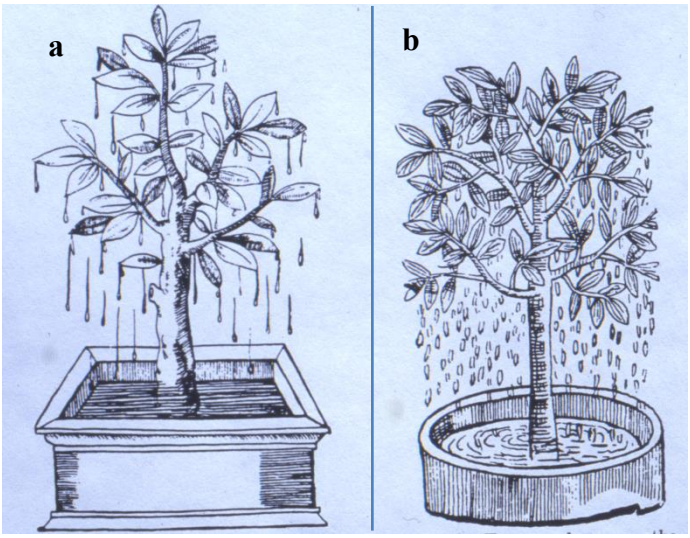

Figure 1.3: Rain tree of the Canary Islands as shown by (a) Duret in *Histoire Admirable* in 1605 and (b) Bauhin and Cherler in *Historia Plantarum Generalis* in 1610 (Photo: Wilhelm Barthlott).

In the past, different fog-collection methods, such as the interception and utilization of intercepted fog by trees and the construction of mound-like different structures in dry regions etc. were documented (mentioned in Prinz and Wolfer 1998; Dower 2002; Nelson 2003; Schemenauer and Cereceda 1994a). Cisterns were also reportedly built under trees in mountain areas in Oman to collect fog (mentioned in Schemenauer and Cereceda 1994a). In the desert areas of Mediterranean and South America, e.g., in the Atacama Desert, different artificial structures, for example stone piles were used to collect mist and dew (mentioned in Prinz and Wolfer 1998; Dower 2002; Nelson 2003).

However, the scientific study of fog collection began at the beginning of the 20th century in the Table Mountains in South Africa (Marloth 1903; Marloth 1905). Marloth, one of the pioneers of fog-collection research, used plants, resembling reeds, above one of the two rain gauges to measure fog precipitation (Marloth 1903). From then, the two rain-gauge system was used by the scientists to measure the volume to quantify the fog collection. It was considered as a standard measuring system for fog precipitation till the

introduction of SFC (Standard Fog Collector) by Schemenauer and Cereceeda (Schemenauer and Cereceda 1994b). Based on Marloth's idea, numerous field experiments were conducted by exploiting mainly wire meshes (Nagel 1956; Nagel 1962; Ekern 1964; Vogelmann *et al* 1968). The first fog-collection project in South Africa was conducted in 1969 by using two large plastic screens (as shown in **Figure 1.4**), each of 28m by 3.6m in size. The project collected an average of 11 $Lm^{-2}day^{-1}$ and supplied to the Air Force personnel living temporarily in the area with water. In 1980, a field experiment was conducted to check the feasibility and measure the amount of fog deposition in El Tofo, Chile, where both small ($0.025m^2$) and large ($40m^2$) fog collectors were installed (Schemenauer *et al* 1988). One of the largest operational projects (100 Raschel mesh fog collectors, each 12m long and 4m high) was conducted in a village in northern Chile (Schemenauer *et al* 1988), which supplied with sufficient water for 300 people; more specifically 33L of water for every person per day (Larrain *et al* 2002). The project continued successfully for a long time until the village politics and the substantial growth of the permanent residents ruined it. The success resulted in the initiation of similar projects in many parts of the world (Schemenauer and Cereceda 1994a) and as of 2010 many fog-collection projects have been implemented in around 40 countries (**Figure 1.5**) of the world (Klemm *et al* 2012).

Figure 1.4: Large fog collectors (LFCs) made of double layer polyolefin mesh located in the Atacama, Chile. (reproduced from: https://www.youtube.com/watch?v=2x2_8RbC2I0; accessed on 22.07.2015). The inset shows the fiber network of a single layer polyolefin mesh (modified after Klemm *et al* 2012; Copyright Royal Swedish Academy of Sciences 2012)

Many operational Projects were conducted and/or have been running in Chile (Schemenauer and Cereceda 1988; Schemenauer *et al* 1988; Schemenauer and Cereceda 1991; Larrain *et al* 2002), Peru (Cereceda *et al* 1998; Lummerich and Tiedemann 2011), Ecuador (Henderson and Falk 2001), Colombia (Molina and Escobar 2008; Escobar *et al* 2010), Guatemala (Schemenauer *et al* 2007), South Africa (Olivier and de Rautenbach 2002; Olivier 2004), Eastern Africa (Klemm *et al* 2012), Eritrea (www.fogquest.org last accessed on 04.07.2015 and searched with the key word Eritrea; Klemm *et al* 2012), Arabian Peninsula (Gandhidasan and Abualhamayel 2007), Oman (Schemenauer and Cereceda 1992; Abdul-Wahab *et al* 2010), Yemen (Osses *et al* 2004), Nepal (www.fogquest.org last accessed on 04.07.2015 and searched with the key word Nepal; MacQuarrie *et al* 2001; Klemm *et al* 2012; Fessehaye *et al* 2014), Croatia (Mileta and Likso 2010), Spain (Estrela *et al* 2008; Estrela *et al* 2009) etc.

Figure 1.5: Maps with the locations where fog-collection projects have been successful or where there is a potential for collecting fog (adapted from Klemm *et al* 2012; Copyright Royal Swedish Academy of Sciences 2012).

Some evaluation projects were conducted in Dominican Republic and Haiti (Schemenauer *et al* 2001), Namibia (Mtuleni *et al* 1998), Ethiopia and Tanzania (Klemm *et al* 2012). Large scale projects are predicted to be successful (Schemenauer *et al* 2001). In several parts of India, some evaluation projects have been being conducted (Klemm *et al* 2012), that has the potential for fog collection at a large scale.

1.3. Existing technologies for fog collection

Fog-collection methods are very simple and inexpensive. Two-dimensional Large Fog Collectors (LFCs) (see **Figure 1.4**) with UV protected polyolefin or other polymer meshes are most widely used for collecting fog. When fog carrying air passes through the mesh, the fog droplets are deposited on the fibers of the mesh, which then drop into a gutter. The water is then transported to a collection reservoir.

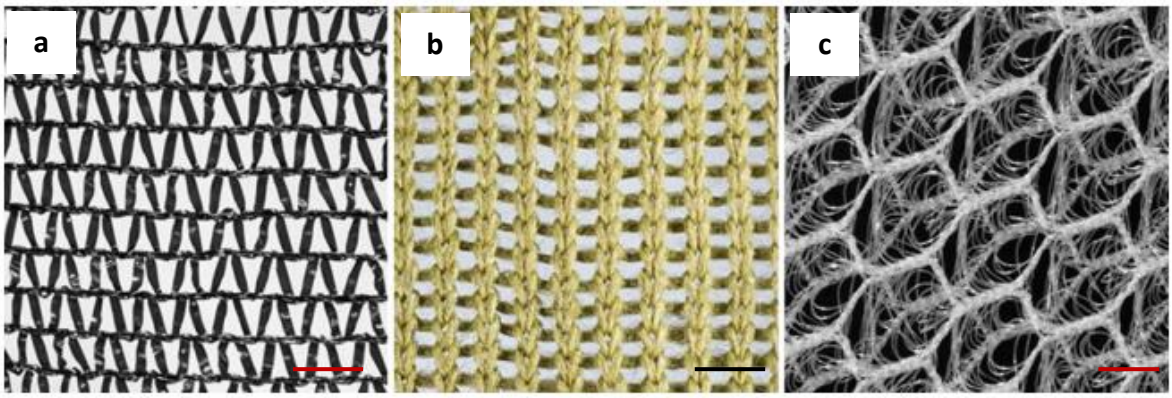

Figure 1.6: (a–c) Three different kinds of mesh designs for fog collection; scale: 1 cm. (a) Raschel/polyolefin mesh that has been used in many countries for decades, (b) polymer yarn mesh co-knitted with stainless steel and (c) a three-dimensional polymer mesh fabric. (adapted from Klemm *et al* 2012; Copyright Royal Swedish Academy of Sciences 2012).

However, fog collectors with a variety of meshes (**Figure 1.6**) of different materials have been tested (Shanyengana *et al* 2003). To enhance the fog-collection efficiency, scientists in different countries tested different kinds of designs of fog collectors, for example the 'Eiffel' collector implemented in Peru (Lummerich and Tiedemann 2011), a fog collector that consists of nine panels of polymer yarn mesh, for an extra strength and stability, co-knitted with stainless steel, arranged in a shape of four equilateral triangles implemented in South Africa (Van Heerden *et al* 2010) and in a very small scale a three-dimensional polymer mesh fabric implemented in the Namib desert (Klemm *et al* 2012). To be noted, a comparison study of the collection efficiency, among the above mentioned fog collectors, has not yet been performed. Fog-collection quantity in different sites varies due to the variation of the parameters, e.g., wind speed, height of LFC installation, liquid water content (LWC), data quality control procedures etc. Therefore, inter-site comparison of fog-collection rates or the prediction of fog-collection rates in different sites is ambiguous. However, the collection rate is on the average of 1–12 $Lm^{-2}day^{-1}$ (**Figure 1.7**).

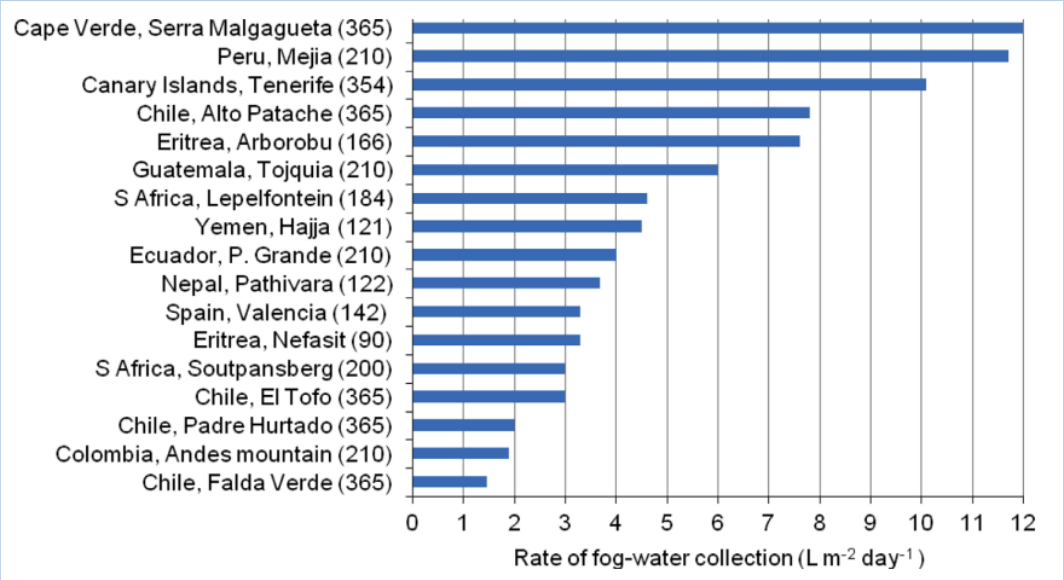

Figure 1.7: Rate of fog-water collection by technical fog collectors (meshes) in different regions of the world. The total fog events (in days) per year are mentioned in the bracket (adapted from Fessehaye *et al* 2014; Copyright Elsevier 2014).

1.4. Physics of surface wettability

The wettability of the solid surfaces is measured by a parameter in surface science called contact angle (CA) (θ). If a liquid drop is placed on a homogenous solid surface, three interfaces, such as a solid-liquid, a liquid-vapor and a solid-vapor interfaces form (**Figure 1.8**). When a tangent along the liquid-vapor interface of the droplet profile is drawn (shown in **Figure 1.8)**, the angle formed is the contact angle of the surface for this liquid. The magnitude of the contact angle is the expression whether the wetting of a surface is favorable or not. A surface with a low contact angle means that the surface favors wetting by the liquid. Therefore, the liquid drop will spread over a large area on the surface.

However, surfaces with a complete wetting (**Figure 1.9a**), with the CAs of < 10° are called superhydrophilic while if the CAs are ≥ 10° and < 90° the surfaces are known as

hydrophilic (**Figure 1.9b**). On the other hand, if the surface does not favor the spreading of the liquid drop on it, rather the liquid drop minimizes its contact with the surface forming a rounder shape with a minimum surface area for a fixed volume.

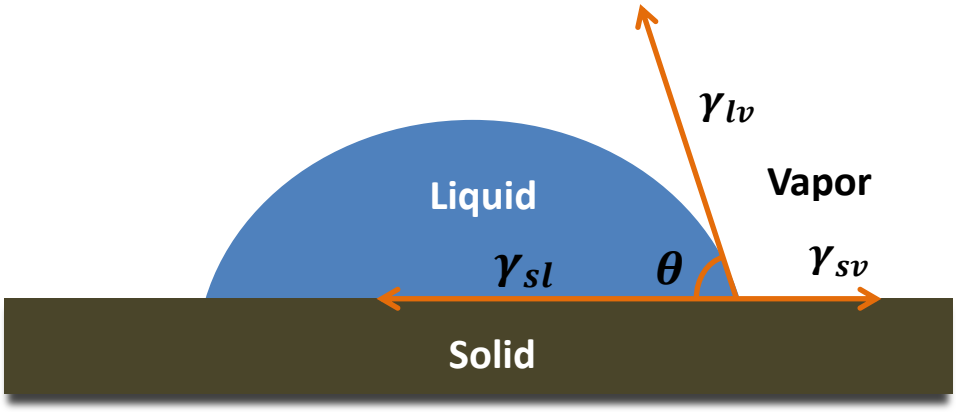

Figure 1.8: Schematic of a liquid drop on a homogenous solid surface. Solid-liquid, solid vapor and liquid-vapor interfaces are shown (indicated by orange lines with arrows).

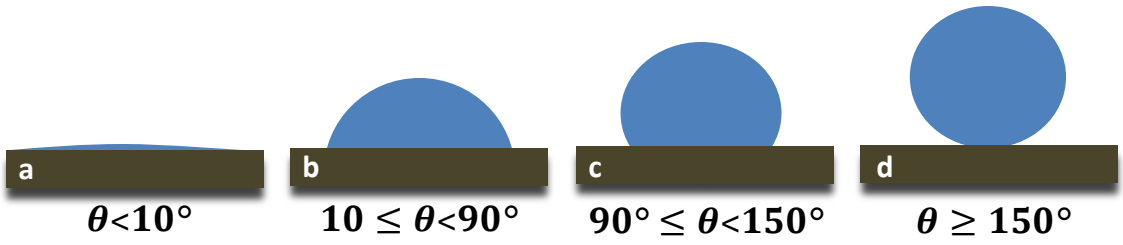

Figure 1.9: Schematic of wettability of different surfaces. (a) A completely wettable surface (superhydrophilic), (b) a wettable surface (hydrophilic), (c) a less wettable surface (hydrophobic), and (d) a non-wettable surface (superhydrophobic). Degree of wettability is shown by θ.

The intermolecular force, responsible for contracting the surface, is called the surface tension (γ). Surfaces exhibiting the CAs of ≥ 90° and < 150°are known as hydrophobic surfaces (**Figure 1.9c**) whereas the surfaces with the CAs of ≥ 150° and the sliding angles (or contact angle hysteresis, which is mentioned later on) of < 10° are known as superhydrophobic surfaces (**Figure 1.9d**). The superhydrophobic surfaces exhibit a very significant property known as self-cleaning or 'Lotus Effect' (Barthlott and Neinhuis

1997). The above classification of surfaces based on CA is adapted from some previous literature (Extrand 2002; Jung and Bhushan 2006; Bhushan and Jung 2007; Jung and Bhushan 2008; Roach *et al* 2008; Zhang *et al* 2008). The static CA is calculated from the following equation-

$$\gamma_{lv} \cos\theta = \gamma_{sv} - \gamma_{sl} \quad \text{..... (1.1)}$$

where γ_{lv} , γ_{sv} and γ_{sl} are the liquid-vapor, solid-vapor, and solid-liquid interfacial tensions, respectively, θ is the CA or Young's CA.

From Young's equation (**Equation 1.1**), which was first described by Thomas Young (Young 1805) in 1805, a unique contact angle is obtained while in a real system, a range of contact angles is obtained; the highest and the lowest are defined as advancing (θ_a) and receding (θ_r) contact angle, respectively. They are also called dynamic contact angles, which are measured by increasing and decreasing the drop volume at a definite speed while the 'three-phase contact line' moves forward and backward, respectively (for the detailed illustration see Gao and McCarthy 2006). The difference between the two is known as the contact angle hysteresis (CAH), which is exhibited by every solid surface (Lam *et al* 2002) unless the surface is ideally smooth and chemically homogenous (Johnson and Dettre 1964; Koch *et al* 2008a; Yuan and Lee 2013).

However, biological and technologically interesting and significant surfaces are not ideal as previously mentioned. Rather they are rough, reactive, or chemically heterogeneous (Gennes *et al* 2004). The equilibrium wetting on rough and heterogeneous surfaces was established by Wenzel (Wenzel 1936) and Cassie-Baxter (Cassie and Baxter 1944). In the following Wenzel's equation, (**Equation 1.2**)

$$\cos\theta_W = r_f \cos\theta \quad \text{..... (1.2)}$$

θ_W is the Wenzel angle, r_f represents the ratio of actual solid-liquid interfacial area to the projected area (1 for smooth surface and >1 for rough surfaces) and θ is the Young's CA.

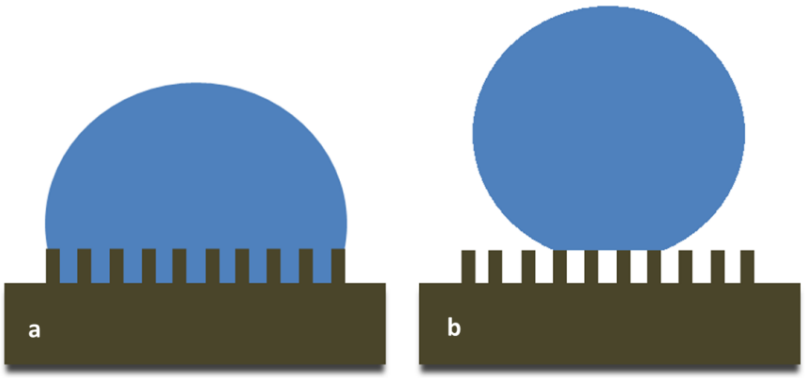

Figure 1.10: Schematic of a droplet in Wenzel state (a) where liquid penetrates into the pockets, and Cassie-Baxter state (b) where air pockets are seen (modified after Yan *et al* 2011).

The Wenzel's equation is based on the assumption that the surface has a homogeneous surface chemistry and much smaller roughness features in comparison to the liquid droplet on the surface; and the pockets/grooves on the surface are filled with the penetrated liquid, resulting in the homogeneous wetting of the surface (**Figure 1.10a).** Therefore, surface roughness controls the wettability on this kind of surface and the equation expresses that the wettability of a smooth hydrophilic surface increases with the increase of the roughness of the surfaces; in contrast the wettability of a hydrophobic surface decreases with the increase of the roughness of the surface (Gennes *et al* 2004). On the other hand, the Cassie-Baxter equation assumes that the liquid cannot penetrate into the pockets/grooves on the rough heterogeneous surfaces (**Figure 1.10b**) due to the presence of air between the solid surface and the liquid. Therefore, the heterogeneous wetting regime reduces the contact area in the solid-

liquid interface, resulting in the increase of the hydrophobicity of the surface (Bhushan and Jung 2008; Koch *et al* 2008a; Nosonovsky and Bhushan 2008b, 2008a). However, Wenzel's equation is applicable for equilibrium wetting not for the dynamic (i.e., advancing and receding CA) wetting of the surfaces. It is well established that the dynamic contact angle measurement system reduces the effects of local irregularities and defects on the surface (Lam *et al* 2002) while the Young's equation cannot take the surface topography into consideration. Moreover, the drop dynamics during droplet deposition on the surfaces can be well understood by the dynamic contact angles. Therefore, the interpretation of the contact angle of a solid surface should be expressed in terms of dynamic contact angle, rather than in terms of the Young's equation.

1.5. Fog collection on plant surfaces

Plants, in the regions with limited rain but regular fog events, do follow fog interception (Burgess and Dawson 2004; Limm *et al* 2009) by their foliage. That is why, in foggy regions, the dripping of water from foliage is one of the most often seen phenomena. Some plants absorb water by their foliage. For example, lower plants, such as mosses (Edelmann *et al* 1998) and lichens (Rundel 1982) take water up by porous surfaces. Some higher plants (vascular plants), such as bromeliads take water up by their superhydrophilic surfaces (Rundel 1982; Benzing *et al* 1985; Benzing 1987; Koch *et al* 2008a; Lüttge 2011). Barthlott and Capesius (1974) demonstrated that some South African xerophytes absorb water, e.g., *Anacampseros papyracea* absorb through dead paper like stipules and *Crassula deceptor* absorb through their leaves. Porous surfaces of some cacti, such as *Discocactus horstii, Opuntia invicta* etc. were also demonstrated to

absorb water (Schill and Barthlott 1973; Porembski 1994). *Trianthema hereroensis*, a Namib plant was also reported to absorb fog water through its leaves (Seely 1979; Van Damme 1991). The authors (Van Damme 1991) commented that *Welwitschia mirabilis,* another Namib plant, may be a fog collector but it is debatable. Spreading of water on superhydrophilic *Ruellia devosiana* leaf surface was revealed (Koch *et al* 2009).

In contrast, some plants drip their intercepted water from their foliage to ground, followed by the uptake by their root system; for example *Sequoia sempervirens* (Redwood) (Dawson 1998; Limm *et al* 2009; Simonin *et al* 2009) and *Pseudotsuga menziesii* (Douglas fir) (Dawson 1998). In a review (Malik *et al* 2014), fog and dew harvesters obtained in nature have been described briefly. The efficiency of fog interception and dripping depends on their surface architecture and chemistry. Various other traits of plants facilitating fog collection, have been analyzed in different studies (Martorell and Ezcurra 2002; Martorell and Ezcurra 2007; Westbeld *et al* 2009; Andrews *et al* 2011; Ebner *et al* 2011; Ju *et al* 2012; Roth-Nebelsick *et al* 2012; Stanton and Horn 2013). For example, increased branchiness of plant species is reported to be an important trait to collect fog (Martorell and Ezcurra 2002; Martorell and Ezcurra 2007; Stanton and Horn 2013). *Tillandsia usneoides*, *Opuntia microdasys, Cotula fallax* etc. have hierarchical structures and have been demonstrated to collect fog efficiently (Martorell and Ezcurra 2007; Westbeld *et al* 2009; Andrews *et al* 2011; Ju *et al* 2012). Conical spines along with the superhydrophilic trichomes of *O. microdasys* (Ju *et al* 2012) and a 3-dimensional orientation of the trichomes and leaves of *C. fallax* (Andrews *et al* 2011) are responsible for their fog-collection ability. Vogel and Müller-Doblies did a study on eight monocotyledon families and some *Oxalis* species in some semi-desert

regions (Namaqualand and adjacent regions) of South Africa, where they demonstrated that these plants did have 'special morphological adaptations' of their aerial parts that facilitate fog and dew collection (Vogel and Müller-Doblies 2011). A comparison of the fog-collection efficiency between a plant species (*Stipagrostis sabulicola*) and an animal species (*Onymacris unguicularis*) showed that plant species were more efficient (Nørgaard *et al* 2012); regardless of the fact that both of the surfaces contained microstructures. Some other studies would be discussed in **Chapter 4–8.**

2. Aims of the thesis

Based on the previous analyses of thousands of plant surfaces by the 'Biodiversity and Bionics' research group led by Prof. Wilhelm Barthlott at the Nees Institute for Biodiversity of Plants, some model plants were selected for this study. Biomimetic models were also considered for analysis.

The main aims of this study are the following:

1. To analyze the fog-collection efficiency of plant and biomimetic models
2. To analyze the influence of the modification of leaf shapes
3. To demonstrate the influence of microstructure and hierarchical architecture of the surfaces
4. To analyze the role of wettability of surfaces
5. To develop novel and/or superior designs for optimized biomimetic fog collectors

3. Material and methods

3.1. Plant and technical material

Plant material

The plants were cultivated in the Botanical Gardens (BG-BONN), University of Bonn. The adaxial surfaces of the leaves/needles/awns of the following plant materials were used.

Abies bracteata (D. Don) Poit. (Accession No. 13140)*, Clerodendrum trichotomum* var. fargesii (Dode) Rehder (Accession No. 6195), *Dendrocalamus brandisii* (Munro) Kurz (Accession No. 22579), *Gunnera tinctoria* (Molina) Mirb (Accession No. 29236), *Hymenanthes maxima* (L.) H. F. Copel (Accession No. 1456), *Hordeum vulgare L.* (Accession No. 19499)*, Iris germanica* var. *florentina* (L.) Dykes (Accession No. 34457), *Pinus canariensis* C. Sm. (Accession No. 17484)*, Ptilotus manglesii* F. Muell (Accession No. 12999), *Prunus laurocerasus* L. 'Caucasica', *Sequoiadendron giganteum* (Lindl.) J. Buchholz (Accession No. 11625), *Sequoia sempervirens* (D.Don) Endl. (Accession No. 12049) and *Tillandsia usneoides* (L.) L. (Accession No. 16078).

Technical material

Copper foil (99.9% copper; Basic Copper, USA), copper wire (98% copper; Lapp Kabel, Germany), polyolefin Raschel mesh (Karatzis S.A. group of Companies, Greece), and polyethylene-terephthalate (PET) fibers of different cross-section profiles and different widths/diameters (Nextrusion GmbH, Bobingen, Germany).

3.2. Sample preparation

3.2.1. Plant samples

(A): Simple leaves (i.e., not divided into leaflets) of 3 different species (*Iris germanica*, *Prunus laurocerasus* and *Hymenanthes maxima*) were modified.

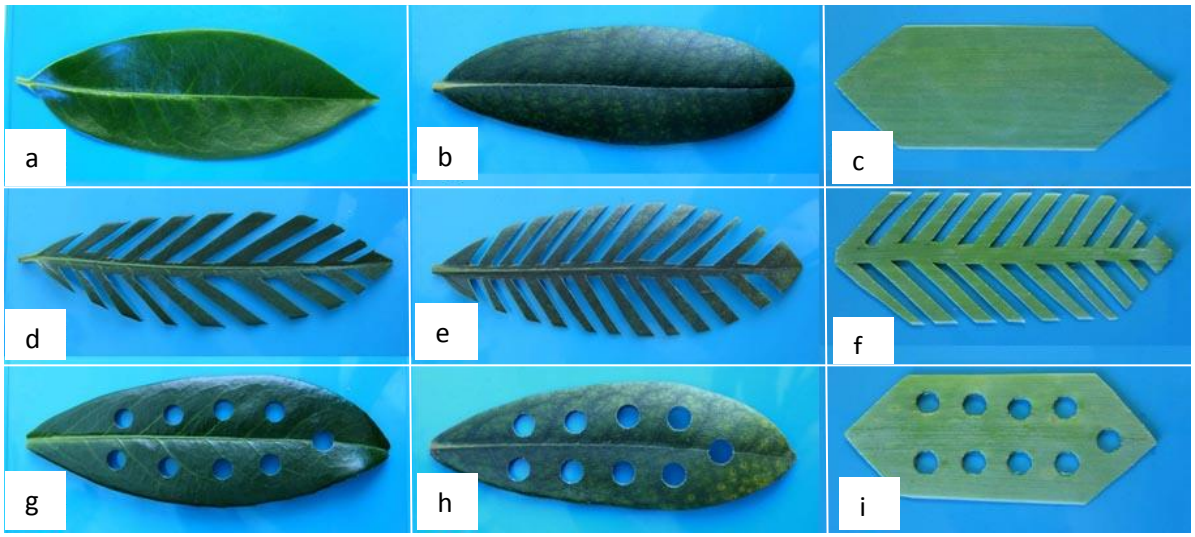

Figure 3.1: (a–c) Simple leaf shapes and (d–i) modified leaf shapes; pinnate (d–f) and perforate (g–i). The left column shows *Prunus*, the middle column shows *Hymenanthes* and the right column shows *Iris* leaf samples. *Iris* leaf sample (c) was cut from a long leaf. (photo: Dorothee Ellerbrok).

In one set of specimens the leaflets were cut at an angle of ~45° from the center vein line. The width of leaflets is 3–4 mm and the width of spaces in between is 1–2 mm. Another set of specimens was perforated carefully. 9 holes (diameter 6 mm) were punched in the same arrangement on the leaves. On each side of the main vein of the leaves 4 holes were made, a hole was in the middle at the bottom of the leaves. **Figure 3.1a–c** shows the simple leaves of *Prunus*, *Hymenanthes and Iris* (actually cut from a long leaf), respectively. Experimentally modified shapes were pinnate (**Figure 3.1d–f**) and perforate (**Figure 3.1g–i**).

(B): In one set, five 2x2 cm^2 samples of each leaf of *Prunus, Dendrocalamus, Gunnera* and *Clerodendrum* were prepared (**Figure 3.2a–d**). They have no drip tip. These are referred as **Type 1** samples in the text. In another set, five 2x2 cm^2 samples of the same leaves were prepared each of them with a drip tip at the middle of the bottom edge (**Figure 3.2e–h**). These are referred as **Type 2** samples in the text.

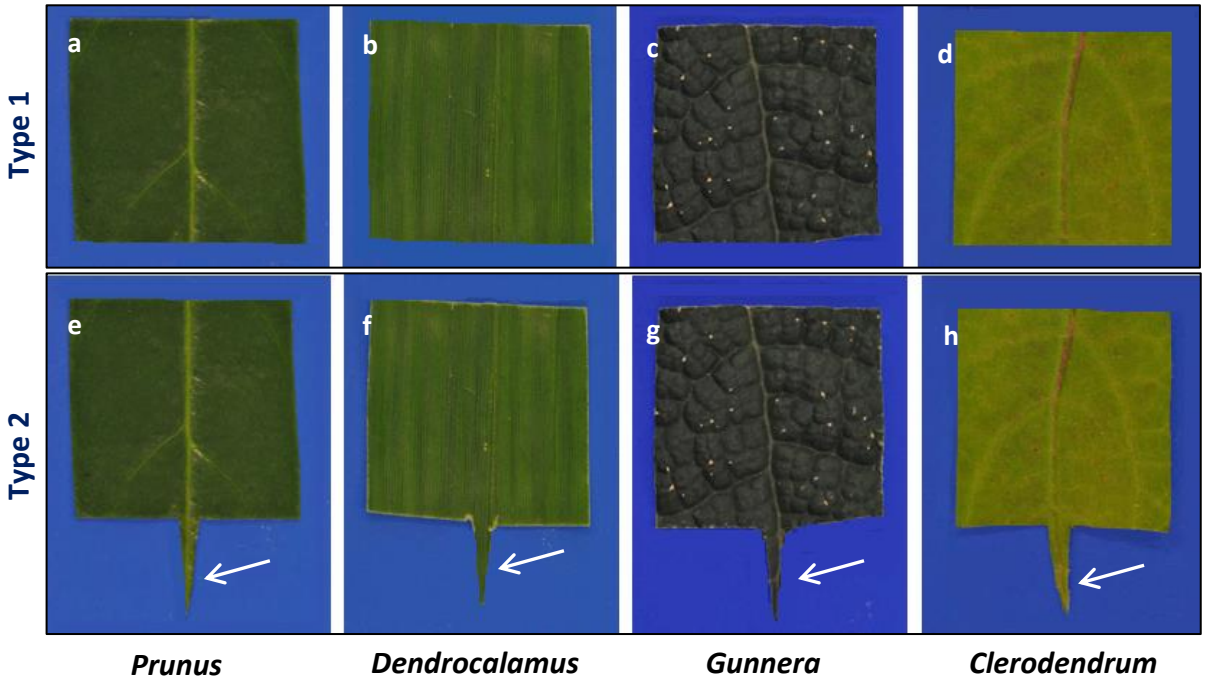

Figure 3.2: (a–d) Type 1 samples: without drip tip and (e–h) Type 2 samples: with drip tip at bottom edges (marked with white arrows). Each pair (in column) was prepared from the plant leaves of the same species; column 1, 2, 3 and 4 represent *Prunus, Dendrocalamus, Gunnera* and *Clerodendrum*, respectively.

(C): 2 cm length of each of the model plant species (**Figure 3.3a–g**), i.e., fresh and dry hydrophilized (DH) awns of *Hordeum* (barely), needle shaped leaves (Ns) of *Abies, Pinus, Sequoiadendron* and *Sequoia*, and leaves (NLSs) of *Tillandsia* were used separately to prepare 2x2 cm^2 samples (**Figure 3.4a**). The needles (Ns) or needle like structures (NLSs) were arranged vertically in such a way that there were gaps (~width of awns/Ns or NLSs) in between. The samples were prepared in such a way that their effective surface area remained close to each other.

Figure 3.3: (a–g) Optical photo of awns, needles and leaves used in the fog-collection experiment; scale bar 1 mm. (a) A fresh and (b) a DH awn of *Hordeum*, (c–f) needles/leaves of *Abies, Pinus, Sequoiadendron* and *Sequoia,* respectively and *(*g) a leaf (needle like structure) of *Tillandsia.* Published in Azad *et al* 2015a.

About 50–55% surface area of each prepared 2x2 cm^2 sample was occupied by the awns/Ns/NLSs and the rest was free to get rid of the impedance of the fog flow. Therefore, the samples have an equivalent effective surface area for fog collection. The measurement of the surface area coverage by the awns/Ns/NLSs was calculated from the images of the samples by Photoshop CS3. For the first set of samples intact Ns/NLSs were used while for the second set, needles of *Abies* and *Sequoia* were cut to reach as close in the diameter of the *Hordeum* awn as possible. The *Tillandsia* leaves (NLSs) of smaller diameter close to *Hordeum* awn were also selected for the second set as well. Samples of 2x2 cm^2 were prepared as previously described.

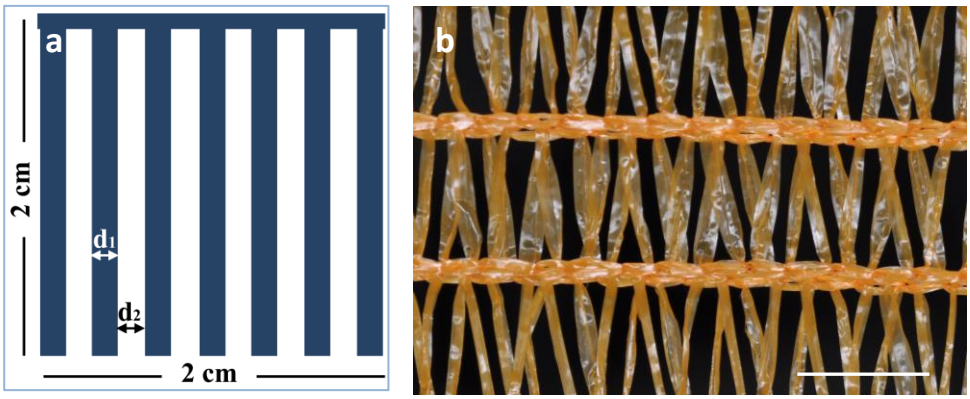

Figure 3.4: (a) Schematic of 2x2 cm^2 sample prepared by awns/needles/leaves/needle like structures/copper wires/fibers; d_1 represents the diameter/width of an awn/needle/leaf (needle like structure)/copper wire/fiber, and d_2 is the gap between consecutive two of them. (b) Double layered polyolefin mesh; scale bar 1 cm. Published in Azad *et al* 2015b.

3.2.2. Technical samples

(A): A copper foil of 15x15 cm^2 and 0.4 mm thickness was cut into smaller pieces of 2x2 cm^2 samples.

(B): Copper wire with the diameter of 1.2 mm was used. First, the plastic outer layer of the wire was peeled off carefully. Then, microgrooves were implemented on the wire surface by using sand paper with korn 80 (kwb–Speziel–Endschliff Finishing Papier-Holz & Lack, Germany) (Korn 80 sand paper contains the particles with the diameter of 190–265 µm (source: Federation of European Producers of Abrasives)). Long wires were cut into smaller pieces (2.4–3 cm length). Then the wires were soldered electrically to prepare copper combs as shown in **Figure 3.4a.** Wires with smooth and microgrooved surfaces were used separately. The gap between two parallel wires is ~1.6 mm. By using the following formula, the surface area of samples exposed to fog was calculated as ~300 mm^2 (for the samples in **Chapter 4**) and ~471 mm^2 (for the samples in **Chapter 5**)

$$A = \pi rl$$

where A = area of the wires exposed to fog, r = radius and l = length of the wires.

(C): A double layered polyolefin Raschel mesh (**Figure 3.4b**) was chosen, which is usually used for packaging purposes. The width of the ribbons of the mesh is ~1.5 mm. There are triangular gaps between the ribbons (2 sides of the triangles are ~11 mm and the base is ~3.5 mm) in the mesh and 1.0 cm spacing between the horizontal lines. The dimension (including the free flow space) of each sample is 8 cm x 5 cm. The double layered mesh was calculated to cover ~59–66% of the total surface area of the sample (measurements done by Photoshop CS3 software by using the images of the samples that will be illustrated later in section 3.7). The rest of the area was open so that the fog stream was not impeded largely.

(D): Smooth glass (microscope slide), and *Gunnera* and *Dendrocalamus* leaf surfaces were replicated by using epoxy resin. A method developed by Koch and co–workers (Koch *et al* 2008b) was followed. The same dental wax, a low consistency polyvinylsiloxane (Coltène® President Plus, ISO 4823, Coltène Whaledent, Switzerland) was used to prepare negative molds, and epoxy resin (Epoxydharz L® No. 236349, Conrad electronics, Hirschau, Germany) with hardener (Härter S, No 236365, Conrad electronics, Hirschau, Germany) was used for filling molds to fabricate the positive replicas (surface area of each replica was 18 mm x 18 mm).

(E): 14 different PET fibers were used for fog collection. They have a width/diameter range between 317 µm and 2300 µm. They were grouped into two categories.

Category A: profiles 1–7 with diameter/width ranges of 317 µm to 999 µm and

Category B: profiles 8–14 with diameter/width ranges of 1000 µm to 2300 µm

Long fibers were cut into small pieces of 2 cm in length and they were used as single fiber samples. Multiple fiber samples were also used. Fibers of 2 cm in length were aligned vertically, parallel to each other, wherein the distance between the adjacent fibers was as identical as possible for every 2x2 cm^2 sample (**Figure 3.4a**). The gap between two fibers was approximately equal to their widths/diameters. The samples were prepared in such a way that they have equivalent effective surface area for fog collection. About ~55% surface area of each sample was occupied by the fibers and the rest was free to get rid of the impedance of the fog flow. The surface area coverage was measured from the images of the samples by Photoshop CS3.

3.3. Contact angle (CA) measurement

Static and dynamic contact angle measurements were performed by a goniometer (DataPhysics OCA 20, Filderstadt, Germany). 5 µl of demineralized water was applied on the samples using an automatic dispense controller to measure static contact angle. Dynamic contact angle measurements were done by increasing the volume of demineralized water droplet from 2 to 5 µl and decreasing from 5 to 2 µl (**in Chapter 4, 5 and 8**) at a rate of 0.1µl/s with a delay time of 5 second; from 1 to 2 µl, followed by a decrease from 2 to 1 µl (**in Chapter 6**) at a rate of 0.1µl/s due to the very low surface area of the samples. Due to the similarity of material properties of the samples **in Chapter 8** (PET fibers), a fiber with smooth surface (profile 14), which have the width enough to place 5 µl of water, had been used. Contact angle hysteresis was calculated from advancing and receding contact angles. All the measurements were taken at room temperature (~21°C). For each sample surface 5 (**in Chapter 4 and 6**) or 10 (**in Chapter 5 and 8**) measurements were taken.

3.4. Light- and Scanning Electron- Microscopy (SEM)

Sample surfaces were analyzed by a Keyence VHX-1000 digital light microscope (Keyence Corporation, Japan) and a Stereoscan 200 SEM (scanning electron microscope) (Cambridge, UK). Fresh-hydrated samples of most of the species were used for SEM analysis while some species (*Prunus*, *Hymenanthes, Iris, Gunnera* and *Clerodendrum*) were critical-point dried. The methods were described elsewhere (Ensikat *et al* 2010). Specimens were coated with gold for 30 s at 60 mA (sputter coater, Balzers Union SCD040, BAL-TEC AG, Liechtenstein) prior to SEM analysis.

3.5. Modification of the chemistry of the sample surfaces

Hydrophilization: Mesh samples (**in Chapter 5**) (untreated mesh is hydrophilic) and dry awns of *Hordeum* (**in Chapter 6**) were dip coated with a water based polymer solution containing TiO_2 (TA 2202, Nadico Technologie GmbH, Langenfeld, Germany) and dried at room temperature for 48 hours. The average primary particle size of TiO_2 is given as <8 nm (manufacturer's information). After evaporation of the solvent the nanoparticles were bonded into a remaining matrix, which prevents their release into the environment. The thickness of the coating was measured by an atomic force microscope (NanoWizard II, JPK Instruments, Germany). The TiO_2 coated mesh was referred as 'superhydrophilic mesh' in the text. Hydrophilized dry *Hordeum* awns were referred as 'DH awns' (D for dry and H for hydrophilized).

Hydrophobization: Mesh samples were dip coated with a hydrophobizing agent (Antispread E 2/200 FE 60, Dr. Tillwich GmbH, Horb, Germany) and dried at room

temperature for 48 h. The Antispread coated mesh was referred to 'hydrophobic mesh' in the text.

3.6. Experimental setup

Droplet deposition behavior on the surfaces of the samples and their fog-collection efficiency were analyzed with the setup (**Figure 3.5**). Samples were mounted vertically at 17 cm from the outlet of an ultrasonic humidifier (Honeywell, BH–860E; outlet diameter 3.2 cm, fog output maximum 0.4 L/h). Fog flow velocity was ~1.6 m/s at 17 cm from the outlet (velocity measured by Testo 416 anemometer, Lenzkirch, Germany). The fog stream had a constant flow. The total setup was placed in a chamber (length/width/height = 100 x 90 x 180 cm) what is named a fog chamber throughout the text. The temperature inside the chamber was 19–20°C and the relative humidity was 75–85% during the experiments.

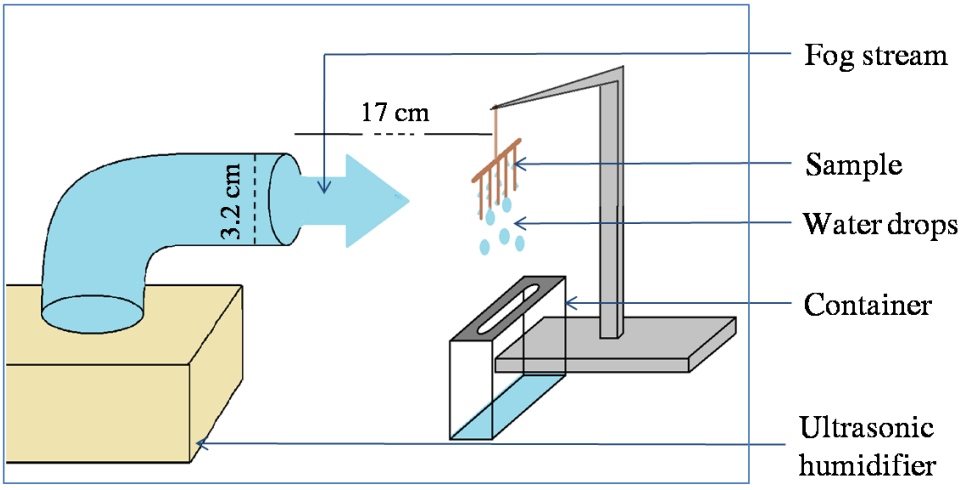

Figure 3.5: Schematic of the experimental setup for fog-collection experiment in a fog chamber. The sample is mounted in a fog stream. Fog droplets deposit on the sample, followed by the dripping into the container under it. Published in Azad *et al* 2015b.

Images were captured by D90 Nikon camera. Videos were captured by the camera as well as by the charged coupled device (CCD) camera equipped with the goniometer (Dataphysics OCA-20) and a Keyence VHX-1000 digital microscope. The efficiency was determined by weighing (by KERN EMB 200-3, KERN & Sohn GmbH, Germany) the amount of fog water dripped from the samples in the container placed under the samples as well as the amount of total water collected by the samples over 10–60 min.

Control experiments were also conducted (5 times each of 10–60 min) without sample. The specific time duration will be mentioned in respective chapters.

3.7. Effective surface area of samples for fog collection

Samples containing free flow (open) spaces should be deducted to measure the effective surface area of samples for fog collection based on what their fog-collection efficiency was compared. To do this, a CS3 version of Photoshop was used. An example (polyolefin Raschel mesh) is illustrated in **Figure 3.6.** A reference scale was set while capturing a photo of a sample. By the use of a tool of the software, in the first step, the reference scale length was converted to pixel length. The pixel length was similar for both in the free flow/open space or in the occupied space of the image in relation to the reference length. In the second step, the total area of a sample was measured, which was converted to the reference length unit from the pixel unit by the software. In the third step, open spaces on the sample image were marked (white dotted lines in the borders of black and yellow spaces shown in **Figure 3.6)** carefully by a tool to deduct the area from the total area that was measured earlier. Therefore, a second area measurement was done where

the area was only for the occupied spaces. From these two values, the percentage of the effective surface area, exposed to collect fog was calculated.

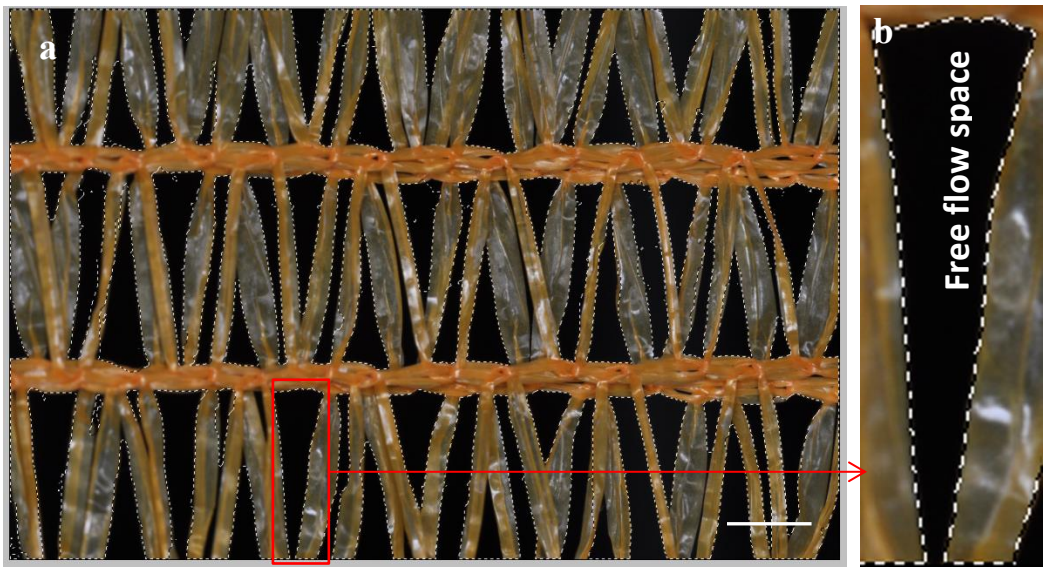

Figure 3.6: (a) A double layered polyolefin mesh sample for fog collection; brown areas represent the effective surface area and black areas represent free flow/open spaces. Scale bar: 500 µm. (b) Small area of Figure (a) is magnified; white dotted lines in the borders of black and brown spaces separated free flow/open spaces (in black). This is done by a tool of the software to deduct the free flow space from the total sample area to calculate the specific surface area for fog collection.

3.8. Statistical analysis

The data were analyzed (**in Chapter 5**) by Statistics analysis software SPSS 22. Normality distribution was tested by Kolmogorov-Smirnov test and Shapiro-Wilk test for paired T-test and one-way ANOVA test was done with Tukey-HSD multiple comparison Post Hoc Test. In both cases confidence interval was 95%.

3.9. Simulation

Fog droplet behavior on surfaces was validated by a numerical simulation. Different surface parameters, e.g., contact angles; dimensions of the grooves etc. were set up in

the simulation. To analyze the behavior of the droplet with time, the continuity and momentum equation, as well as an additional transport equation for the phase fraction gas/liquid have been solved using the *interDyMFoam* algorithm of the open source software *OpenFOAM* (Version 2.3.1). To determine the gas-liquid interface *OpenFOAM* applies the *Volume-of-Fluid-Method* (VOF). **Figure 3.7** shows a schematic of a wavy microgrooved surface, the initial position of the water droplet, as well as values for the geometry, surface and fluid properties. The discretization schemes are of second order in time and first/second order in space. The basic mesh consists of 75600 hexahedral cells with an average non-orthogonality of 8.26°**.** During calculation an increase in number of cells took place; every second time step a mesh refinement at both sides of the liquid/gas interface led to an improved interface capturing.

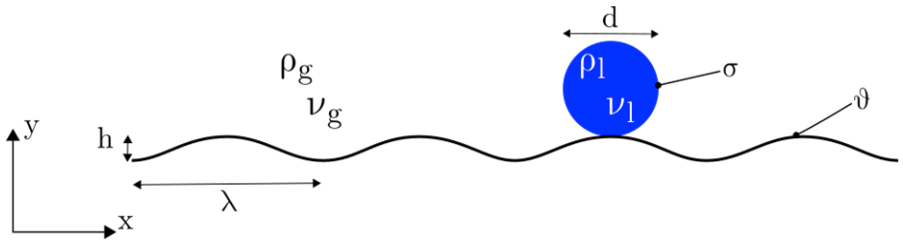

ρ_l	=	$1000\,\mathrm{kg/m^3}$	ρ_g	=	$1\,\mathrm{kg/m^3}$
ν_l	=	$1 \cdot 10^{-6}\,\mathrm{m^2/s}$	ν_g	=	$1.48 \cdot 10^{-5}\,\mathrm{m^2/s}$
σ	=	$0.072\,\mathrm{kg/s^2}$	θ	=	$62°$
h	=	$15\,\mu\mathrm{m}$	λ	=	$113\,\mu\mathrm{m}$
d	=	$100\,\mu\mathrm{m}$	L	=	$1000\,\mu\mathrm{m}$

Figure 3.7: Schematic of a wavy microgrooved surface (wave length *λ*, amplitude *h/2*, length in *z* direction *L*) and initial position of a spherical water droplet (diameter *d*). Densities *(ρ)* and viscosities (*ν)* are given for the liquid- and gas phase indexed with *l* and *g*, respectively. The contact angle on the surface is *ϑ* and the surface tension is *σ*. The gravitational force is pointing in the negative *z* direction.

4. Fog collection on plant surfaces: Influence of leaf shape modification and directed water transport on the surfaces

4.1. Introduction

The amount of fog interception by the plants may vary depending on the size and shape of the leaves in combination with other physical traits, e.g., microstructures on the surfaces and/or chemical traits, e.g., the superhydrophilicity of the surfaces (Rauh *et al* 1973; Benzing *et al* 1976; Rundel 1982; Ju *et al* 2012; Roth-Nebelsick *et al* 2012). Despite the large number of measurements of fog collection by trees, it was not possible to compare their collection efficiency quantitatively. Here, we propose a quantitative comparison. In this study, the shape of the leaves from same species was considered as a single variable maintaining other parameters/characteristics exactly the same to characterize the influence of leaf shape modification on fog collection. To do this, shape of simple leaves was modified experimentally, i.e., perforate, pinnate etc. (**Figure 3.1 in Chapter 3**) while all other parameters, e.g., chemistry of surfaces remained same. Simple leaves of same dimensions from same species were used as controls. A set of representative technical samples, e.g., copper foil and copper wire was also considered in the analysis separately. Droplet deposition and water drainage/transport efficiency are important factors in developing an efficient and large capacity system for fog collection. Direction controlled movement of tiny water drops was demonstrated in several studies (Bai *et al* 2010; Zheng *et al* 2010; Ju *et al* 2012; Chen *et al* 2013) but the distance was

limited (maximum 5 mm by Chen *et al* 2013). Moreover, here the study is focused on the surfaces with channels. The fog-collection ability of the surfaces with channels as well as flat technical surfaces has been compared in a study (White *et al* 2013). Though, no significant difference in the efficiency of the samples was found but it could describe the difference in the drop dynamics on the surfaces. A 'Y' shaped hydrophilic channel on a hydrophobic technical surface was shown to control water transport, although the study was limited to the spraying of water by a syringe on the surface (Shirtcliffe *et al* 2009). However, an extended study based on the fog collection and the transport of the collected fog water on the surfaces with channels is presented here in this chapter. A flat/smooth surface was used as a control.

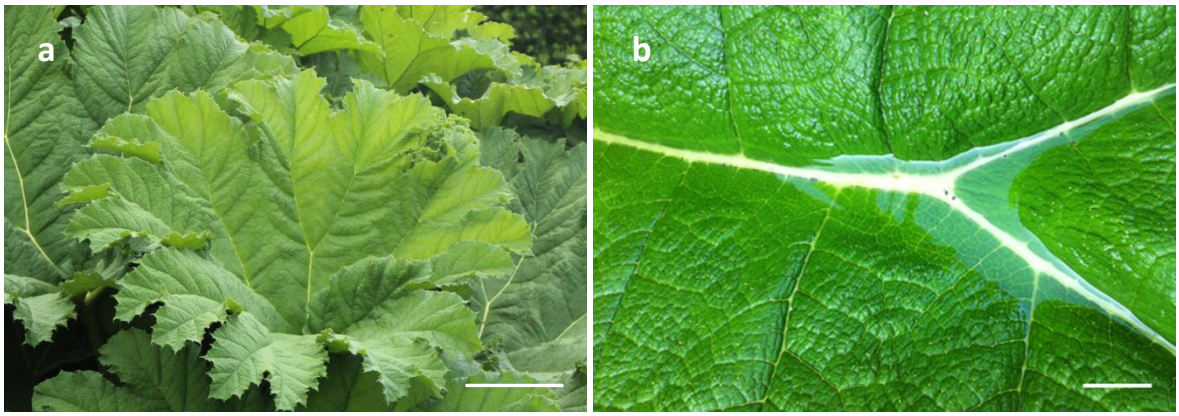

Figure 4.1: (a) Large leaves of *Gunnera* (~1.5 m diameter) plant cultivated in the Botanical Garden, Bonn, (b) dew water collected by *Gunnera* leaf; interconnected channel networks can be seen. Scale bar: (a) 20 cm and (b) 2 cm.

In summer 2014, *Gunnera* leaves, with their directed channel network formed by their reticulate venation (i.e., interconnected), collected the highest amount of dew among the samples investigated in an open field experiment.

Inspired by this fact, fog-collection efficiency of plant surfaces with channels was compared with other plant surfaces (*Dendrocalamus* and *Clerodendrum*) both having different kinds of channels, and a flat leaf surface (*Prunus*). Moreover, a drip tip (**Figure 3.2e–h** in **Chapter 3**) was prepared at the bottom edge of each sample surface of a set that showed interesting results during fog-collection experiment.

The experimental setup for fog collection has been illustrated in **Chapter 3 Figure 3.5**.

4.2. Results

4.2.1. Structural characterization of the samples

Upper surfaces of leaf samples and technical sample surfaces were characterized, which are described briefly in **Table 4.1**.

Table 4.1: Structural characterization of leaf and technical samples

Sample	Structural characterization
Prunus	Smooth surface
Hymenanthes	Apparently rough surface with cuticle folding in microstructures
Iris	Large grooves on the surfaces with the width of about 1–2 mm
Dendrocalamus	Width of the grooves at the base 74.6 ± 5.1 µm, width of the ridges at the base 204 ± 11 µm, peak to peak width between the ridges 290 ± 12.8 µm
Gunnera	Narrowest channels (105–177 µm wide and ~400 µm deep) are connected to the channels of 288–303 µm wide which are then connected to the widest channel of the sample. The widest channel of every 2x2 cm^2 sample is at the middle (from the top to the bottom) is 800–915 µm. Height of the trichomes in the channels 196–517 µm; distance between the trichomes 311–668 µm
Clerodendrum	Height of the trichomes 153 ± 94 µm, density of the trichomes 12 ± 2/mm^2
Copper foil and wire	Smooth surface

4.2.2. Surface wettability

Advancing contact angle (θ_{adv}), receding contact angle (θ_{rec}), and contact angle hysteresis (CAH) of all sample surfaces are given in **Table 4.2**.

Table 4.2: Surface wettability of leaf and technical samples

Sample	**Advancing contact angle (θ_{adv})**	**Receding contact angle (θ_{rec})**	**Contact angle hysteresis (CAH)**
Prunus	76 ± 3	45 ± 2	31 ± 2.5
Hymenanthes	70 ± 3.5	43 ± 2.5	27 ± 1.3
Iris	152 ± 0.2	150 ± 0.5	2 ± 0.6
Dendrocalamus	63 ± 2	45 ± 2.1	17.4 ± 1.3
Gunnera	0	0	-
Clerodendrum	0	0	-
Copper foil	95 ± 1	54 ± 5	41 ± 6
Copper wire	82 ± 4	57 ± 5	25 ± 5

4.2.3. Surface microstructure

The leaf surface of *Prunus* is smooth and contains no channels (**Figure 4.2a**) except the main vein at the middle of the leaf, kept in the middle during the preparation of both kinds of samples (**Figures 3.1a,d,g** and **3.2a,d**) which forms a channel on the upper surface of the leaf. *Hymenanthes* leaf surface contains cuticle foldings (**Figure 4.2b**) that make the surface a bit rough. *Iris* has wax particles (**Figure 4.2c**) on the leaf surface resulting in the superhydrophobicity (**Table 4.2**).

Leaf surface of *Dendrocalamus* contains grooves (**Figure 4.2d**), *Gunnera* contains papillate microstructures and channels with trichomes inside (**Figure 4.2e**), and *Clerodendrum* has channels and trichomes (**Figure 4.2f**). Both copper foil and copper wire contain similar smooth surfaces (**Figure 4.2g** and **h,** respectively).

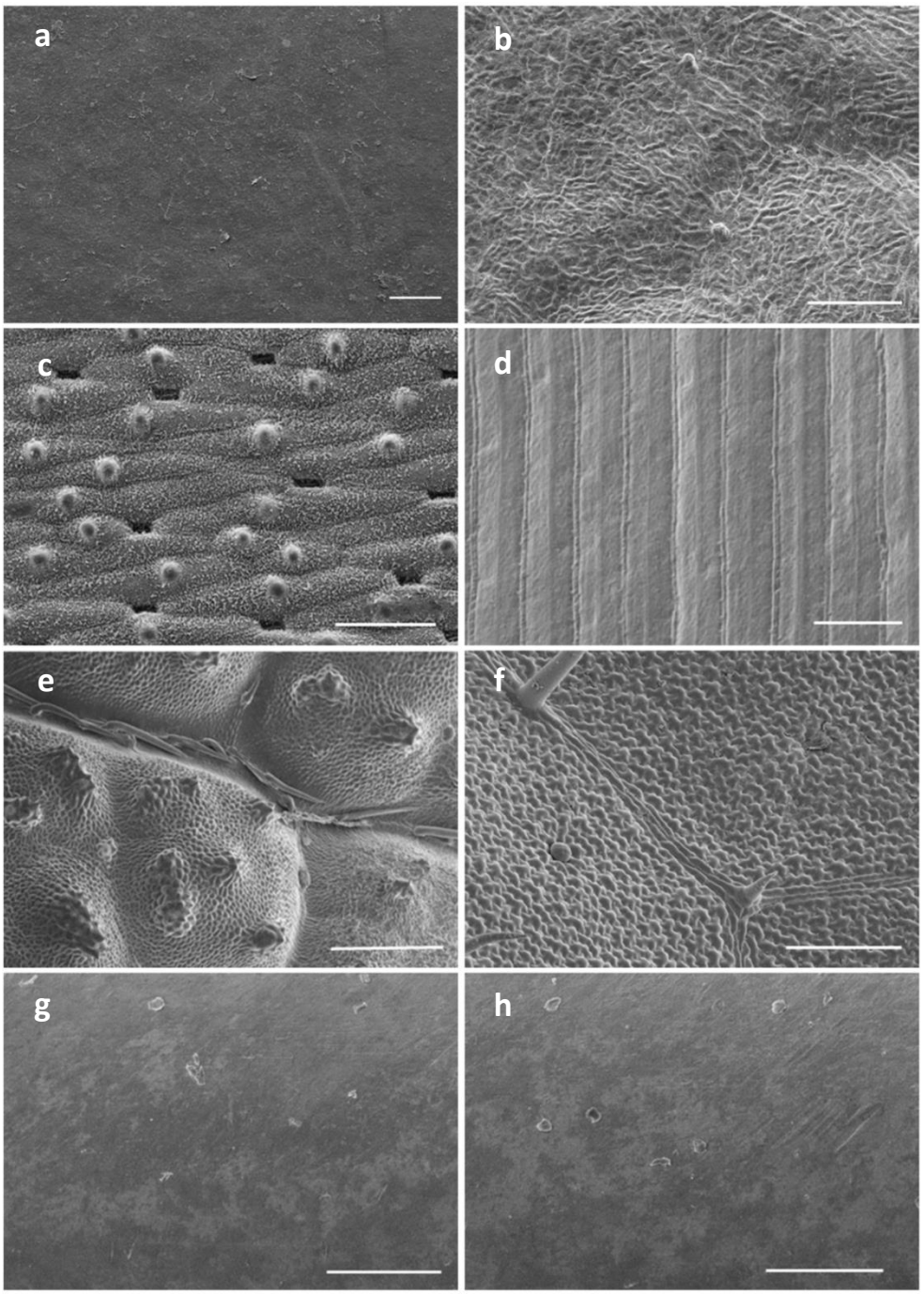

Figure 4.2: Scanning electron micrographs (SEMs) of critical-point dried leaf surfaces of (a) *Prunus*, (b) *Hymenanthes* (c) *Iris* (e) *Gunnera* and (f) *Clerodendrum,* and SEMs of (g) smooth copper foil and (h) smooth copper wire; scale bar (a) 200 µm, (b) 100 µm*,* (c) 100µm, (d) 500 µm, (e) 500 µm, (f) 200 µm, (g) 200 µm and (h) 200 µm.

4.2.4. Influence of leaf shape modification

Fog collection by simple leaves as well as their modified shapes (shown in **Figure 3.1 in chapter 3**) was analyzed. The experimental modification of leaf shapes influenced their fog-collection efficiency (**Figure 4.3a**). The amount of water collected by pinnate leaf sample was much higher than simple or perforate shape. The amount of water collected by pinnate shape of *Prunus* leaf was 2.5 and 5 times higher than perforate and simple shape, respectively.

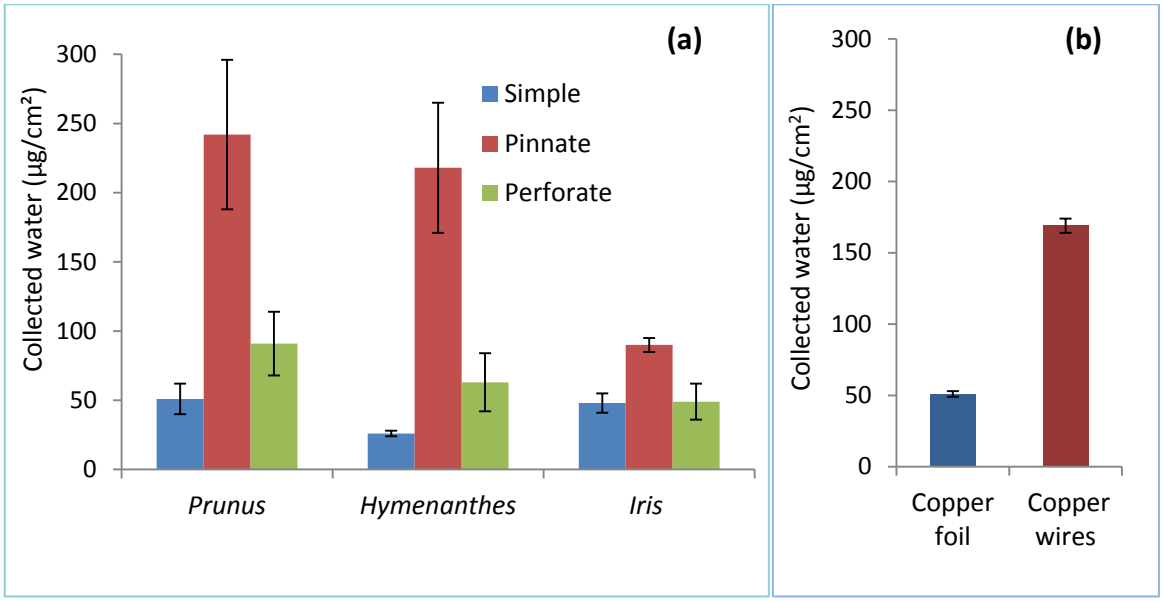

Figure 4.3: (a) Fog collection over 60 min by the samples of simple and modified leaf shapes (pinnate and perforate). (b) Fog collection over 30 min by smooth copper foil and copper wire sample (2x2 cm^2). Average values from 5 measurements and standard deviations are shown here.

For *Hymenanthes* species pinnate sample showed 3.5 and 8 times higher efficiency than perforate and simple leaf shape, respectively (**Figure 4.3a**). For *Iris* the amount of water collected by pinnate sample was 2 times higher than both perforate and simple leaf samples. Here, perforate and simple leaf samples showed nearly the same efficiency (**Figure 4.3a**) possibly because of their hydrophobicity (see **Table 4.2**).

Copper wire samples having gaps in between to ease the fog flow showed higher efficiency in comparison to copper foil samples (**Figure 4.3b**). A thick water layer (shown by the dotted rectangle in **Figure 4.4a**) adhered at the bottom edge of copper foil samples, while droplets were observed to hang at the bottom (**Figure 4.4b**) of copper wire and drip (marked by a white arrow) after a definite time interval (~300 s).

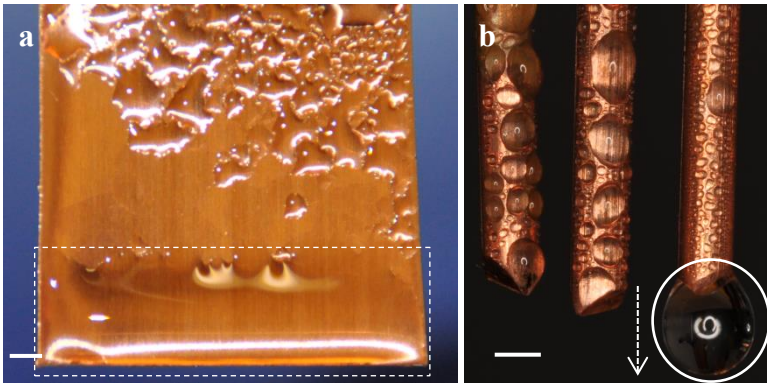

Figure 4.4: (a) Adhesion of a thick water layer at the bottom of copper foil (marked with a dotted rectangle), (b) a droplet hanging at the bottom of a copper wire (in the white circle); it drips continuously over time when large enough (the arrow indicates the direction). Scale bar 1 mm.

4.2.5. Influence of directed water transport on the surfaces

The influence of directed channels on the surfaces on fog collection was analyzed (**Figure 4.5**) by comparing the amount of collected fog water by the samples (**Type 1 in Figure 3.2a–d**) with and without channels on the surfaces as well as the addition of a drip tip at the middle of the bottom edge of the samples (**Type 2 in Figure 3.2e–h**). All the samples surfaces with channels, such as *Dendrocalamus*, *Gunnera* and *Clerodendrum* collected more water (**Figure 4.5**) than the smooth leaf sample of *Prunus*. *Clerodendrum* samples collected the highest amount of fog among the samples investigated here. Drip tip

improved the fog-collection efficiency of samples by 17%–60% (*Prunus* 17%, *Dendrocalamus* 37%, *Gunnera* 44% and *Clerodendrum* 60%).

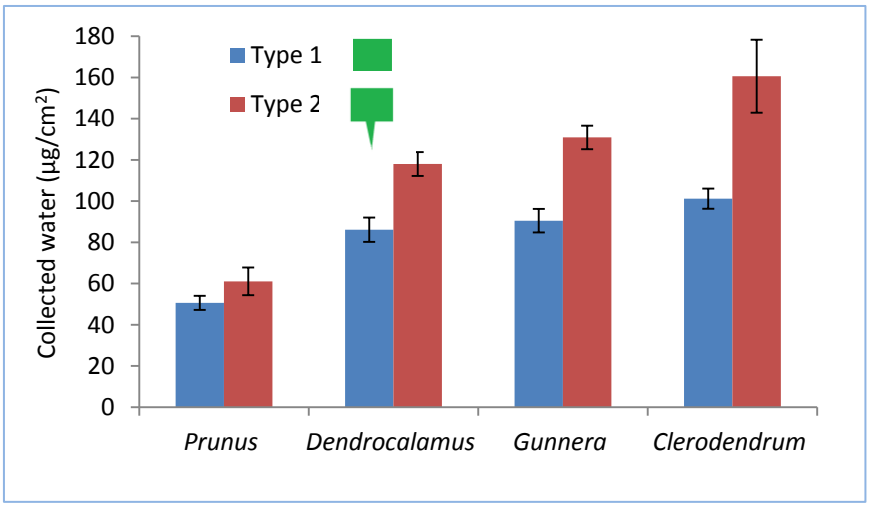

Figure 4.5: Fog collection over 30 min by different leaf surfaces (2x2 cm^2) without drip tip (Type 1 samples) and with a drip tip (Type 2 samples) at the bottom edges of the samples. Type 2 samples show better efficiency than type 1 samples. Smooth *Prunus* surface collected the lowest amount of water compared to the surfaces with directed channels of *Dendrocalamus, Gunnera* and *Clerodendrum*.

However, though there was hardly any dripping from the smooth leaf sample of *Prunus*, a discontinuous dripping was observed on the sample surfaces with channels, such as *Gunnera*. For type 2 samples, adhesion of a thick water layer was observed at the bottom edges of the samples (**Figure 4.6a–b**) while a drip tip on the type 2 samples (dotted rectangles in **Figure 4.6c–d**) improved the dripping though adhesion of larger water droplets (marked with a dotted rectangle in **Figure 4.6c)** at *Prunus* was still observed.

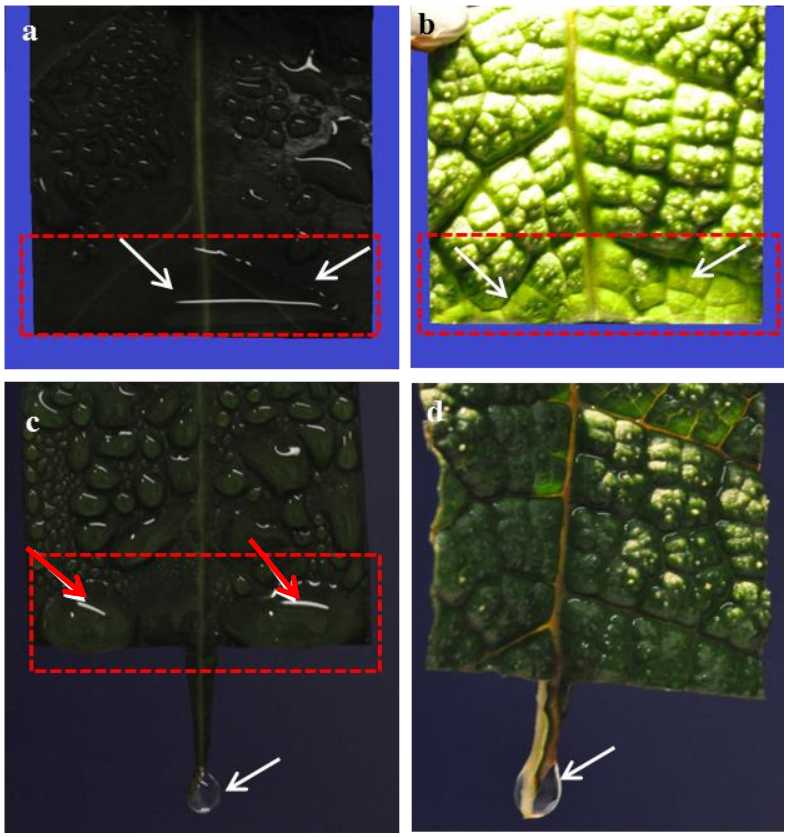

Figure 4.6: (a,b) Adhesion of a thick water layer (marked with white arrows in red rectangles) at the bottom edges of the leaf samples without a drip tip (Type 1 samples); (a) *Prunus*, (b) *Gunnera*; (c,d) drip tips at the bottom edges of the samples (Type 2 samples) help transport water (water dripping marked with white arrows) and thus overcome surface saturation. In *Prunus* sample (c) the drip tip is not as effective as in *Gunnera* (d); still surface saturation can be seen on *Prunus* sample (marked with red arrows) due to the absence of any directed channel on the surface.

4.3. Discussion

4.3.1. Influence of leaf shape modification

Both pinnate and perforate shaped leaf samples showed higher yields of water than simple leaf shape. They are both permeable for the air carrying the fog, although the pinnate sample shape is more open to fog flow. Pinnate samples collected the highest amount of water among 3 different sample shapes; thus a shape, which has a lower flow

resistance for the air carrying fog, is much better for fog collection. This is because if air strikes an impermeable surface, i.e., simple leaf shape, air passes around the surface.

A certain portion of the fog droplets that are carried out by the air tend to be deposited on the obstacles, i.e., plant surfaces in the path of the moving air. Fog droplets, moving with the air, while approaching a permeable and open structured body, i.e., pinnate or perforate leaf sample, a change of the perturbation of the air (Nagel 1956) and/or much turbulence occurs (Suga *et al* 2010). Thus, the air moves multiple times over the samples, resulting in the deposition of more droplets on their surfaces. Moreover, the areas of the leaf samples, where modifications were done, are believed to become sharp and increase the wettability, resulting in the capture of more fog droplets.

The fraction of the fog, that comes in contact with the sample surface, depends on the drag co-efficient of the surface (C_d), which is directly proportional to the force component in the direction of the flow velocity and the flow resistance (C_0) of the surface. It is expressed by the following equation

$$\eta_{AC} = \frac{S}{1+\sqrt{C_0/C_d}} \qquad \text{..... (4.1)}$$

where S is the shade co-efficient that represents the fraction of the area of the sample surface capable of capturing droplets.

From the **Equation 4.1** it is clear that the modification of the leaf shapes that decreases the flow resistance should enhance the aerodynamic collection efficiency (η_{AC}), resulting in the increase of the total fog-collection efficiency. Therefore, pinnate samples guarantee the least possible flow resistance to create turbulences and simultaneously

provide a large surface for the droplets to impinge on. However, there should be an optimized ratio of projected surface area (i.e., ~ 55 %) for fog droplet deposition to the free flow space (i.e., ~ 45 %) for a fog collecting system (**Chapters 5–6** to be followed).

4.3.2. Influence of directed water transport on the surfaces

Results (**Figure 4.5**) exhibit an influence of directed channels or grooves on the surfaces and a drip tip at the bottom edge of the sample surfaces on fog collection. Directed channels transport collected fog water to the bottom generating an unsaturated or free space for further fog droplets to impinge (Cao *et al* 2015). Moreover, thinner boundary layer due to the surface asperities created by the channels or grooves (Vogel 1994; Nørgaard *et al* 2012; Azad *et al* 2015b) facilitates the process, resulting in the increase of aerodynamic fog-collection efficiency. Thus, the fog-collection efficiency of the samples of *Dendrocalamus, Gunnera* and *Clerodendrum* was higher than *Prunus*. It should be noted that, the presence of superhydrophilic trichomes as well as the superhydrophilic surface chemistry (see **Table 4.1** and **4.2** and **Figure 4.2f**) also played a role in the highest fog collection among the samples by *Clerodendrum*. However, the scenario at the bottom edge of the sample surfaces differs concerning the transport due to the adhesion of a thick water layer. Similar results were reported in earlier studies (Lee *et al* 2012; White *et al* 2013). Lee and co-workers during their dew condensation experiment, on the patterned surfaces other than channels, tried to solve the problem by the addition of tiny channels at the bottom edge of the sample surface. Due to the retention of the water on the hydrophilic to superhydrophilic surfaces still water transport from the adhered thick water layer was not improved. Nevertheless, they recommended a narrow channel (1–2

mm) at the bottom edge. The adhesion of a thick water layer cannot be overcome though the samples investigated here contained channels. White and co-workers did not consider the case of the adhesion of a thick water layer. Shirtcliffe *et al* 2009) demonstrated 'Y' shaped branched hydrophilic channels on the middle of the hydrophobic surfaces; in contrast to that lots of studies suggest using hydrophilic to superhydrophilic surfaces to collect dew and fog (Muselli *et al* 2002; Beysens *et al* 2003; Beysens *et al* 2007; Lekouch *et al* 2010; Comanns *et al* 2011; Lekouch *et al* 2011; Lee *et al* 2012; Beysens *et al* 2013; Azad *et al* 2015b). Moreover, earlier studies (Shirtcliffe *et al* 2009; Lee *et al* 2012; White *et al* 2013) conducted the water transport experiment by spraying water by syringes. However, in this study, the addition of a drip tip at the middle of the bottom edge of the samples reduced the saturation, solved the overflow of the channels and thus improved the drainage efficiency, resulting in the higher fog-collection efficiency. The increase of the efficiency for *Prunus* sample by a drip tip cannot be expected due to the absence of any channels on the surface and/or superhydrophilicity. Thus, the increase was very small. On the other hand, a significant increase of the efficiency by the addition of drip tip for other samples suggests that drip tip would work better only with the channel networks on the surface and with superhydrophilic surfaces.

4.4. Conclusion

The ratio of occupied space to free flow space on a fog collector should be in such a way that fog carrying air can flow without having much resistance and there is enough surface area for droplet deposition. A technical sample, a comb like structure, prepared from copper wires based on the idea of pinnate samples, was found more effective than a

copper foil in collecting fog. Improved results are expected by the further modifications of the copper wire samples, i.e., microstructures on the surface, which will be discussed in the next chapter.

Improved water transport was achieved by directed channels and a drip tip at the bottom edge of the samples. The results indicate an influence of directed channels or grooves as well as wettability of the surfaces on fog collection. Even on superhydrophilic surfaces the channels help improve water transport and consequential collection shown in the results from *Clerodendrum and Gunnera*. A drip tip at the sample surface could help overcome the saturation, resulted from the adhesion of a thick water layer, and improve water transport, resulting in the increase of fog-collection efficiency. The study also found that the trichomes can improve the ability to capture fog droplets continuously as seen on the *Clerodendrum* leaf samples, if the saturation of the surface can be overcome. The saturation of the trichomes influences their long term efficiency. However, stable trichomes (that do not bend because of the mass of water adhered on them but remain erected during fog collection) and a drip tip could optimize the efficiency. Dew collectors are large hydrophilic and/or superhydrophilic plates where transport of water from the surface is an important issue. A system having interconnected channels terminally connected to the large channels as well as drip tips at the bottom edge could also be important for the development of efficient dew collectors.

5. Fog collecting biomimetic surfaces: Influence of microstructure and wettability

(Results and figures presented in this chapter have been published in Azad MAK, Ellerbrok D, Barthlott W and Koch K (2015), Fog collecting biomimetic surfaces: Influence of microstructure and wettability in *Bioinspiration & Biomimetics,* **10** 016004, IOP publishing)

5.1. Introduction

In nature, many biological surfaces possess special functionalities resulting from the presence of unique micro-/nano-structures and their intriguing wetting properties (Hamilton and Seely 1976; Barthlott and Neinhuis 1997; Sun *et al* 2005; Nørgaard and Dacke 2010). Scientists have been experimenting on these naturally evolved principles and functionalities to implement into different technologies, which is known as the biomimetic approach (Rawlings *et al* 2012). Fog collection by the plants to survive in arid condition is one of the principles, which has drawn attention and has been studied for decades. Some important studies have been collectively discussed in a recent review (Malik *et al* 2014).

This chapter focuses on microstructures and wettability of biomimetic surfaces for fog collection. Some studies (Garrod *et al* 2007, Thicket *et al* 2011 and Lee *et al* 2012) compared the water collection efficiency of hydrophilic-hydrophobic patterned surfaces with smooth surfaces. However, in these studies microstructures of the patterned surfaces were of different material than that of the background or smooth surfaces. Therefore, we cannot separate the influence of microstructures versus chemistry on the

collection efficiency. In contrast to that, in this study, the smooth and microstructured surfaces in each set (replica or copper wire) were fabricated with the same material (i.e., only epoxy resin to prepare replicas; hence the surface chemistry was similar). The experimental setup allows the analysis of the influence of both parameters, e.g., chemistry and surface structures on the efficiency of water collection separately. Another relevant parameter that has not yet been addressed was the comparison of the quantity of water collection between smooth and microgrooved technical surfaces that contained consecutive open and occupied spaces in the sample. In the studies of Thicket *et al* (2011) and Lee et *al* (2012) condensation, as opposed to fog collection was investigated. Most importantly, this study showed that polyolefin meshes with a superhydrophilic surface chemistry of the fibers collected a higher amount of water than hydrophilic or hydrophobic meshes. These findings, important and relevant for the development of more efficient fog harvesting devices, have not been previously demonstrated.

Microstructured replicas of the surfaces of *Gunnera* and *Dendrocalamus* leaves were fabricated based on a replication technique (Koch *et al* 2008b). Microgrooves were implemented on copper wire surfaces, and polyolefin mesh surfaces were modified with a hydrophilizing and a hydrophobizing agent.

In this chapter, the fog-collection efficiency of 3 different sets of samples – replica (with and without microstructures), copper wire (smooth and microgrooved) and polyolefin mesh (hydrophilic, superhydrophilic and hydrophobic) were analyzed. The collection efficiency of the samples was compared in each set separately to investigate the influence of microstructures and/or wettability of the surfaces on fog collection. Based on the

chosen controlled experimental conditions, large differences in their efficiencies were found. The experimental setup has been illustrated in **Chapter 3** in **Figure 3.5**.

5.2. Results

The fog-collection efficiency of 3 different sets of samples (1. smooth, papillate and microgrooved replica, 2. smooth and microgrooved copper wires and 3. hydrophilic, hydrophobic and superhydrophilic mesh) was compared separately. Sample from set 1 was not compared with set 2 or 3. For every different set of samples, the parameters were same and hence the influence of fluid dynamics was same for the samples in each set. Collection container did not influence the fluid dynamics of fog flow as the container was placed under the sample where the fog stream was not impeded. The control experiment (without mounting the samples) showed a very negligible (12 ± 5 µl) fog collection in the container. Important findings of the study are described below.

5.2.1. Surface microstructure

Replica: The Scanning electron micrographs (SEMs) (**Figure 5.1a–c**) of the epoxy replicas illustrated the surface microstructures that seemed to contribute to efficient fog collection. The glass replica has smooth surface where as *Gunnera* replica had papillate (technical term convex shape) microstructure and random channels with hairs inside the channel. The height of the papilla is 190–380 µm; the width of the channels is 118 ± 73 µm (mean ± standard deviation) and the depth of the channels is ~200 µm. The length of the cone shaped hairs is 535 ± 362 µm. *Dendrocalamus* replica has a microgrooved

surface. The width of the grooves is 51.75 ± 2.22 µm; the depth of the grooves is approx. 30 µm and the distance between two grooves is 378.35 ± 15.59 µm. The ridges have apexes between two grooves and the distance from the ridge apexes to the grooves is 190 ± 8.2 µm.

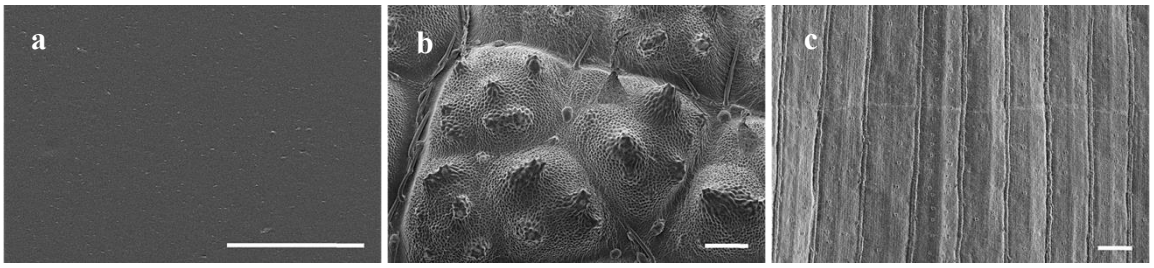

Figure 5.1: Scanning electron micrographs of (a) a smooth surface of a glass replica, scale bar 200 µm; (b) a papillate surface with random channels and hairs inside the channels of *Gunnera* leaf replica, scale bar 300 µm and (c) a microgrooved surface of *Dendrocalamus* leaf replica, scale bar 300 µm.

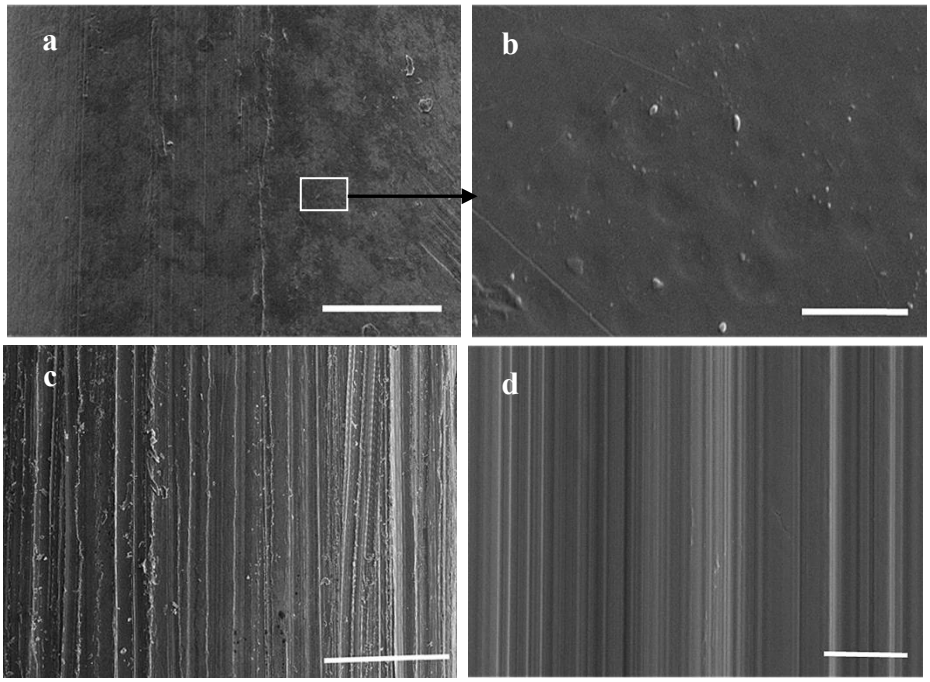

Figure 5.2: Scanning electron micrographs of (a, b) a smooth surface of a copper wire, scale bar 200 µm (a) and 4 µm (b); (c) microgrooved surface, scale bar 200 µm; and (d) sub-microgrooves on the surface of a copper wire, scale bar 5 µm.

Copper wire: One type of sample was prepared by the smooth copper wires (SEMs in **Figure 5.2a–b**) and another type by microgrooved wires (**Figure 5.2c–d**). The

microgrooved wires have microgrooves (**Figure 5.2c**) with the width of 29.68 ± 8.85 µm; and sub-microgrooves (**Figure 5.2d**) with the width of 2–10 µm.

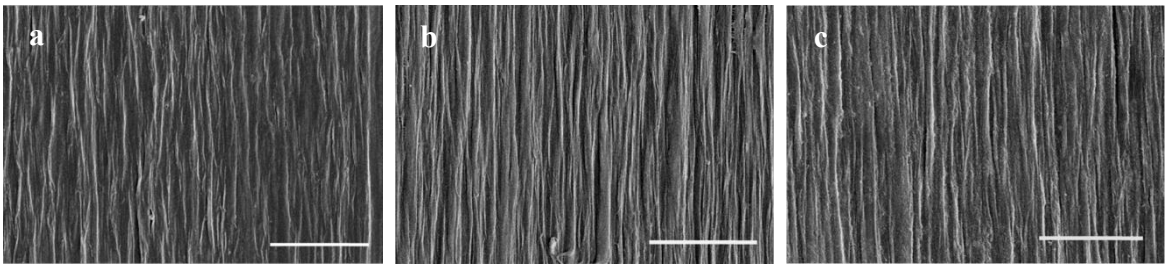

Figure 5.3: Scanning electron micrographs of a ribbon surface of (a) hydrophilic mesh; (b) hydrophobic mesh and (c) superhydrophilic mesh. Scale bar 10 µm.

Polyolefin Raschel mesh: Microscopic analysis showed that there are some channel microstructures on the ribbons of the mesh (**Figure 5.3a–c**). The channels are not continuous from the top to the bottom of the ribbons; the channels discontinue at some random points.

5.2.2. Surface wettability

Table 5.1: Contact angles (CA) of 3 different sets of samples

Sample	Type	Advancing CA (θ_{adv})	Receding CA (θ_{rec})	Contact angle Hysteresis (CAH)	Static CA (θ_{static})
Replica	Smooth	84 ± 2	71 ± 6	13 ± 5	78 ± 5
	Papillate	72 ± 7	55 ± 10	17 ± 5	65 ± 4
	Microgrooved	78 ± 4	65 ± 3	14 ± 1	72 ± 5
Copper wire	Smooth	82 ± 4	57 ± 5	25 ± 5	72 ± 7
	Microgrooved	79 ± 6	58 ± 4	21 ± 6	69 ± 3
Polyolefin mesh	Hydrophilic	97 ± 6	59 ± 5	38 ± 3	80 ± 7
	Hydrophobic	124 ± 4	98 ± 5	26 ± 7	114 ± 4
	Superhydrophilic	-	-	-	5 ± 3

Advancing contact angle (θ_{adv}), receding contact angle (θ_{rec}), contact angle hysteresis (CAH) and static contact angle (θ_{static}) of all 3 different sets of samples are given in **Table 5.1**.

5.2.3. Influence of microstructure

Samples were exposed to artificial fog stream in a fog chamber and their fog collection was quantified over 30 min. Fog stream during the flow while approaching an impermeable, rigid surface (such as replica) changed its direction to get rid of the impedance. Nevertheless, some percentages of total droplets hit the surface and based on the surface microstructure the number of droplet impingement, as well as fog collection varied.

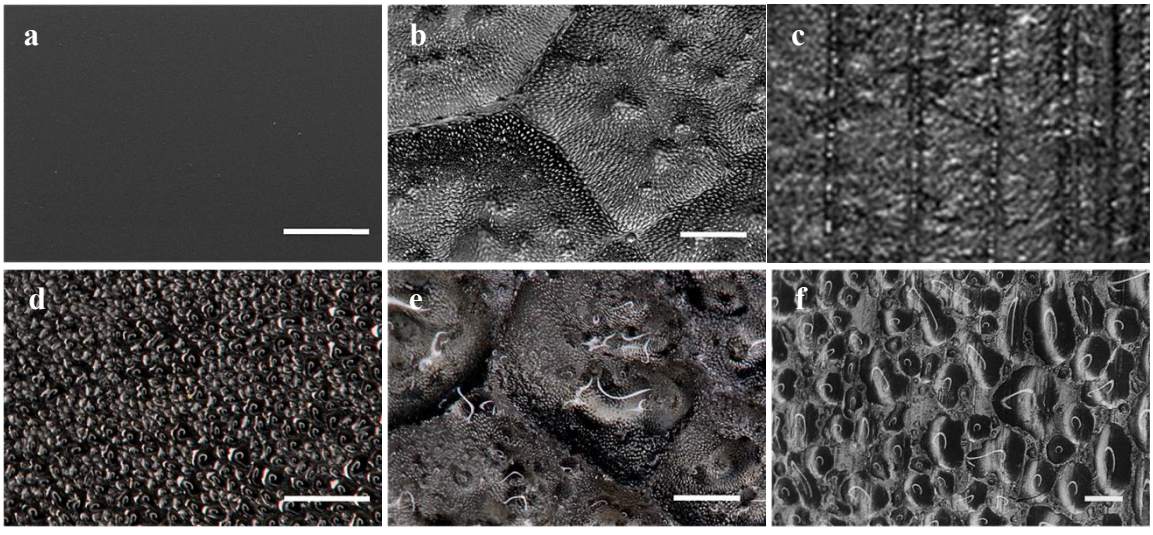

Figure 5.4: (a–c) Images of the dry surfaces before the experiment; (d–f) Images of the surfaces with fog droplets on them after 30 s. (d), (e) and (f) show the comparison of fog droplet deposition on replica surfaces without and with microstructures after 30 s exposure in front of artificial fog stream in the fog chamber. Innumerable fog droplets impinged on the structured surfaces and after coalescence they grew larger as shown in (e) and (f). On the other hand the drop on drop impingement on the smooth surface (d) was less than that of microstructured surfaces by 30 s. Scale bars 500 µm.

Replica: **Figure 5.4a–c** show the dry replica surfaces before the experiment started. In **Figure 5.4d–f** the droplet deposition state on replica surfaces without and with microstructures after 30 s exposure has been shown. On microstructured surfaces innumerable tiny fog droplets were captured, coalesced and grew larger. Consequently, the larger droplets seemed to be ready for moving downwards as the replicas were vertically placed. But on the smooth surface very tiny droplets were seen as the drop on drop impingement as well as coalescence with the neighboring drops was insignificant. That is why large droplets could not be formed over 30 s.

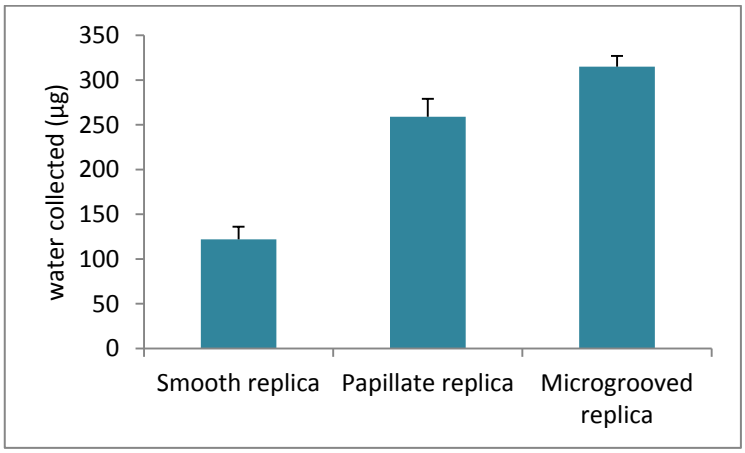

Figure 5.5: Fog collection over 30 min by smooth, papillate and microgrooved replicas (surface area 324 mm^2). $p < 0.001$ indicated that the differences were highly significant for all sample types between each other.

Structured surfaces had an enhanced ability to capture and collect fog droplets with an efficiency > 2 times higher compared to the smooth surfaces. Smooth glass replica collected 122 ± 14 µl of water while *Gunner*a replica with papillate surface collected 259 ± 20 µl and *Dendrocalamus* replica with microgrooved surface collected 315 ± 12 µl of water. Among the three different surface types microgrooved surface had the highest efficiency (**Figure 5.5**). The difference in the fog-collection efficiency was tested by a one-

way ANOVA test (n = 10), and in all cases $p < 0.001$ indicated that the differences were highly significant.

For smooth replica fog collection was the lowest because of the lowest number of droplet impingement. Due to the papillate structures, conical hairy structures and some random channels on *Gunnera* replica, the number of droplets attached was higher than that of smooth surface and hence its fog collection was higher than that of smooth surface. *Dendrocalamus* replica had groovy microstructures directed from the top to the bottom of the replica that improved the ability to capture higher number of droplets and enhanced an effective drainage.

Copper wire: Microgrooved sample collected 1634 ± 73 µl of water while smooth wire sample collected 627 ± 30 µl (**Figure 5.6a**). The difference in the fog-collection efficiency was tested by a paired T-test (n = 10). $p < 0.001$ indicated that the difference was highly significant. The comparison of the onset of dripping of water droplet from the bottom of the smooth and the microgrooved wires is shown in **Figure 5.6b**. The two different, smooth and microgrooved copper wire surfaces showed different behaviors of the fog stream. The smooth surface allowed the fog stream to pass the surface with minimal droplet impingement. In contrast, the microgrooved surface captured many droplets on the sharp corners and over time grew larger from coalescence with the neighboring droplets. After coalescence with the neighboring droplets the droplet shape became more round on smooth wire surface than that on microgrooved surface. They remained attached to the surface unless the droplets grew to the size of capillary length to have an influence of gravity on them (**Figure 5.7a–b**). The experiments were conducted for each sample separately and the flow parameters remained the same.

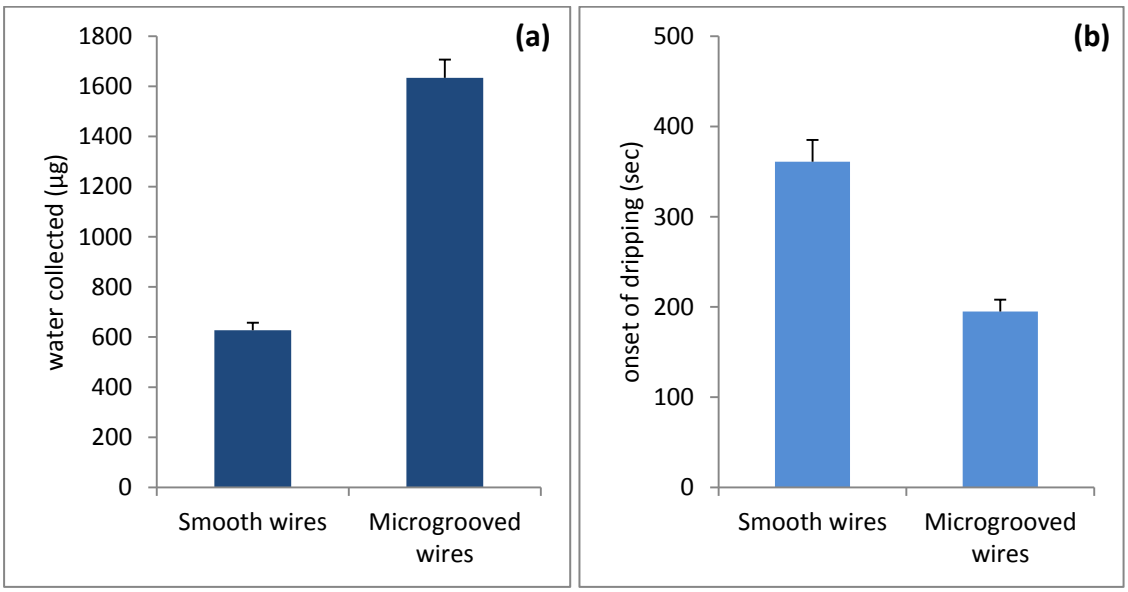

Figure 5.6: (a) Fog collection over 30 min by smooth and microgrooved copper wires (surface area ~471 mm^2). $p < 0.001$ indicated that the difference was highly significant; (b) Comparison of onset of dripping of water droplet from the bottom of the smooth and the microgrooved wires. $p < 0.001$ indicated that the difference was highly significant.

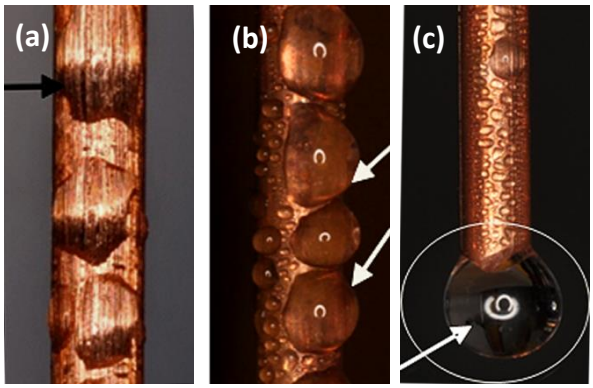

Figure 5.7: (a) Downward movement of fog water collected on the microgrooved surface of the copper wire (marked with a black arrow) due to the capillary force inside the grooves and lower contact angle hysteresis than that of a smooth surface while in (b) droplets (marked with 2 white arrows) were seen to remain stuck on the smooth surface of the copper wire; (c) The hanging droplet (marked with a circle and an arrow) waits for another drop to fall on it along the smooth wire surface to start dripping.

Moreover, the onset of dripping of water droplets from the copper wires was also compared (**Figure 5.6b**), where smooth wires took ~6 min while microgrooved wires took ~3 min. The difference in the onset of dripping was tested by a paired T-test (n = 10). $p < 0.001$ indicated that the difference was highly significant. The drop appeared at the bottom of the smooth wire after ~3 min and the dripping did not start until another accumulated droplet fell on the hanging drop (**Figure 5.7c**). On the contrary, the first drop appeared at the bottom of the grooved wire after 1.8 ± 0.2 min proving that a higher number of fog droplet impingement on the grooved surface than that of the smooth surface; and for dripping to start it is not necessary that another accumulated drop to fall on the first drop at the bottom of the grooved wires. No clogging was observed in the grooved wire sample but in the smooth wire sample because of the large droplets attached in between two adjacent wires.

5.2.4. Influence of wettability

The surface chemistry of the polyolefin meshes was modified to change their wettability and their fog-collection efficiency was compared with that of hydrophilic mesh samples. Superhydrophilic mesh was proven the most efficient (**Figure 5.8**). The amount of collected water by hydrophilic, hydrophobic and superhydrophilic mesh samples was 443 ± 217 µl, 1284 ± 406 µl and 2384 ± 328 µl, respectively. The contact angle of the ribbon surfaces of the meshes, after 30 min exposure to fog stream, had been measured again to make sure that the coating was stable enough during the experiment; on hydrophobized sample the contact angle reduced by ~ 5°, on hydrophilized sample the contact angle increased to 16° ± 11. The difference in the fog-collection efficiency was tested by a one-

way ANOVA test (n = 10), and in all cases $p < 0.001$ indicated that the differences were highly significant.

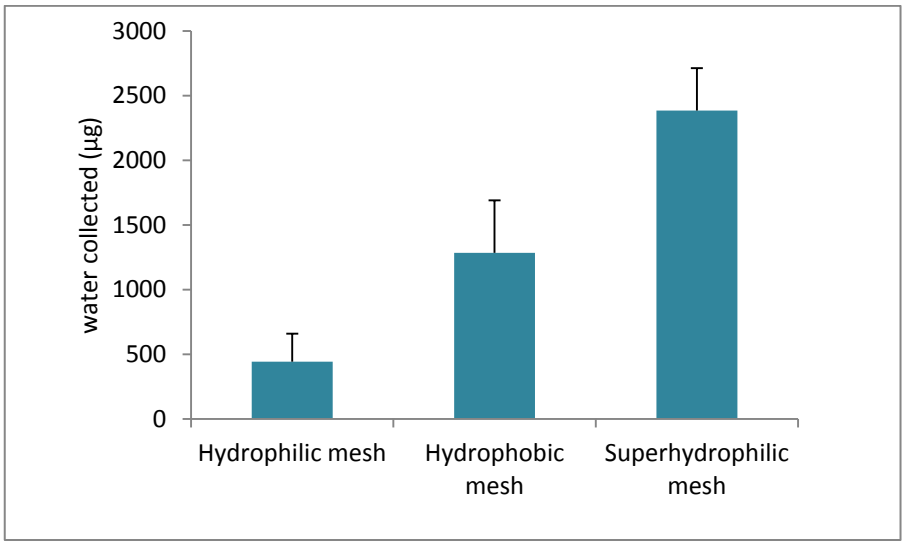

Figure 5.8: Fog collection over 30 min by polyolefin meshes (surface area ~24 cm^2) with different degrees of wettability. $p < 0.001$ indicated that the differences were highly significant for all sample types between each other.

Fog droplets were not impinged much on hydrophobic ribbon surface of the mesh as on superhydrophilic mesh; even the tiny droplets that impacted on the surface did not fuse together as fast as in superhydrophilic surfaces. As a result, every single droplet tended to grow larger until their gravitational force was high enough to overcome the attachment force. Droplets attached on the surfaces and between two adjacent ribbons reduced the open space and consequently hindered the fog flow.

For hydrophilic mesh, the amount of collected fog water was the lowest. Faster dripping rate from superhydrophilic mesh samples clearly indicated that the number of fog droplets from the stream impinging on the superhydrophilic surfaces was very high. Only a continuous flowing film on the surface was seen rather than clogged droplets between

the ribbons. Therefore, the balance between the open and the occupied space in the mesh remained the same, resulting in the minimum blockage of the fog flow.

5.3. Discussion

5.3.1. Influence of microstructure

The results of this study showed that fog-collection efficiency was strongly influenced by the surface structures of the test samples. Several studies showed similar results, i.e., a higher condensation rate of water on patterned surface than smooth surface had been demonstrated from humid air (Thickett *et al* 2011) and mist flow (Garrod *et al* 2007), provided that they (Thicket *et al*) cooled the surfaces below the dew point. Both of the research groups used different materials for every hydrophilic-hydrophobic patterned surface; in contrast, the surfaces with the same material (for replica and copper wires) were used in this study. Compared to the smooth surface, papillate and microgrooved surface may have a thinner boundary layer which enhanced the fog collection (Vogel 1994). The trichomes of *Gunnera* replica were believed to improve the fog collection. The backside of the replicas contained flat glass that had to be used during replication procedure. The size, chemistry and geometry of the backsides of the replica samples did not contribute to fog collection as the surface was impermeable (no open space in the sample). On the other hand, copper wire and polyolefin mesh samples contained consecutive open and occupied spaces and the backsides had the same surface properties as on front sides; hence the backsides contributed in fog collection. Freely moving droplets on a vertically placed surface, i.e., the movement of droplets by capillary force,

coalescence and gravity were considered. The flow from the fog stream may contribute to the kinetics in the system but the flow remained same for all samples.

Numerous studies showed that water drops spread spontaneously on the solid grooved surfaces because the surfaces favor the generation of non-axisymmetric drop flow (anisotropic wettability) on them (Chen *et al* 2005; Sommers and Jacobi 2006; Chung *et al* 2007; Kusumaatmaja *et al* 2008). Similar results were found in the current study. Tiny water drops were observed to penetrate inside the microgrooves. Consequently thin water filaments along the grooves developed and advanced towards the tip of the vertically oriented wires. Similar liquid filaments were reported in earlier studies (Kannan and Sivakumar 2008b; Kannan *et al* 2011). The lamella front of the continuously impacted droplets, as well as the large drops, was believed to have sufficient momentum to push the liquid in the grooves, so that the water filaments ran until the end facilitating faster dripping. Bussmann *et al* 2000 indicated that this is caused by the surface asperities. Due to this fingering or filament formation on the grooved surface the water drops exist in a collapse state and anisotropic wetting was observed. That's why the contact angle in the direction parallel to the grooves was lower even though the surface roughness increased (Bliznyuk *et al* 2011; Xia *et al* 2012). The droplets that grew large enough started to move downward along the edge of the grooves as it is energetically more advantageous (Kannan and Sivakumar 2008a); provided that the contact angle hysteresis of the microgrooved wire surface was 4° less than that of smooth wire surface. The water from the flowing film and/or the water through the narrow grooves due to the capillary flow along with the gravitational force accelerated the dripping. Roth-Nebelsick *et al* 2012) also demonstrated hanging droplets far away from each other on a

quadrilobal filament and they mentioned that very small droplets disappeared in the furrows of the grooves. Therefore, the groove-corners enhanced the impingement of a large number of droplets from the fog stream and the grooves themselves facilitated an effective drainage.

5.3.2. Influence of wettability

Capturing of small droplets as well as, their transportation is highly expected for a continuous and efficient collection (Bai *et al* 2012; Bai *et al* 2011), that is what had been achieved by superhydrophilic surface property on the mesh. Garrod *et al* 2007) showed that the hydrophobic (e.g., $\theta_{adv}/\theta_{rec}$ = 126°/113°) and superhydrophobic surfaces (e.g., $\theta_{adv}/\theta_{rec}$ = 154°/152°) collected more water than hydrophilic (e.g., $\theta_{adv}/\theta_{rec}$ = 86°/75°) surfaces. This study showed the similar result in case of hydrophilic (e.g., $\theta_{adv}/\theta_{rec}$ = 97°/59°) and hydrophobic (e.g., $\theta_{adv}/\theta_{rec}$ = 124°/98°) mesh samples. Moreover, the efficiency of superhydrophilic (e.g., θ_{static} = 5°) mesh samples was compared with hydrophilic and hydrophobic samples and it could be demonstrated that superhydrophilic surface property improved the fog-collection efficiency than hydrophobic surfaces. This finding is in agreement with the earlier study (Lee *et al* 2012) that demonstrated that superhydrophilic surfaces were more effective than uniformly hydrophobic or hydrophilic-hydrophobic patterned surfaces. They also mentioned a higher condensation rate (not studied here) on superhydrophilic surfaces than that of hydrophobic and superhydrophobic surfaces. Another recent study (Ju *et al* 2013) demonstrated that the droplet growth rate on hydrophobic conical wire was higher than that of hydrophilic one but the transport velocity was much lower (about 2.5 times lower). In contrast, Bai *et al*

(2014) described that the superhydrophilic area of a patterned surface with different wettability enhanced droplets capture but their transport was hindered due to the patterns. Consequently, the fog-collection efficiency of the superhydrophilic surface was lower than superhydrophobic surface. Park *et al* 2013) demonstrated the re-entrainment of the droplets from superhydrophobic surfaces. Therefore, the surface has to have enough adhesion force to capture the droplets from fog stream and simultaneously the droplets captured on the surface have to be transported to the bottom of the vertically oriented ribbons of the mesh. Superhydrophilicity offered the highest affinity for tiny fog droplets to impinge on the surface (Bai *et al* 2014), as well as fast spreading. On the other hand hydrophobic surfaces had lower affinity but the droplets captured on them rolled off. The surface of the hydrophilic mesh had a higher affinity than hydrophobic surfaces but the transportation on them was the lowest. Therefore, the droplets attached on them neither spread nor rolled off easily (Park *et al* 2013). Usually a water droplet, to be moved on a solid surface by gravitational force, has to have a critical size larger than the capillary length (Gennes *et al* 2004). The disadvantage of the large droplets during fog collection is the hindrance in fog-collection cycle and clogging. Hence, they inhibited the rebirth of the fog-collection cycle and re-evaporation was supposed to happen (Bai *et al* 2011). Consequently, the overall efficiency of fog collection would decrease. These clarified the reason for the highest fog-collection efficiency of superhydrophilic mesh and the lowest for the hydrophilic mesh.

5.4. Conclusion

Microstructure and wettability are very important factors to be considered during designing efficient biomimetic fog collecting systems. Both microstructure and superhydrophilicity enhanced droplet impingement from the fog stream, as well as effective transport of collected water. Consequently, the rebirth of the fog-collection cycle continued and the efficiency increased. Polyolefin meshes, which have been being used to collect fog for last few decades (Schemenauer and Cereceda 1994b; Shanyengana *et al* 2003), can be modified with superhydrophilic surface property to improve their fog-collection efficiency. The results of the study can be materialized to develop an efficient fog collector.

6. Hierarchical surface architecture of plants as an inspiration for biomimetic fog collectors

(Main results and figures (except Figure 6.9) presented in this chapter have been published in Azad MAK, Barthlott W and Koch K (2015), Hierarchical surface architecture of plants as an inspiration for biomimetic fog collectors in *Langmuir*, 31, 13172-13179, ACS publications)

6.1. Introduction

Fog collectors can enable us to alleviate the water crisis in certain arid regions of the world. In the last few decades the only technology for collecting fog has been large fog collectors (LFCs) made of polyolefin mesh; it has been used in 40 countries in South America, Europe, Africa and Asia where suitable persistent fog is present (Schemenauer and Cereceda 1991, 1994b; Klemm *et al* 2012). With the aim to increase the amount of fog collection, a multi-funnel fog collector has been proposed (Holmes *et al* 2015) Although the simulations showed that the multi-funnel fog collector is more efficient than the old design of the LFC, the design can be further improved by using elements based on the hierarchical architectures of plants. Inspired by the cactus spine (Ju *et al* 2012), conical copper (Ju *et al* 2013) and zinc-oxide (Heng *et al* 2014) wire, and fog collecting impermeable surfaces with cone arrays (Ju *et al* 2012; Cao *et al* 2014; Ju *et al* 2014) have been demonstrated. Though the cone arrays were proved highly efficient for a continuous

fog collection, there were not enough indications in these publications how the structures can be implemented to build a large fog collector, with one exception (Ju *et al* 2012) where the proposed prototype surface lacks free flow (or open) spaces that may result in the hindrance of the fog carrying air to flow. The fog carrying air has the tendency to deviate the direction while approaching an impermeable obstacle. This is why fog collectors, or effective fog collecting trees, have an open structure with collecting surfaces a millimeter or less wide. Therefore, a mesh-like structure with a continuous fog collecting ability is proposed as a viable solution. A continuous fog-collection cycle consisting of a persistent capture of fog droplets and their fast transport to the target is a prerequisite for developing an efficient fog collector. In regard to this topic, a biological superior design has been found in the hierarchical surface architecture of barley (*Hordeum vulgare*) awns. The barbed (barb = conical structure) dry hydrophilized (DH) (advancing contact angle 16° ± 2.7 and receding contact angle 9° ± 2.6) awn of *Hordeum vulgare* (barely) is demonstrated here as a model to develop optimized fog collectors based on a high fog capturing capability and an effective water transport. The hierarchical architecture of the plant species also provides a solution of the problem of the clogging of fog droplets observed in an earlier study (Park *et al* 2013). It should be noted that, when the droplets, attached to the fiber surfaces of a mesh or net, block the open space between the fibers and consequently hinder the flow of the fog carrying air, the phenomenon is defined as ‘clogging’. A comparison of fog-collection efficiency between the model samples with and without barbs has been conducted here for the first time.

6.2. Results

6.2.1. Structural characterization of the samples

Structural characteristics of the samples are presented in **Table 6.1**. The awns of *Hordeum* (both DH and fresh) have barbs (conical structure), the leaves of *Sequoiadendron* have barb like conical structures and other samples do not have barbs. *Pinus, Abies, Sequoia* and *Sequoiadendron* have needle shaped leaves which refers to 'needles' (Ns) in **Table 6.1**.

Table 6.1: Structural characterization of plant samples

Sample		Structural characteristics
Barbed awns	*Hordeum* (DH awn)	Width of the awns: 708 ± 113 µm, barb length: 173 ± 26 µm with an apex angle (2α) of 22° ± 3, tilted angle of the barbs with the main axis of the awns: 37° ± 4, distance between two barbs: 370 ± 106 µm on both sides and ~twice in the middle of the awn in some areas and irregular in some other areas.
	Hordeum (Fresh awn)	Width of the awns: 706 ± 108 µm, barb length: 163 ± 21 µm with an apex angle (2α) of 19.4° ± 2.9, tilted angle of the barbs with the main axis of the awns: 31° ± 4, distance between two barbs: 349 ± 107 µm on both sides and ~twice in the middle of the awn in some areas and irregular in some other areas.
Leaves (Ns)	*Pinus*	Width of the Ns: 913 ± 87 µm.
	Abies	Width of the Ns (intact): 1374 ± 100 µm. For the second set of samples, Ns were cut to a width of 717 ± 75 µm.
	Sequoia	Width of the Ns (intact): 2645 ± 175 µm. For the second set of samples, Ns were cut to a width of 814 ± 54 µm.
	Sequoiadendron	Ns have cone like structures on the main axis; diameter of the Ns: 1074 ± 91 µm (**Figure 6.1**).
Leaves (NLSs)	*Tillandsia*	Diameter of the NLSs: 600–1800 µm. For the second set of samples, NLSs with diameter of 600–800 µm were used.

DH: dry hydrophilized, Ns: needles, NLSs: needle like structures

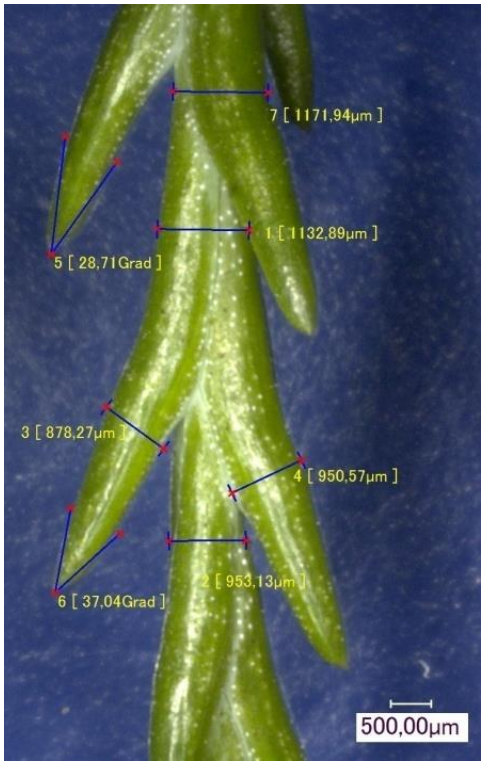

Figure 6.1: Structural characteristics of a leaf of *Sequoiadendron*; cone like structures of varying dimensions are attached to the main axis of the leaf.

6.2.2. Surface microstructures

The awns of *Hordeum*, fresh or dry have similar surface microstructures. A combination of the microstructures of different dimensions result in the hierarchical architecture (Lakes 1993). They have barbs (**Figure 6.2a,b**) on both sides as well as along the mid-section of the awns, and microgrooves on the surfaces of the awns (**Figure 6.2b,c**). Moreover, SEMs in **Figure 6.2b,c** show that the thin coating (~300 nm) of TiO_2 does not fill the microgrooves (groove height 3–3.6 µm). Wax crystals are visible on the hydrophobic surfaces of the leaves of *Abies* and *Sequoiadendron* (**Figure 6.2d,e**).

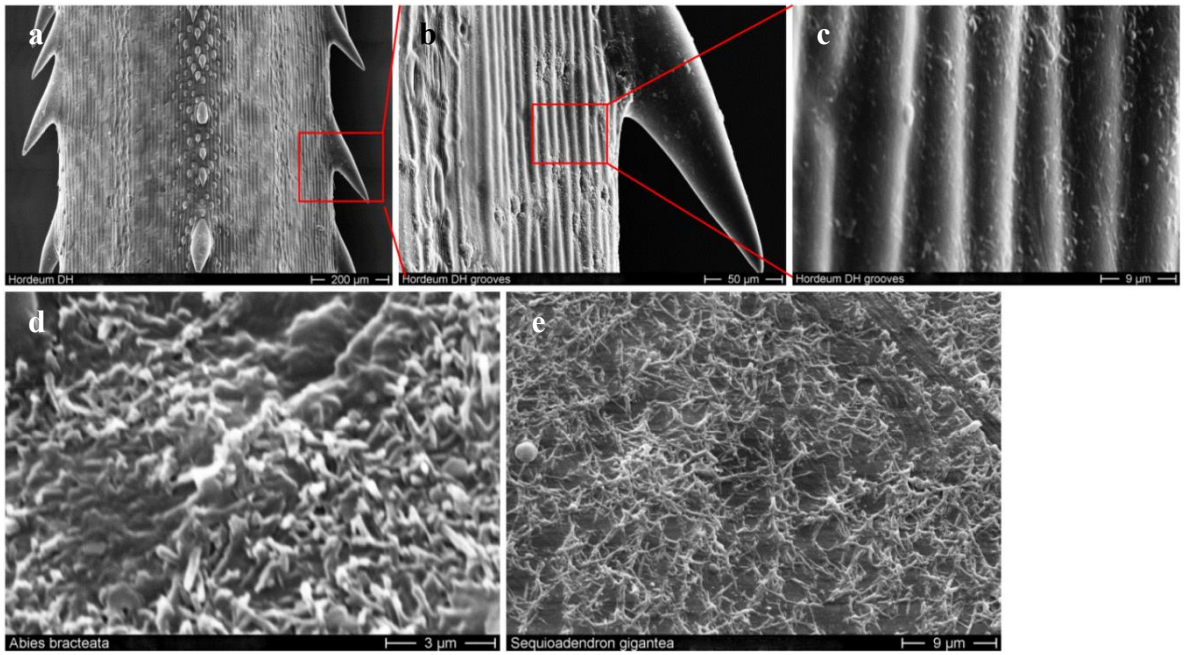

Figure 6.2: Scanning electron micrographs of (a) a DH awn of *Hordeum* shows hierarchical surface architecture; (b) a single barb attached to the microgrooved main axis of the awn; (c) microgrooves of the awn surface; waxy surfaces of the leaves of (d) *Abies* and (e) *Sequoiadendron*.

6.2.3. Surface wettability

The presence of wax crystals on the surfaces of the leaves of *Pinus, Abies*, *Sequoiadendron* etc. (**Figure 6.2**d–e) and a thin wax film on the surface of fresh *Hordeum* awn leads to their hydrophobicity (Neinhuis and Barthlott 1997; Wilhelmi and Barthlott 1997; Stabentheiner *et al* 2004; Koch and Barthlott 2009) as exhibited by the droplet behavior on the surface during the fog-collection experiment (**Figure 6.3a,b**). The degree of wettability of the samples is shown in **Table 6.2**.

Table 6.2: Surface wettability of the samples

Sample	Advancing contact angle (θ_{adv})	Receding contact angle (θ_{rec})	Contact angle hysteresis (CAH)
Hordeum (DH awn)	16 ± 2.7	9 ± 2.6	7 ± 1.8
Hordeum (Fresh awn)	112 ± 2.9	84 ± 3.6	28 ± 1.2
Pinus	114 ± 4	78 ± 5.6	31 ± 6.4
Tillandsia	0	0	-
Abies	120 ± 2.8	94 ± 2.6	25.8 ± 2.4
Sequoia	94 ± 2.7	60 ± 4.5	33.5 ± 4.2
Sequoiadendron	115 ± 7	85 ± 3.9	29.5 ± 5.3

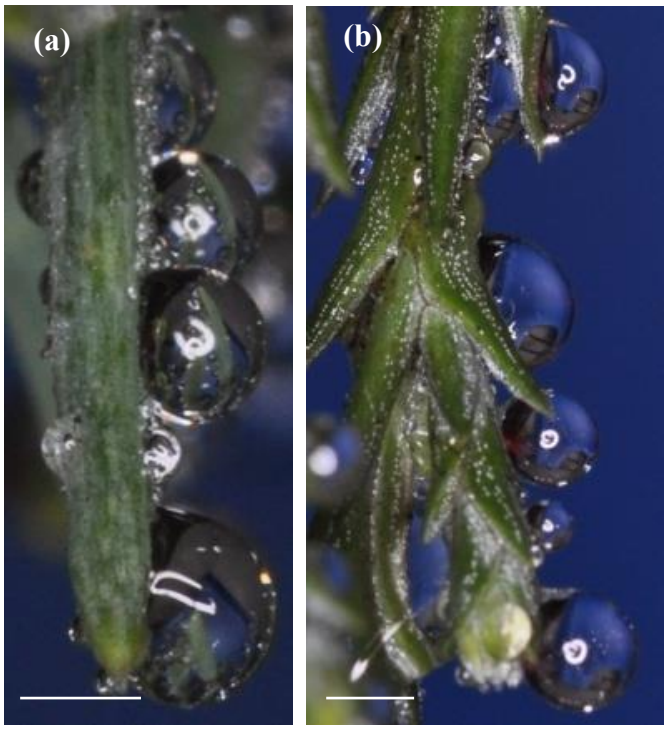

Figure 6.3: Fog droplet behavior on the surfaces of the leaves of (a) *Pinus* and (b) *Sequoiadendron* are shown. Scale bar 1 mm. Droplets remain attached on the surfaces unless large enough to roll off.

6.2.4. Comparison of fog-collection efficiency

Barbed samples were found more effective than the samples without barbs (**Figure 6.4**). Highly wettable (θ_{adv} = 16°±2.7 and θ_{rec} = 9°±2.6) DH awns showed a higher efficiency

than hydrophobic fresh awns (θ_{adv} = 112° ± 2.9 and θ_{rec} = 84° ± 3.6). The efficiency of superhydrophilic (contact angle = 0°) *Tillandsia* was higher than any other hydrophobic samples (see contact angle in **Table 6.2**) and hydrophilic *Sequoia*.

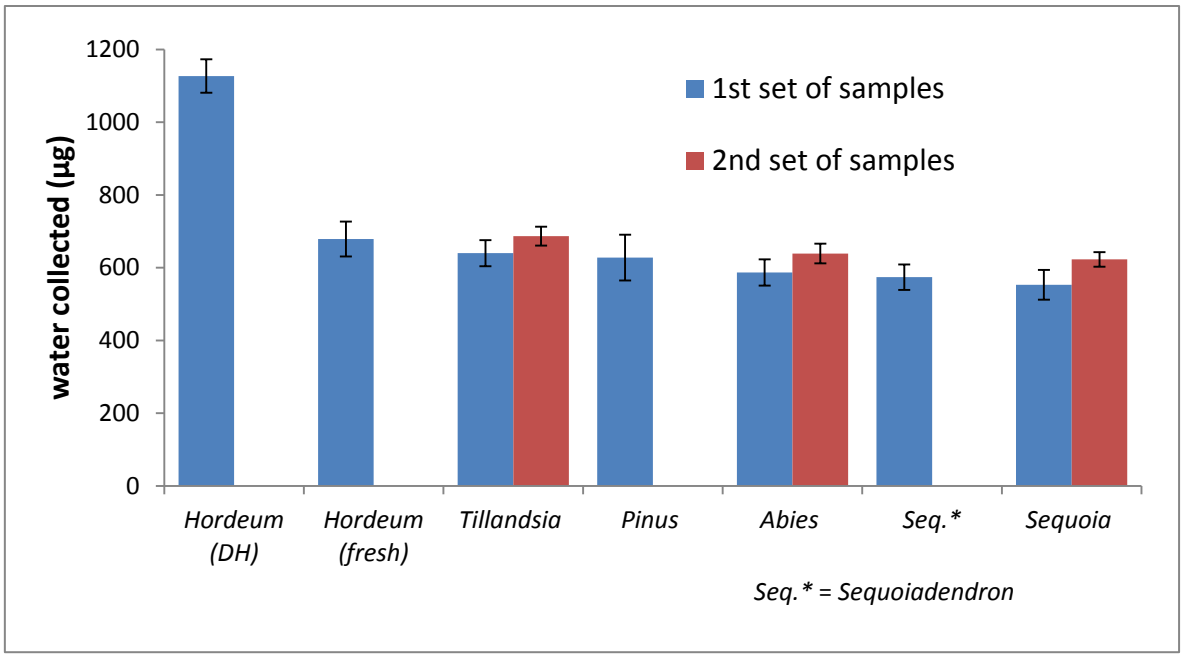

Figure 6.4: Fog collection by samples over 10 min. (In the 1st set of samples intact awns/Ns/leaves were used but diameters/widths of *Tillandsia, Abies* and *Sequoia* leaves were too large as compared to that of *Hordeum* awns. In the 2nd set the width of the Ns of *Abies* and *Sequoia* was reduced by cutting; and *Tillandsia* leaves of smaller diameter were used. Awns/Ns/leaves in each 2x2 cm^2 samples in both sets occupied similar percentage of area and therefore an equivalent effective surface area for fog collection).

Leaves of *Sequoiadendron* and *Sequoia* showed the least efficiency among the samples. DH awns of *Hordeum* were found to be the best among the samples analyzed here. The control experiment (without mounting the samples) showed that 10±4 µl of fog settled down in the container, which is negligible.

Fog collection by the samples with barbs: The mechanism of fog collection on DH awns is shown cycle wise in **Figures 6.5** and **6.6**; **Figure 6.5a–g** represent the first cycle, **Figures 6.5h–l** and **6.5m–o** represent the next cycles of fog droplet capture and transport.

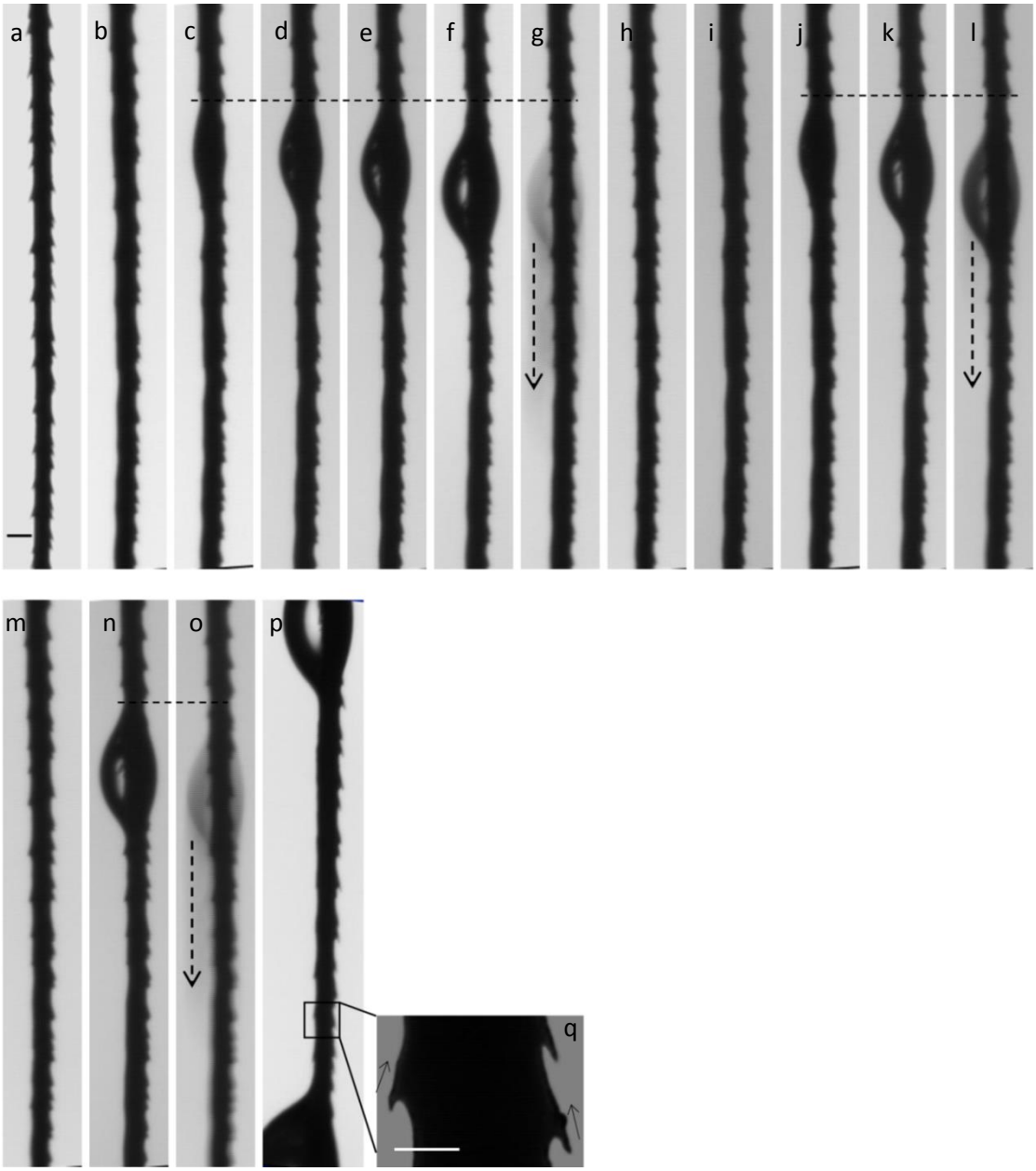

Figure 6.5: Mechanism of fog droplet capture and transport by the DH awns: capture, then coalescence, followed by the transport to the target. The first cycle (a–g) takes about 15–25 s and afterwards every cycle (h–l or m–o) takes 4–10 s, depending on the width of the awns. From (c–f) the droplet is getting larger and (g) shows the downward movement of the droplet. (h–l) or (m-o) shows next similar cycles; (p) two droplets increasing in size, one anywhere in the middle and another at the bottom of the awn; the gap between two droplets forming on the DH awn is also shown; (q) magnified image of a portion of (p) shows the directional movement of fog droplets from the tip to the base of the barbs. Scale bar (a–p) 650 µm; (q) 300 µm.

The droplets that hit the surface, with the exception of the barbs of the awn (DH), spread and/or followed the grooves. A second mechanism occurred when droplets hit the barbs;

in this case, the droplets captured on the barbs moved from the tip to the base. As a direct consequence of the process, an enlargement of a droplet encompassing a tiny area of the awn was observed (**Figure 6.5c–f**). The droplet pulled other adjacent water droplets accumulated at the base of the barbs towards itself. With the increase of the amount of water in the droplet, it moved downward (shown by the horizontal dotted lines in **Figure 6.5c–g,j–l** and **n–o**). The droplets moved to the bottom of the awn, when large enough, (shown by the vertical dotted arrows in **Figure 6.5g,l,o**) after a time frame of between 4 and 25 s. The first cycle of fog collection on the DH awn, starting with drop formation to falling downwards (**Figure 6.5a–g**), took 15–25 s depending on the width of the awns. The subsequent cycles (shown in **Figures 6.5h–l** and **6.5m–o**) took 4–10 s depending on the width of the awns. The cycle continues. Over a length of 2 cm, mostly in one place, rarely in two, the droplet(s) was seen to form and obviously a droplet at the tip (**Figure 6.5p**). A magnified image of a portion of Figure **6.5p** is also shown in **Figure 6.5q** to demonstrate the movement of fog droplets from the tip to the base of the barbs.

Figure 6.6 describes the final collection of water from the bottom of the awns. The droplet moved to the bottom of the awn and there the droplet increased in size (shown in the direction from **Figure 6.6a–d**) by pulling the droplets from the nearby barbs and the surface of the awn, resulting in the formation of a film on the DH awn. Simultaneously, other larger droplets forming continuously anywhere in the middle of the awn were also combining with the droplet at the bottom (the shadow and the arrow in **Figure 6.6e**). Therefore, both the water film flow and the droplets falling from anywhere in the middle of the awn resulted in the enlargement of the droplet at the bottom, as well as continuous dripping every after about 27–58 s from the bottom (**Figure 6.6f**).

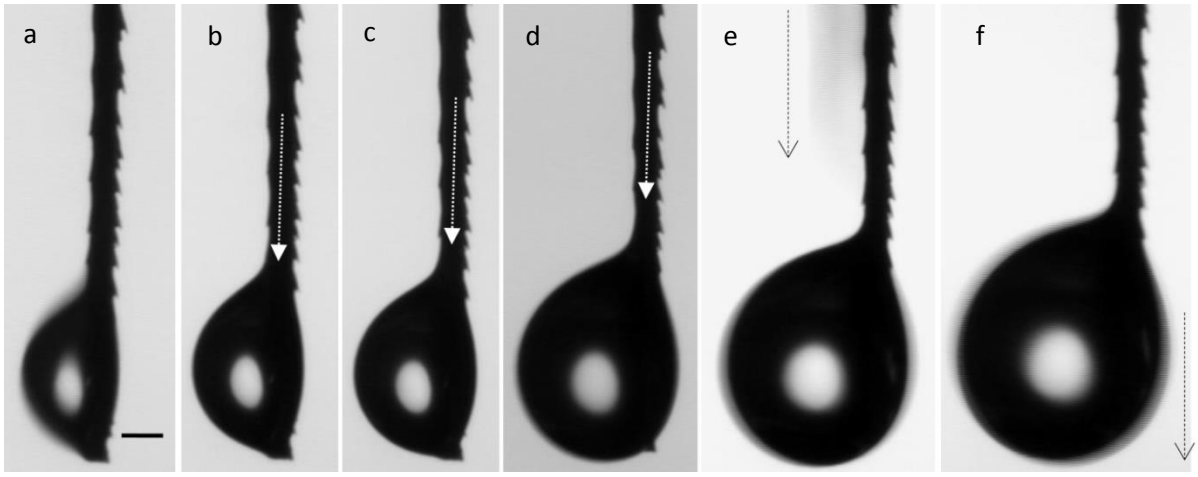

Figure 6.6: Size of the droplet at the bottom is increasing over time (a–d). It pulls the water film on the awn. Hence, the fog droplets captured by all the barbs above are moving downwards with the film (shown by the white arrows in b–d). Another drop anywhere from the middle of the awn moving downward (shadow can be seen) shown by the arrow (e); droplet about to start dripping shown by the arrow (f); scale bar 1 mm.

The hydrophobic awns did not have an efficient capture of fog droplets because of the saturation of the barbs due to the accumulation of water at their bases (**Figure 6.7a**).

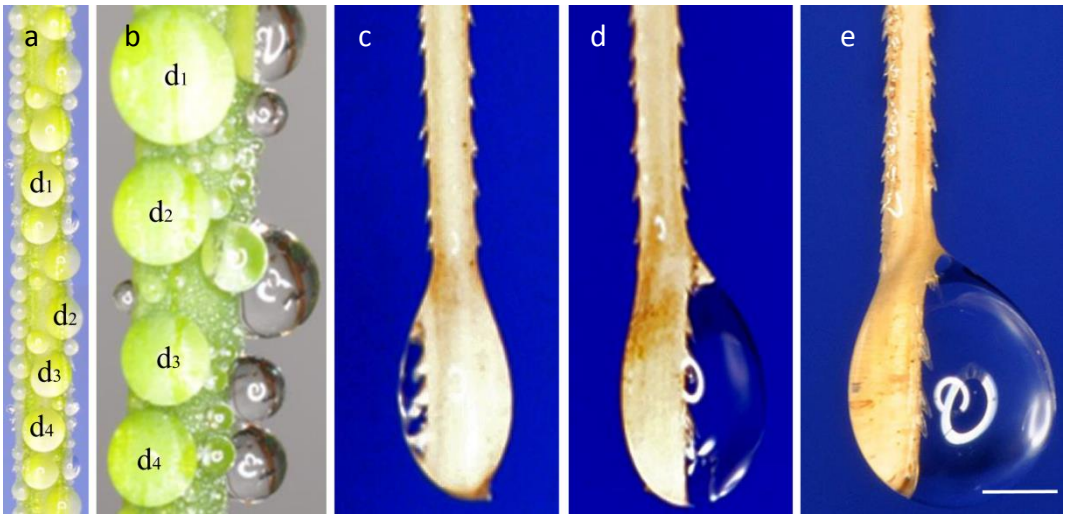

Figure 6.7: Fog droplet behavior on a fresh hydrophobic awn of *Hordeum* (a); hydrophobic needle shaped leaves of *Abies* (b). Fog droplet behavior on the DH awn at different moments during fog collection; after (c) 30 s, (d) 60 s and (e) 90 s, free barbs are seen on both sides of the awns. Scale bar 1 mm.

However, in some instances it was observed that when a large droplet from the top fell down it hit other droplets on the way, leading to a cascade where the droplets further down the awn fell down together. Only then can a new cycle start on the awns (especially

on the barbs). The accumulated water at the bases of the barbs covered the barbs (**Figure 6.7a**) and reduced the fog droplet capture by those barbs. For convenience, we name the 4 larger droplets on the awn/needle (**Figure 6.7a,b**) d_1, d_2, d_3 and d_4 from the top to the bottom, respectively. If d_1 falls first it will collect other droplets available on its way down. Similar results were seen for d_2 and d_3; logically d_4 cannot influence the downward movement of d_1, d_2 and d_3. In contrast, DH barbs followed a continuous fog-collection cycle as they were never saturated (**Figures 6.5, 6.6 and 6.7c–e**) at their bases. Due to a film formation there was an overall influence of the fog droplets on the DH awns. Droplets captured on the barbs (DH awn) were subsequently transported to the base of the barbs followed by the transport downwards (observed and documented by the CCD camera). No droplets were seen attached on the sides of the awns (observed and documented by the CCD camera and a camera with Nikor medical lens). Even the film on the surface was not thick enough (**Figures 6.5, 6.6 and 6.7c–e**) to reduce the free flow space between two awns because the film was continuously flowing downwards due to the grooves directed from the top to the bottom and due to the gravitational force as well. Other orientations of the awns, e.g., horizontal, upward orientation etc. resulted in a lower transport of water. Thus, a reduced efficiency was observed.

For 50% coverage of the sample of DH awns, no clogging was observed except at the bottom for a short time due to the fast transport of the tiny droplets from the tips of the barbs to their bases, followed by the downward movement. Even if we increased the coverage by DH awns to about 65%, we did not observe any clogging, with the exception of at the bottom for a short period of time.

Fog collection by the samples without barbs: After 2–5 min of effective fog capture by *Tillandsia* leaves (NLSs), the trichomes were saturated (**Figure 6.8**) and remained attached

to the leaf. Consequently, during the last half (5 min) of fog flow duration, the dripping of water from the samples reduced. Nevertheless, due to their superhydrophilic trichomes (Koch and Barthlott 2009**)** on the leaves, they showed moderate fog-collection efficiency (**Figure 6.4**). It is to be noted that, the amount of water remaining on the surface was less than those of the hydrophobic samples, e.g., *Hordeum* (fresh awn), *Abies* etc. but one of the highest among all the samples due to their absorption of water in *Tillandsia*.

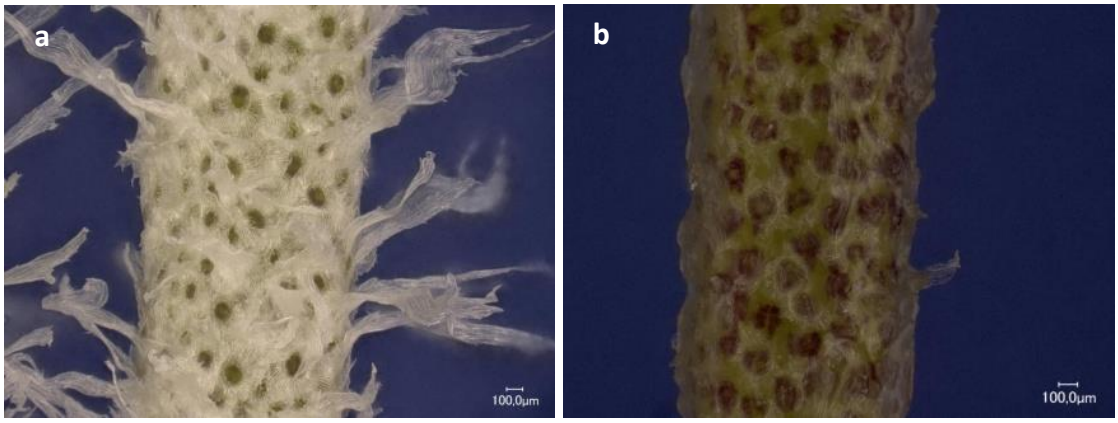

Figure 6.8: (a) A dry leaf (needle like structure (NLS)) of *Tillandsia* shows trichomes all around it; (b) a wet and saturated leaf after a few minutes of fog collection. The trichomes are seen to attach the surface of the main axis.

Droplets remained pinned to the surfaces of *Abies, Pinus* and *Sequoiadendron* (**Figures 6.7b** and **6.3a,b**) until they were large enough to be dominated by the gravitational force, which is consistent with the contact angle and CAH (**Table 6.2**) of the surfaces. The illustration of the droplet behavior of one example *Abies* is shown in **Figure 6.7b**. It showed similar droplet behavior to that of the hydrophobic *Hordeum* awn. *Pinus* also showed similar behavior (**Figure 6.3a**), but the droplets on the leaves were more elongated than those of *Abies* and *Sequoiadendron* due to higher CAH and the presence of microgrooves. The droplets attached elongated after getting larger and fused with similar droplets forming a thick film on the hydrophilic leaves (see contact angle and CAH in **Table 6.2**) of *Sequoia.*

In the second set of samples, the diameter of *Sequoia* and *Abies* needles/leaves was reduced by cutting them. This resulted in the increase of the sharpness and surface area of the edges of the leaves. *Tillandsia* NLSs of smaller diameter (**Table 6.1**) was also used. Though the effective surface area occupied by the Ns/NLSs remained the same (50–55% coverage), their fog collection increased by 7–13% (*Tillandsia* 7.3%, *Abies* 9%, *Sequoia* 12.6%). Despite the increase, only *Tillandsia* from them could reach the efficiency comparable to the barbed *Hordeum* awn (fresh), but it was still only about 60% of the efficiency of DH awns. However, the efficiency of *Tillandsia* decreased over time due to the saturation of the whole NLSs, and therefore there were no free trichomes to capture fog droplets after a few minutes. Moreover, a drastic decrease (**Table 6.1**) of the width of *Sequoia* was a possible cause for a total of 12.6% increase of fog collection (**Figure 6.4**).

6.2.5. Simulation

A simulation was conducted where a water droplet with a diameter of 50µm was applied on the virtually prepared (in the software) microgrooved and smooth surfaces with different wettabilities. The simulation was conducted in cooperation with Prof. Dr. Albert Baars and Leon Danter, Bremen University of Applied Sciences, Germany. An aspect ratio (depth to width) of 0.8 was used for the grooves, which is comparable to the aspect ratio of the microgrooves of a DH awn. To be noted rectangular grooves were tested here. The results showed similar surface phenomena observed on the plant samples. The water droplet was observed to spread and enhance the film formation on the microgrooved hydrophilic surface (θ_{adv} = 16° and θ_{rec} = 9°) (**Figure 6.9a**) while on the other experimental surfaces, for example on the hydrophilic smooth surface (**Figure 6.9b**) water spread but to a limited extent; even if the experimental surface was designed in such a way that the

grooves were hydrophilic and the ridges were hydrophobic, the water droplet did not spread all through the grooves (**Figure 6.9c**).

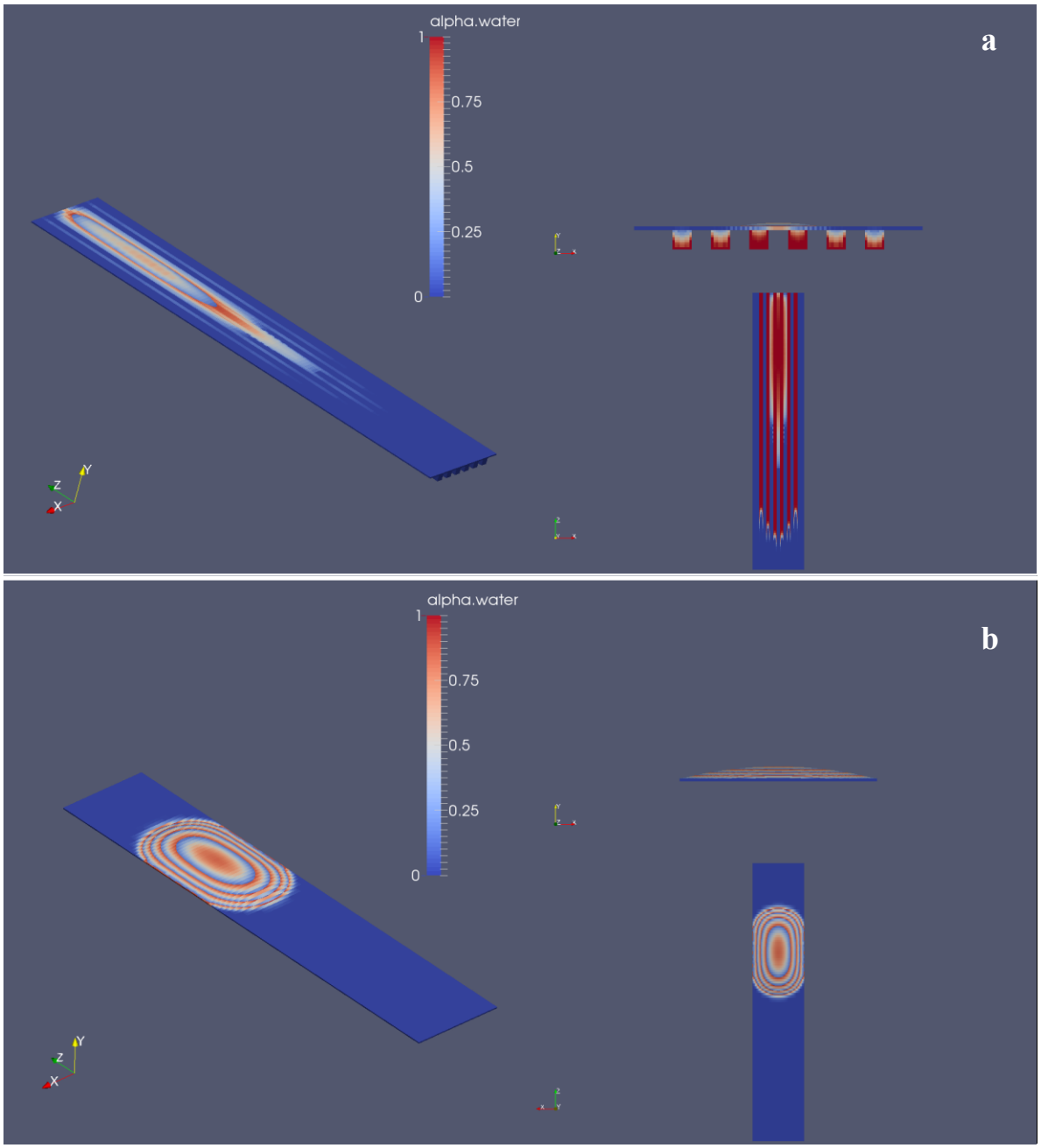

Figure 6.9a–b: Simulation of water droplet behavior on the microgrooved and smooth surfaces with different wettability; (a) microgrooved-hydrophilic surface: water spreads along the microgrooves, (b) smooth hydrophilic surface: water spreads to a very limited extent.

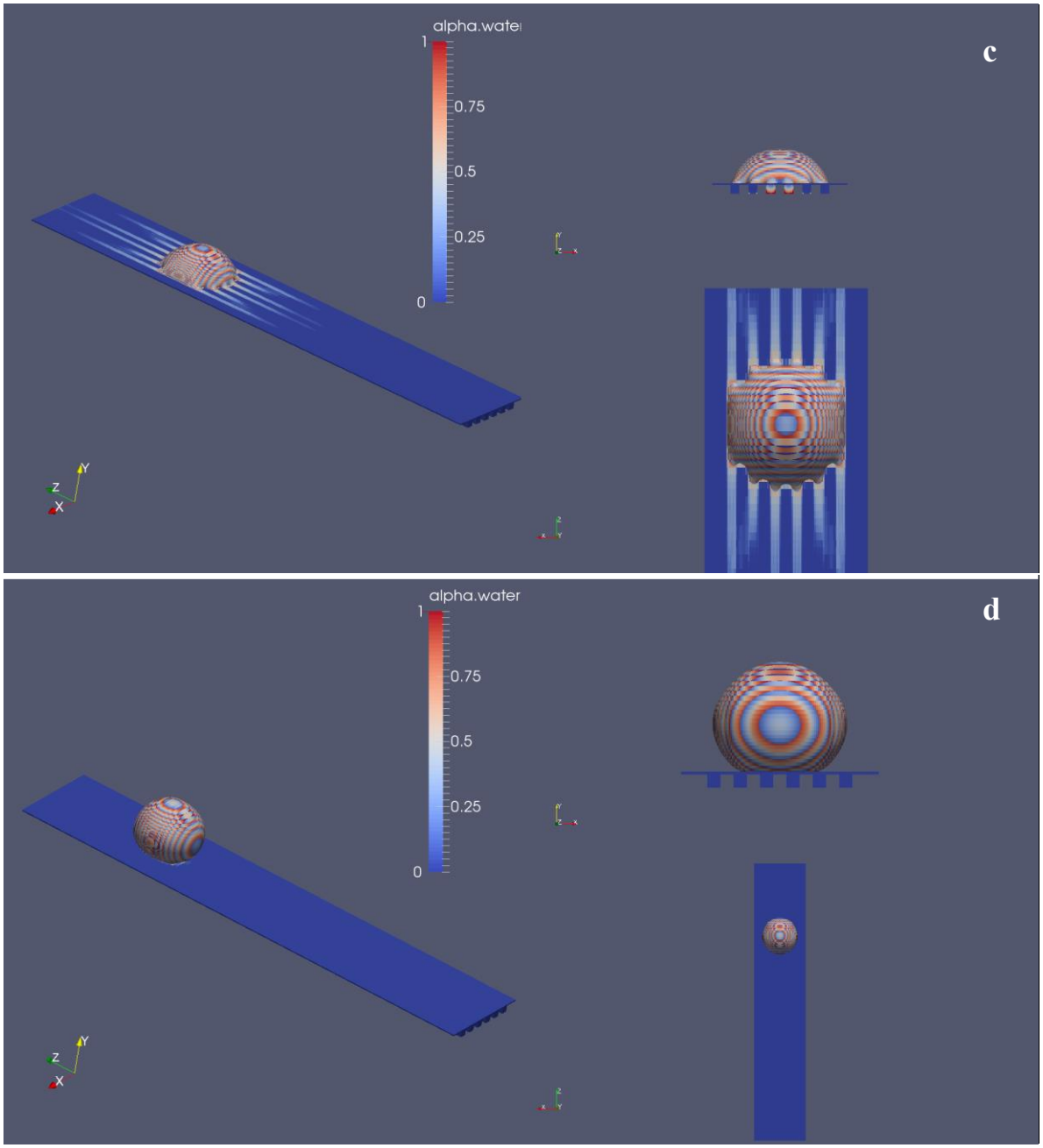

Figure 6.9c–d: Simulation of water droplet behavior on the microgrooved and smooth surfaces with different wettability; (c) hydrophilic grooves and hydrophobic ridges: water spreads along the microgrooves to a limited extent and most of the water of the droplet remains at one place of the sample surface, and (d) microgrooved hydrophobic surface: water droplet remains adhered on the surface.

Moreover, a large part of the water remained attached with the hydrophobic ridges. On the hydrophobic surface water did not spread at all (**Figure 6.9d**), rather the water droplet remained attached to the surface as observed on the hydrophobic fresh awn surface (**Figure 6.7a**).

6.3. Discussion

The size, form and surface structure of the samples where fog droplets can be captured are very important factors in fog collection. The fog droplet carrying air, while approaching an obstacle in front of it, tends to deviate its direction to right or left according to the space available. If the obstacle is a mesh like structure, the edges of the fibers (i.e., the awns or needles of the samples in this study) play a crucial role in capturing fog droplets. Not only the influence of edges of the Ns/NLSs was checked, but their diameters also controlled, as closely as was possible, so that they were comparable in size. The increase in fog collection by the modified samples is caused by the reduced diameter, increase of edge for higher impingement and increase of sharpness and wettability of the edges due to cutting. Despite these measures being taken, the amount of water collected by *Hordeum* (DH) was almost twice as high as any other samples. Here, an effective transport of the water captured played the major role in keeping the barbs free to continuously capture more fog droplets. The efficiency of the DH awns was attributed mainly to the conical shape of the barbs; this generates a Laplace pressure gradient between the two opposite sides of the drop on the barb (Lorenceau and Quéré 2004). It can be described as follows:

$$\Delta P_{barb} = -\int_{R_1}^{R_2} \frac{2\gamma}{(R+R_0)^2} \sin\alpha \, dz$$

where γ is the surface tension of water, R is barb's local radius (**Figure 6.10** shows two local radii (R_1 *and* R_2) of the barb at the two opposite sides of the drop), R_0 is the radius of the drop, α is the half-apex angle of the barb (**Figure 6.10**) and dz is the integration variable.

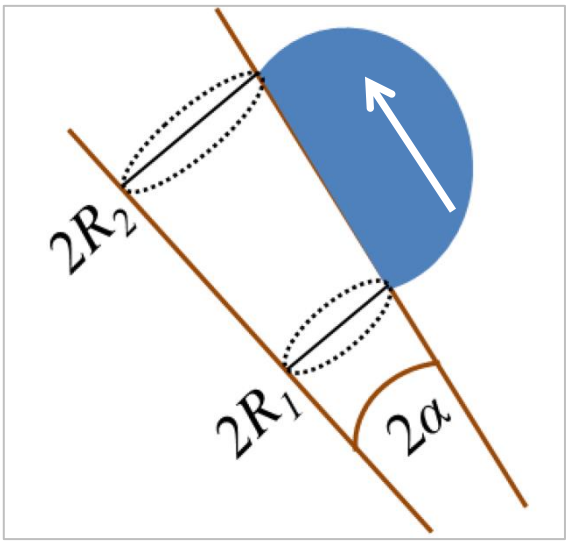

Figure 6.10: A schematic of the movement of a water droplet from the tip to the base of a barb. The region near the tip (radius R_1) of the barb has larger pressure than the base region (radius R_2); thus water droplet moves from higher to lower pressure. The direction of droplet movement is marked by an arrow.

The region near the tip of the barb (region with a smaller radius R_1) has a larger Laplace pressure than that near the base (region with a larger radius R_2). The energy generated from the pressure difference (ΔP_{barb}) drives the droplet to move from the tip to the base of the barb (Ju *et al* 2012).

The combination of higher wettability and barbs on both sides proved to be the major factors for a high capture rate. In the previous study (**Chapter 5**; Azad *et al* 2015b)**,** it was shown that both microstructured and superhydrophilic surfaces have higher capability to capture fog droplets than those of flat and/or hydrophilic or hydrophobic. Due to the influence of morphological differences in the samples, the influence of their wettability on fog-collection efficiency cannot be expected to be exactly similar to the earlier study. However, a higher efficiency of superhydrophilic (θ = 0°) *Tillandsia* than the hydrophobic samples (**Table 6.2**) tends to show a similarity. In case of hydrophobic surfaces, such as the *Hordeum* awns (fresh) and needles of *Abies, Pinus* and *Sequoiadendron* water droplets remained attached on the surfaces (**Figures 6.7a,b** and **6.3a,b**). The droplets that

remained attached on the surfaces hinder the continuous generation of free surfaces resulting in the discontinuous fog-collection cycle (Cao *et al* 2015).

If the amount of water remaining on the hydrophobic samples is deducted, their efficiency would be much lower, i.e., 10–20% lower. It is to be noted that, even after 30 min the amount of water remained on the surface would be the same as it was after 10 minutes, but ultimately the presence of these droplets influence the total amount of fog collection. If only the amount of water collected in the container under the sample is considered, excluding the water remaining on the sample after 10 or 30 min observation, again the DH awn is expected to be the most efficient among the samples investigated, because it retained the lowest amount of water on the sample.

The hydrophilization of the hierarchical architecture of the barbed awn attributed higher wettability of the entire surfaces. Higher wettability of the conical structures, as well as other parts of the awns allowed the droplets to spread. Consequently, the presence of a precursor liquid film on the surface provided a lubrication effect that increased the velocity of the drop motion on the surfaces (Lorenceau and Quéré 2004; Ju *et al* 2013). Nature also provides logic to support it. Many lower plants, such as lichens, mosses etc. and higher plants, such as Bromeliads, epiphytic orchids etc. have evolved superhydrophilic surface property to uptake water (Rauh *et al* 1973; Koch *et al* 2008a; Koch and Barthlott 2009). Moreover, the presence of microgrooves on the surface of the awns improved the downward movement of water. In other words, a faster transport on the surface has been achieved by higher wettability along with the microgrooves (Liu *et al* 2009; Roth-Nebelsick *et al* 2012; Azad *et al* 2015b). The droplets that hit the grooved surface of the awns tend to fuse with neighboring droplets and grow larger. Capillary forces cause the droplets that accumulate at the base of the barbs, to be pulled into the

grooves. Then, their movement is influenced by the energy barrier in different directions. The first thing that helps downward movement is the vertical orientation of the awns. Second thing is the zero energy barrier parallel to the groove direction (Kannan and Sivakumar 2008a). Therefore, the droplets form an elongated filament shape in the aforementioned direction, where it finds another similar source to follow the path till the end and a spontaneous spreading of water along the direction occurs as it gathers sufficient momentum to do so (Chen *et al* 2005; Kannan and Sivakumar 2008b; Kusumaatmaja *et al* 2008; Kannan *et al* 2011) as validated by the simulation (**Figure 6.9a**). Furthermore, during the accumulation of the fog drops on the surfaces (actually condensation) heat transfer is an important issue. Hydrophilic surfaces could be an advantage compared to the hydrophobic surfaces in this respect (Liu *et al* 2009). Therefore, directional microgrooved surfaces with higher wettability enhance the drainage performance along with a high rate of droplet condensation and/or accumulation. To reduce entrainment in fog collection, highly adhesive superhydrophobic surfaces, i.e., peanut leaf surface, have been studied by a research group (Yang *et al* 2014). The surfaces remains occupied with the droplets attached on them unless the droplets have been influenced by the gravitational force. Moreover, this effect would have a negative influence for the hierarchically barbed samples by blocking the barbs.

The meshes with 50% coverage theoretically remove 50% of the droplets approaching them (Schemenauer and Joe 1989). Although, the barbs on the edges of the fibers (as seen on the awn sample) only occupy a low space they can capture a high percentage of the fog droplets that would otherwise be lost if there were no barbs. Park *et al* 2013) showed that clogging would be a problem in hydrophilic meshes. Provided that their samples contained no barbs, and hence the droplets remained attached at the edges of

the fibers resulting in clogging. The clogging observed only at the bottom of the DH awn for a short period of time would not be a problem as it did not hamper the flow of the fog. It should be noted that it is also possible to overcome this problem with design optimization (see **Chapter 9**). Therefore, even superhydrophilic meshes of barbed fibers could solve the clogging problem. Moreover, because of the higher wettability, the droplets captured on the surface of the awns could not be blown away by the air what has been shown a major problem for the superhydrophobic surface of the mesh during fog collection (Park *et al* 2013). Thus, the superhydrophilic surface property also would nullify the possibility of re-entrainment (loss of captured droplets by the air). Due to adequate adhesion at hydrophobic surfaces (a function of CA and CAH; see **Table 6.2**) there is no possibility of entrainment from the hydrophobic samples (not superhydrophobic) used here (Yang *et al* 2014).

6.4. Conclusion

An approach to improve the efficiency of biomimetic fog collectors was discussed in this study. A potential design (described in **Chapter 9)** based on the hierarchical architecture of the model sample can be proposed to fabricate meshes with hierarchical architecture by using inexpensive materials for the target user of people in poor communities in water deficient dry areas. With the new design, fog droplet capturing could be optimized, clogging and re-entrainment problems could be solved and transport of water along the fog collector can be greatly improved. Therefore, the investigation of fog collection on the hierarchical, barbed surface architecture may open new possibilities to develop highly efficient fog collectors.

7. Trichomes of *Ptilotus manglesii*: An integrated system for efficient fog collection

7.1 Introduction

Fog collection on microstructured plant surfaces including the model sample, dry hydrophilized awn of *Hordeum* (barely), has been analyzed and presented in Chapter 6. However, nodose/knotty trichomes of *Ptilotus manglesii* (Family: Amaranthaceae) is another potential model plant sample. Most of the species of the genus occur in arid Western Australia (Hammer *et al* 2015). The plant inhabits the sandy land in the eastern Swan Coastal Plain, Western Australia (Davis and Tauss 2011). It is presented in this chapter separately since it is too tiny to prepare a 2x2 cm^2 sample to compare it with other samples treated in **Chapter 6**.

A *Ptilotus* plant with flowers, and a flower with the trichomes attached on the petals are shown in **Figure 7.1**a-b. The species usually commences flowering at the end of October when the soil is very dry (Davis and Tauss 2011). Most probably, then their trichomes help collect moisture from the environment. Physical characteristics of the trichromes and their fog collection have been analyzed here. A possible fog-collection mechanism is also proposed.

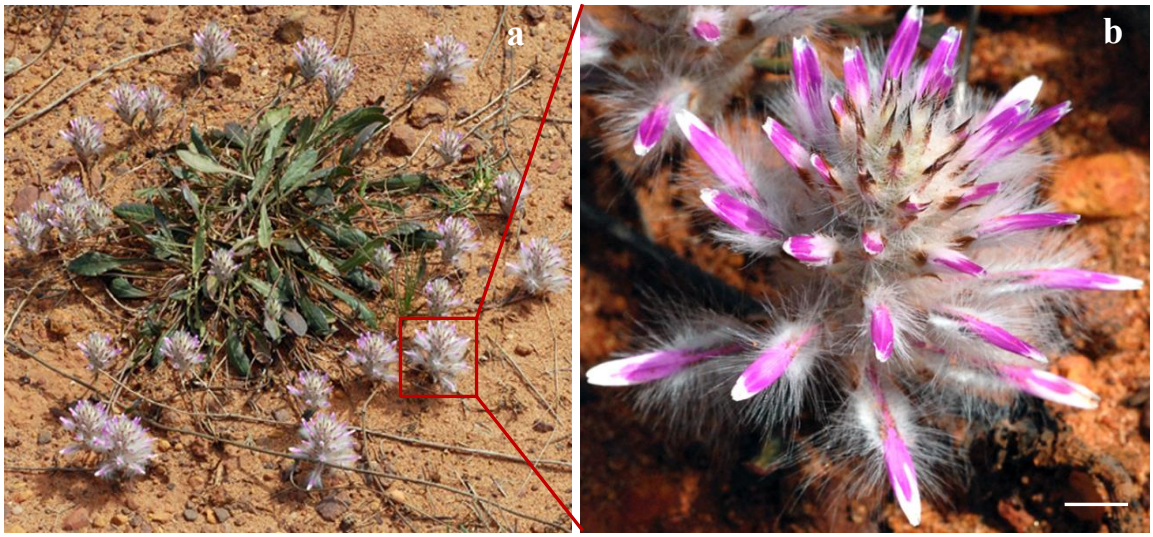

Figure 7.1: (a) A *Ptilotus* plant with flowers grown in a sandy land, (b) a flower with trichomes on both sides of petals Scale bar: 5 mm. (Photo credit: ukwildflowers.com).

7.2. Results and discussion

7.2.1. Characterization of trichomes

Dense, long multi-cellular trichomes (6–9 mm) are attached on the petals of the flowers. The trichomes have sharp tips and a very low gradual increase of the diameter of the trichomes from the tip to the base (**Figure 7.2a**). Cone shaped tiny structures, called barbs, are oriented surrounding the nodes of the trichomes every after a distance of about 149 ± 41 µm (**Figure 7.2b**). Barbs have an average length of about 20–41 µm.

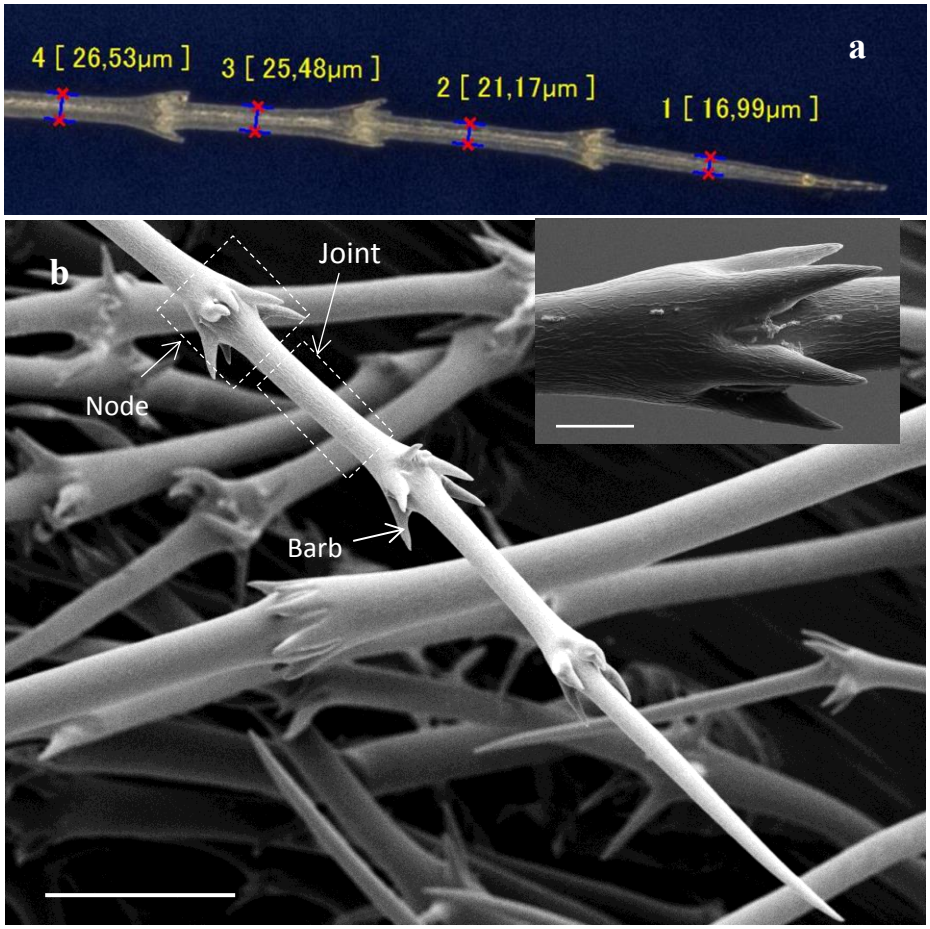

Figure 7.2: (a) An optical micrograph of a *Ptilotus* trichome shows a very low gradual increase of the diameter from the tip to the base, (b) Scanning electron micrograph of the trichomes; barbs, joints and nodes are marked; the inset shows the orientation of the barbs surrounding a node; scale bar: (b) 100 µm and in the inset 20 µm.

7.2.2. Fog collection by trichomes

Barbed and nodose/knotty structures of the trichomes might provide unique fog-collection ability. A petal with dense trichomes when placed in a fog flow, trichmoes captured fog droplets (**Figure 7.3a**) very efficiently. The trichomes were transporting water droplets from the tip to the base (**Figure 7.3a–c**). Every node with the barbs was actively capturing the droplets (nodes with fog droplets were marked with the arrows in

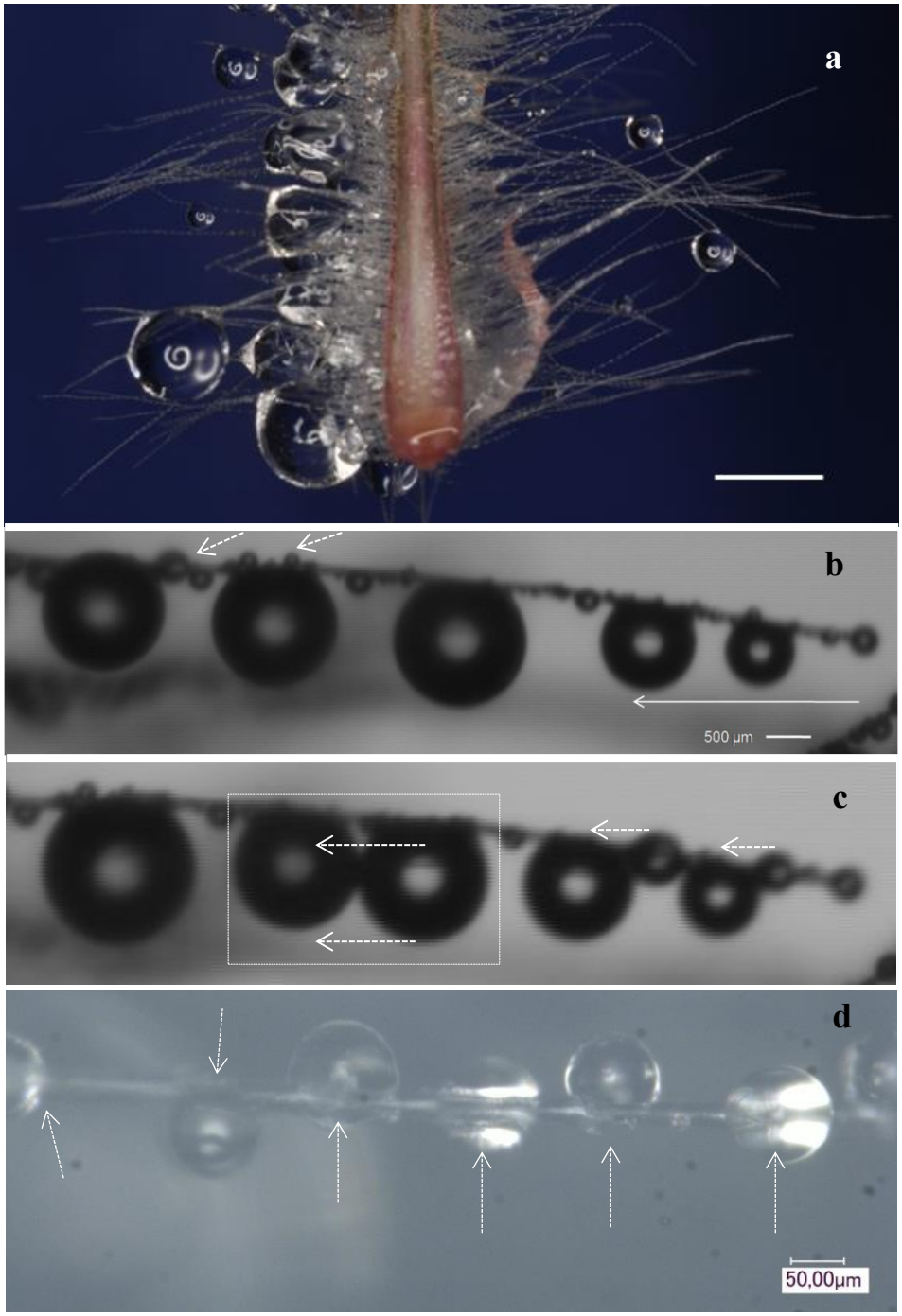

Figure 7.3: Fog collection by (a) a petal with the trichomes (scale bar 3 mm) and (b,c) a trichome of the plant; the movement of water droplet from the tip to the base (marked with the arrows) is visible in both cases, (d) accumulated droplets at the nodes are marked with the arrows (droplets captured by the barbs on the node; droplets moved from joints to nodes).

Figure 7.3d). Similar droplet movement was also happening for the barbs. Droplets were also moving from the joint to the nodes. A detail of the fog-collection process on a

vertically placed trichome is described in **Figure 7.4**. Droplet deposition in the beginning was observed (**Figure 7.4a,b**). The first 5 distinguishable droplets at the tip area were named as 1, 2, 3, 4, and 5. The tiny droplets fused with the neighboring droplets above their position and increased in size (**Figure 7.4c–h**). The movement of the droplets occurred against the gravity. The arrows indicate the direction of the movement of the fog droplets in **Figure 7.4d–h**.

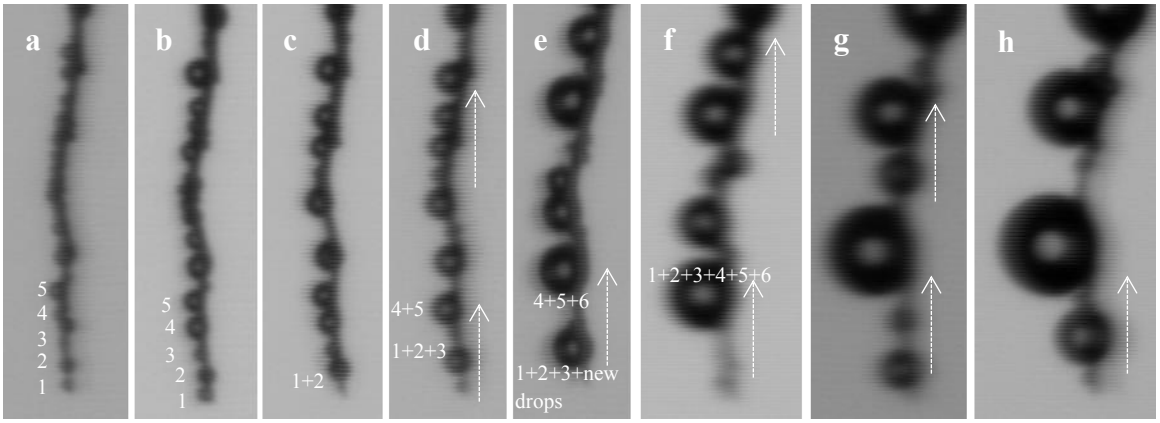

Figure 7.4: Fog-collection process on a vertically placed trichome; (a,b) droplet capture, the droplets are numbered 1–5 at the tip area, (c–h) droplets increasing in size after fusing with the neighboring droplets, droplet movement (marked with the arrows) occurs from the tip to the base against the gravity.

This kind of movement of liquid droplet was first demonstrated on a conical wire by a group of researchers in 2004 (Lorenceau and Quéré 2004) and after that on the spine of *Opuntia microdasys* (Ju *et al* 2012) and on bristle grass (Xue *et al* 2014). Even though the function of the barbs of the trichomes was similar to the barbs of *O. microdasys*, bristle grass and barely awns, there are differences in other structures of the trichomes and over all functional mechanism. The physics behind the movement of the droplets from the tip to the base has already been described in **section 6.3 in Chapter 6.** In short, the gradient of Laplace pressure is the primary reason for the movement (Lorenceau and Quéré 2004; Renvoisé *et al* 2009; Bai *et al* 2010).

The proposed mechanism of the fog-collection process at the joints and node can be illustrated as the following:

Droplet capture (**Figure 7.5a**) → fusion with the neighboring droplets (**Figure 7.5a,b**)→ movement along the Laplace pressure gradient generated from the diameter gradient (on the barb as well as from the joint to the node) (**Figure 7.5a–c**) → droplet accumulation on or under a node (**Figure 7.5b,c**) → large drop hanging underneath a node or in between two nodes (**Figure 7.5c,d**).

The movement was also to a limited distance when the trichome was placed vertically, keeping the tip down (**Figure 7.4**). This is because the movement was against the gravity and a lower dimeter gradient of the trichomes. However, the movement of droplets from the joints to the nodes occurred in all conditions. In their fog collection mechanism the first step was droplet capture. Though the capture of fog droplets was observed on the whole trichomes, a better efficiency was observed on the node (**Figure 7.3d**) surrounded by the barbs, because of their 3-dimensional orientation. The second step was the fusion of the neighboring droplets (**Figure 7.5a,b**). Then the droplets were moving along the Laplace pressure gradient generated from the diameter gradient on the barbs as well as from the joints to the nodes (**Figure 7.5a,b**). There the drops were observed to move either from the tip to the base of the trichomes or to the lower part of the node (**Figure 7.5b**).

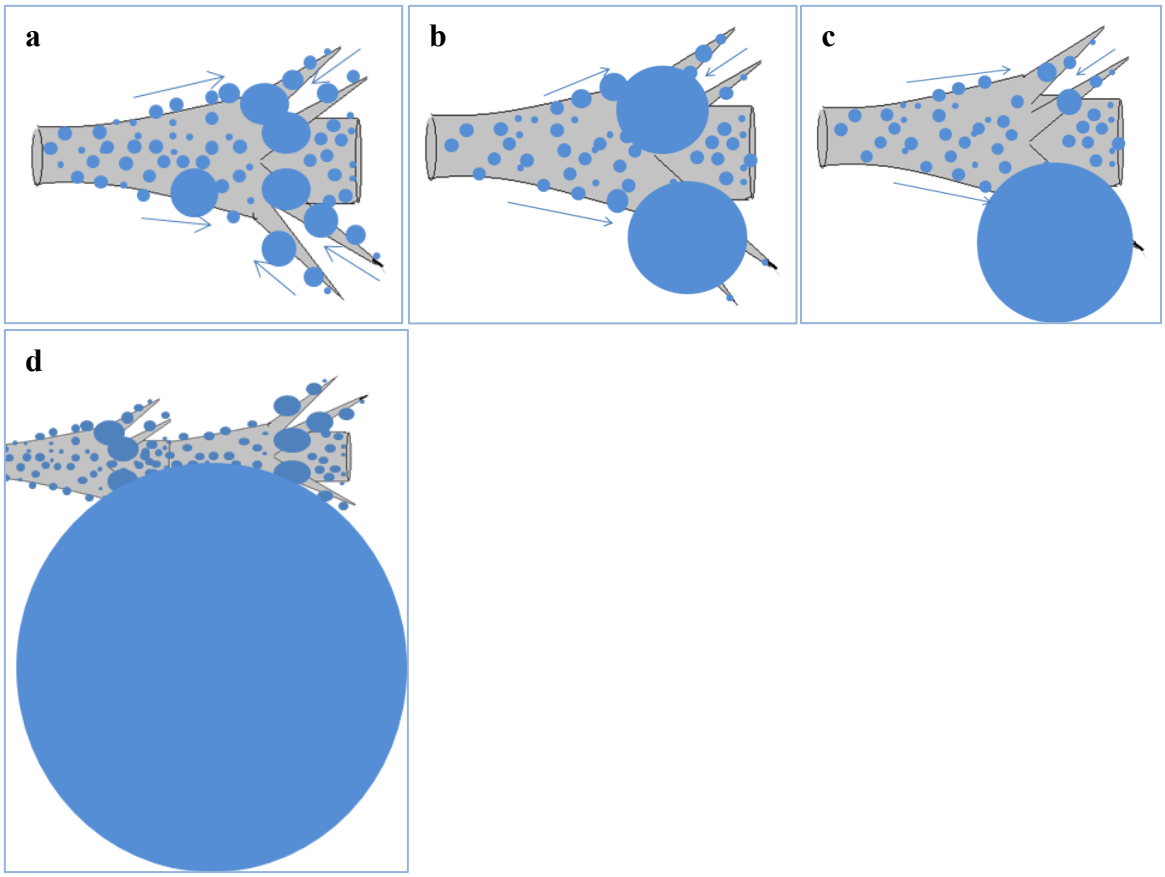

Figure 7.5: A schematic of the proposed fog-collection mechanism of the trichomes, more specifically at the joints and node: (a) droplet capture and movement on the barbs as well as from the joint to node, (b) droplet accumulation on the upper and lower part of the node, (c) fusion of two large droplets into one and finally (d) a large droplet hanging at the joints between two nodes along with the barbs at the lower part of a node.

The determining factors for the movement were the size of nearby droplets and the structure of the droplet's position. If the size of the droplet is smaller than the nearby droplet along the direction from the tip to the base of the trichomes, it moved to the larger droplet. Otherwise, the droplet fused with the droplet at the lower part of the node. Therefore, the 2nd order movement was on the trichomes from the tip to the base along the Laplace pressure gradient generated from the diameter gradient, though this movement became limited if the droplets were large enough to be dominated by the gravitational force (Gennes *et al* 2004).

When a droplet hung under a node remaining attached with the barbs there, other barbs at the node were free to capture new fog droplets (new fog droplets observed to deposit and accumulate shown in **Figure 7.3b,c**). Moreover, a high hanging ability of the node was observed (**Figure 7.3b**). However, the larger droplets fall down when they overcome the adhesive force. Depending on the arrangement and location of the petals and trichomes some droplets reach to the shoots and some fall to the ground, where their absorption through roots can be expected.

7.3. Conclusion

The efficient fog droplet capturing by the 3-dimentsional orientation of the barbs surrounding the node and droplet movement property of the trichomes are demonstrated. It could be beneficial for developing biomimetic fog collector as well as in other fluid dynamics applications, such as directional transport, filtering etc.

8. Fog collection on polymer fibers: Droplet behavior and collection efficiency influenced by cross-section profiles and surface structures

8.1. Introduction

Numerous fog-collection projects have been conducted by exploiting mainly wire and fiber meshes (i.e., harp designs, such as screens of wire or a cylinder type) (Nagel 1956; Nagel 1962; Ekern 1964; Vogelmann *et al* 1968; Goodman 1985; Schemenauer and Cereceda 1988; Schemenauer and Joe 1989). Fog collecting meshes show a great potential to ensure a supply of drinking water in many arid regions in the world. However, the optimization of these meshes is a major challenge. Fog collectors made of polyolefin mesh have been used for decades (Schemenauer and Cereceda 1994a; Klemm *et al* 2012) with the aim of improving the daily life of the people affected by acute water shortage. However, there are many opportunities to modify the meshes originally used in the fog collectors to optimize their fog-collection efficiency. For example, development of a three-dimensional fabric has been reported (Sarsour *et al* 2010), the use of multi-panel fog collector has been proposed (Holmes *et al* 2015), water collection and release behavior of a temperature sensitive polymer coated cotton fabric has been demonstrated (Yang *et al* 2013), some design rules of fiber network, e.g., theoretical optical diameter of the fiber, gap length between the fibers, low CAH of the fiber surface with a contact angle of ~100°, etc. for fog harvesting were proposed (Park *et al* 2013). The potential of artificial

silk fiber (Bai *et al* 2010; Bai *et al* 2011; Bai *et al* 2012; Hou *et al* 2012; Chen *et al* 2013; Hou *et al* 2013) and electrospun nanofibers (Dong *et al* 2012; Birajdar and Lee 2015) to collect fog and dew was shown.

Plants capable of fog collection in different foggy regions have structured leaves, needle shaped leaves, spine shaped structures etc. (Martorell and Ezcurra 2007; Westbeld *et al* 2009; Andrews *et al* 2011; Vogel and Müller-Doblies 2011; Ju *et al* 2012; Roth-Nebelsick *et al* 2012; Stanton and Horn 2013; Xue *et al* 2014). For example, pine, redwood and fir with needle shaped leaves were reported to show a good fog-collection efficiency (Goodman 1985). Their leaf morphologies are being considered as possible models for developing fog collecting meshes. The needles or needle like structures of the plants have different cross-section profiles, e.g., round, rectangular, rectangular with round corners and/or edges, triangular etc., and they have different surface microstructures as well. In contrast, the surface of the ribbons or fibers of the mesh that have been used for the last few decades to collect fog is apparently smooth or not structured enough. However, the influence of different fiber cross-section profiles on the fog-collection efficiency has not yet been studied so far. Therefore, fog droplet behavior on polyethylene-terepthalate (PET) fibers with different cross-section profiles and surface structures, e.g., microgrooves, is analyzed to investigate their influence on fog-collection efficiency.

8.2. Results

8.2.1. Cross-section profiles and surface structures of the fibers

Profiles: The horizontal cross-sectional view and dimension of 14 different fibers are given in **Figure 8.1a–n**. The widths/diameters of the fibers shown in cross-sectional view increased compared to real widths/diameters of the fibers due to the expansion of their edges during cutting. Real widths/diameters of the fibers are given in **Table 8.1**.

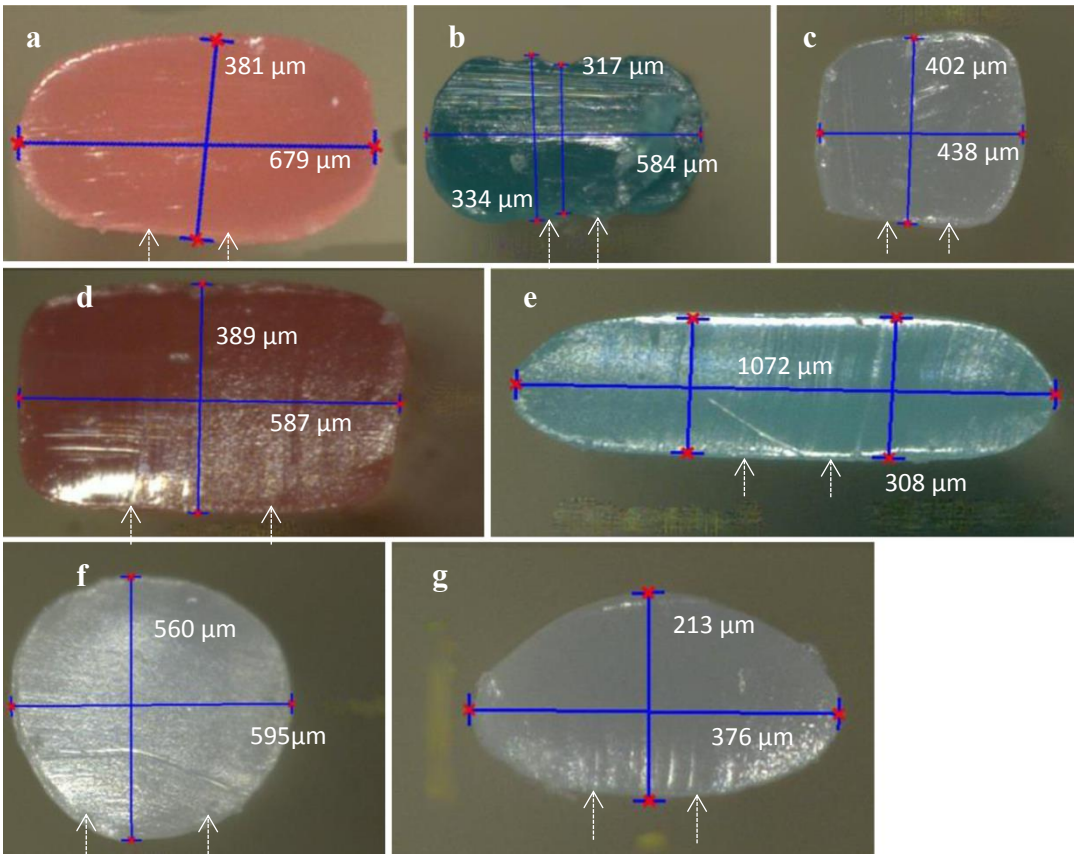

Figure 8.1(a–g): Fiber cross-section profiles, category A: Horizontal cross-sectional view of different fiber profiles with different widths/diameters. The dotted arrows in each profile indicate the surface where the fog flow was directed during the fog-collection experiment (for both single and multi-fiber samples).

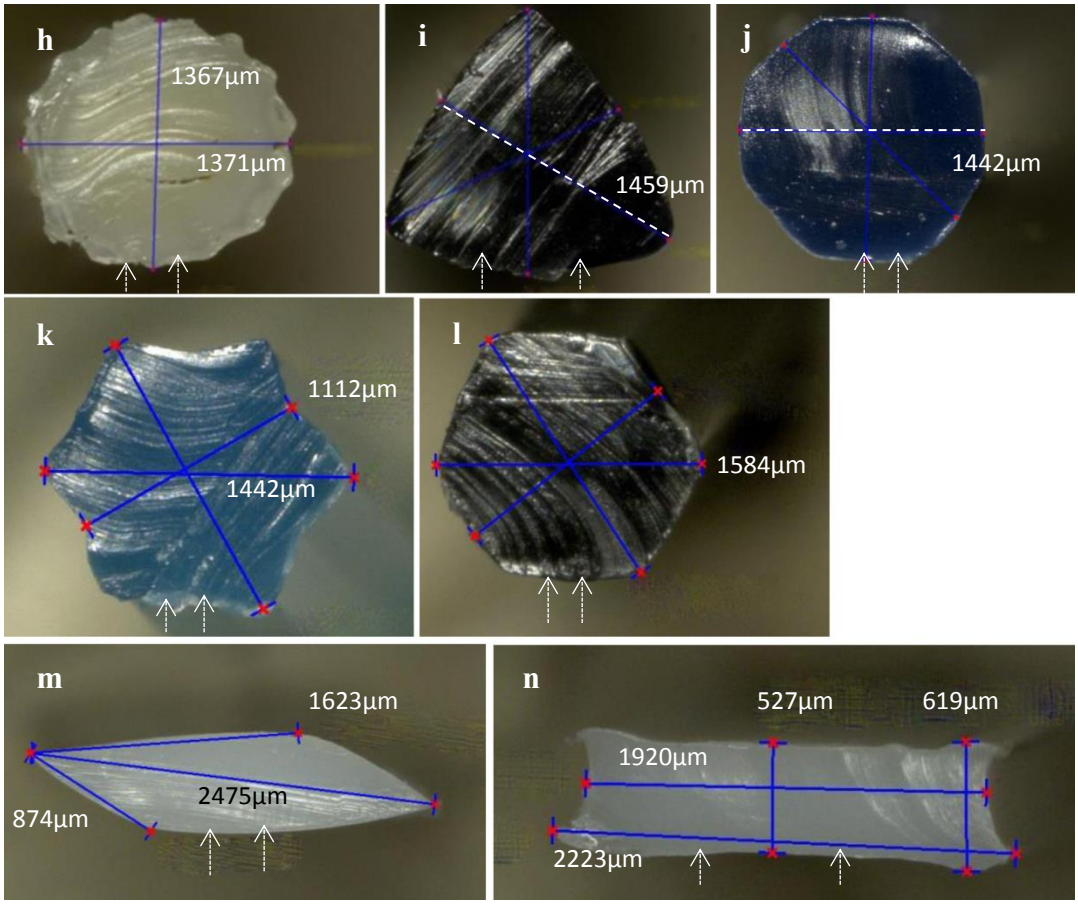

Figure 8.1(j–n): Fiber cross-section profiles, category B: Horizontal cross-sectional view of different fiber profiles with different widths/diameters. The dotted arrows in each profile indicate the surface where the fog flow was directed during the fog-collection experiment (for both single and multi-fiber samples).

Table 8.1: Real diameters/widths (average ± standard deviation) of the fiber profiles

Profiles in Category A	**1**	**2**	**3**	**4**	**5**	**6**	**7**
Widths/diameters (µm)	640 ± 2	570 ± 1	439 ± 1	556 ± 1	988 ± 2	490 ± 2	317 ± 2
Profiles in Category B	**8**	**9**	**10**	**11**	**12**	**13**	**14**
Widths/diameters (µm)	1277 ± 1	1337 ± 1	1243 ± 4	1372 ± 2	1503 ± 2	2289 ±2	2122 ± 3

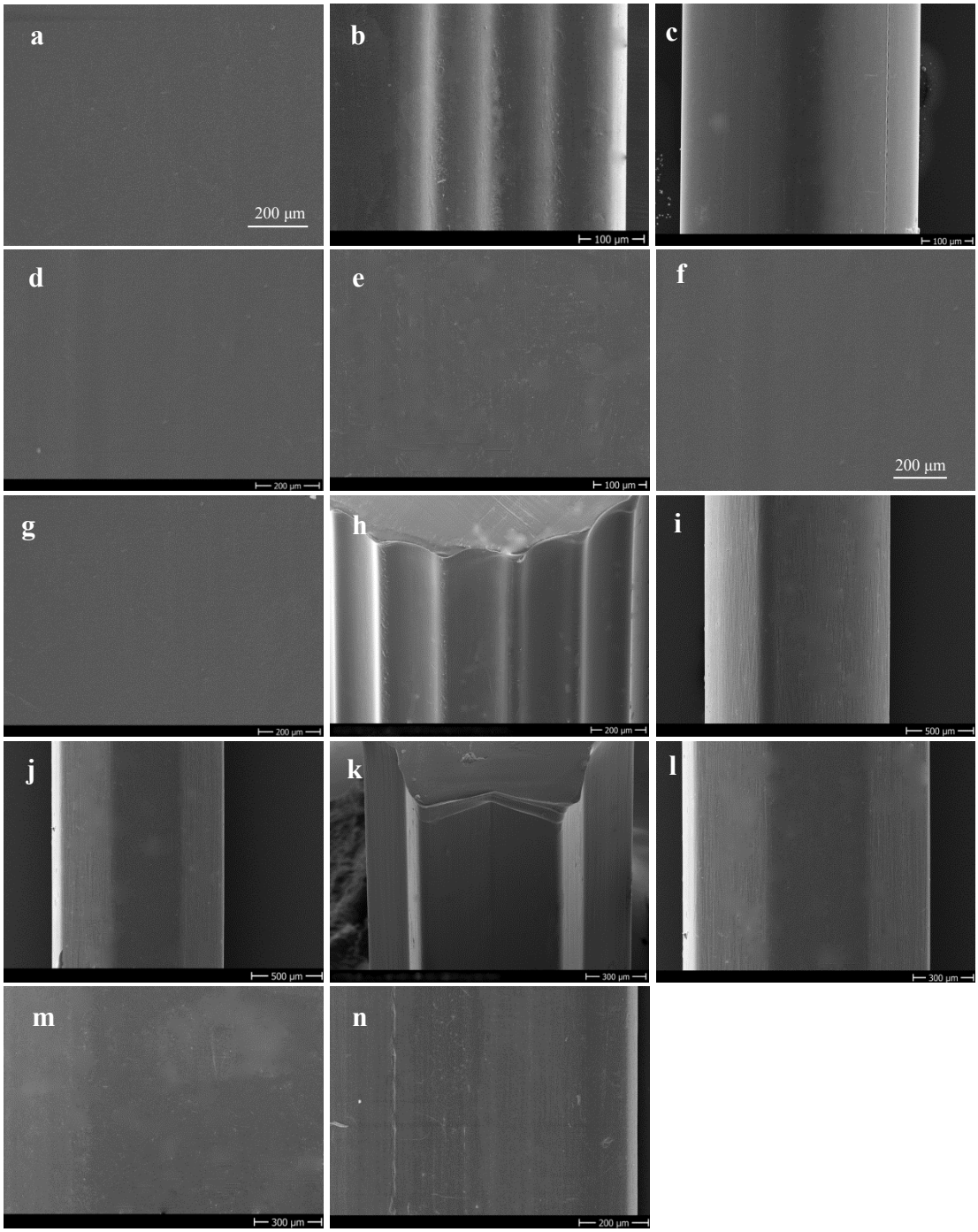

Figure 8.2: Scanning electron micrographs (SEMs) of the surfaces of different fiber profiles. Figures (a–o) represent the fiber profiles 1–14, respectively. Surfaces of fiber profiles 1, 3, 4, 5, 6, 7, 9, 13 and 14 are smooth (a, c, d, e, f, g, i, m and n respectively). Microgrooves can be seen on the surfaces of profile 2 in (b), profile 8 in (h) and profile 11 in (k). Edges of fiber profiles 10 (**j**) and 12 (**l**), due to their polygonal shapes, can be seen on their surfaces.

Surface structures: Surface structures of profiles 1–14 are shown in **Figure 8.2a–n**. Surfaces of fiber profiles 1, 3, 4, 5, 6, 7, 9, 13 and 14 are smooth (**Figure 8.2a,c,d,e,f,g,i,m** and **n** respectively). Profiles 2 (**Figure 8.2b**), 8 (**Figure 8.2h**) and 11 (**Figure 8.2k**) have microgrooves on their surfaces. Edges of fiber profiles 10 (**Figure 8.2j**) and 12 (**Figure 8.2l**), due to their polygonal cross-section, can be seen on their surfaces.

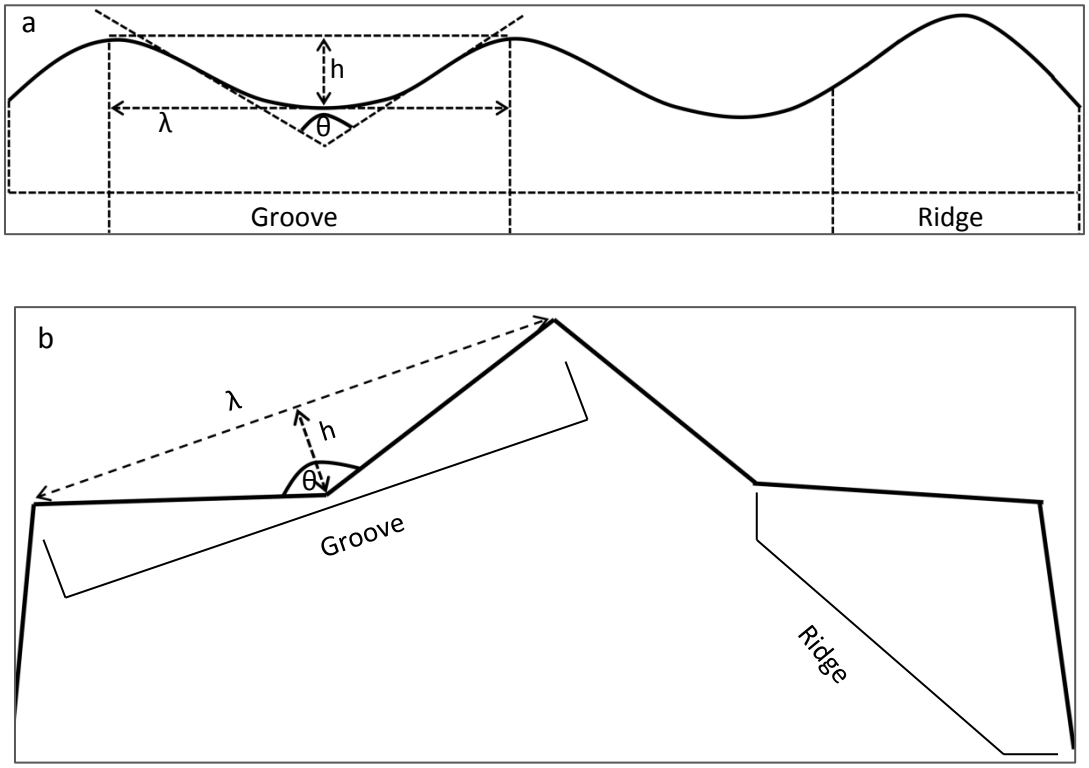

Figure 8.3: Illustration of the characteristics of (a) wavy microgrooves of profile 2 and 8, and (b) V-shaped microgrooves of profile 11. The ridges are also marked on the right side of the figures. Here, λ is the peak to peak distance of the grooves, h is groove-depth and θ is the angle between the walls of the grooves.

Wavy microgrooves on the surfaces of profiles 2, 8 and v-shaped microgrooves on the surface of profile 11 are schematically illustrated in **Figure 8.3a-b,** respectively. Characteristics of the microgrooves have been summarized in **Table 8.2.**

Table 8.2: Characteristics of the microgrooves on fiber profile 2, 8 and 11. The values represent average ± standard deviation.

Characteristics	Profile 2	Profile 8	Profile 11
Groove depth (h in µm)	15 ± 0.6	28 ± 0.7	111 ± 0.6
Peak-peak distance (λ in µm)	117 ± 1.4	260 ± 0.8	686 ± 2
Angle between the walls of a groove (θ in degree)	130 ± 1.3	126 ± 1	146 ± 1.4

8.2.2. Surface wettability

Dynamic contact angles were measured on a smooth PET fiber (Profile 15). Advancing contact angle (θ_{adv}) was 78° ± 2, receding contact angle was (θ_{rec}) 45° ± 3 and contact angle hysteresis (CAH) was 34° ± 2.

8.2.3. Influence of cross-section profiles and surface structure on fog collection

The amount of water dripped down as well as the amount of total collected water by the samples was measured (**Figure 8.4**). In **category A,** profile 2 with microgrooved surface collected the highest amount of fog water (2121 ± 156 µg) followed by profile 7 with an oval cross-section (1772 ± 118 µg). Profiles with rectangular cross-sections with round corners and smooth surfaces were not as efficient (1109 ± 221 µg, and 1203 ± 226 µg by profile 3 and 4, respectively) as profiles 2 and 7. Profiles 1 (elliptical cross-section) and 6 (round cross- section) showed higher efficiency (1534 ± 130 and 1349 ± 116 µg, respectively) than profiles 3 and 4. Provided that profile 1 has a higher diameter than

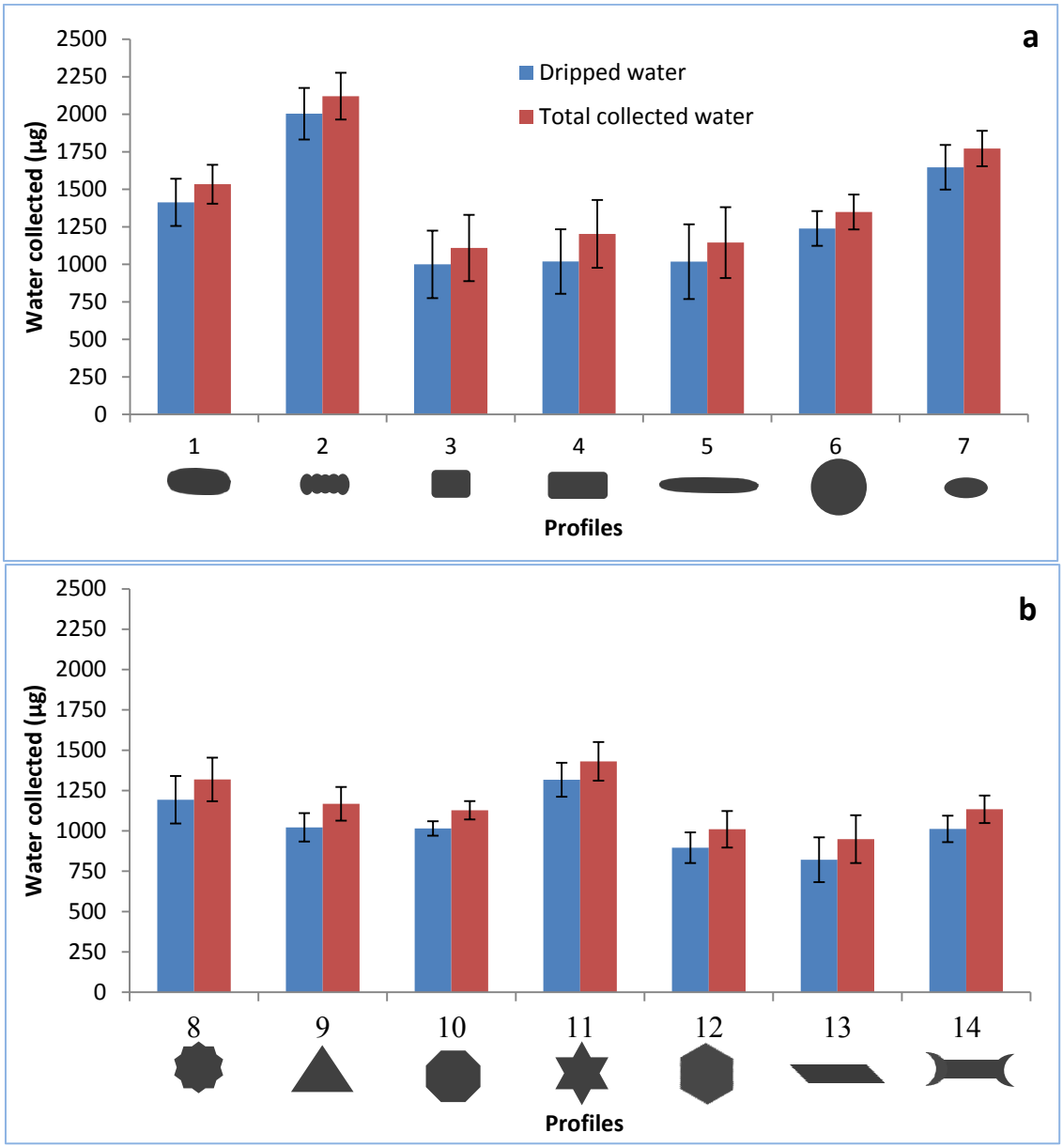

Figure 8.4: Amount of water dripped from samples, and total water collected by samples over 30 min. (a) Category A: profile 1–7, (b) Category B: profile 8–14.

profile 3 and 4; and profile 6 has a higher diameter than profile 3. Profile 5, though has an elliptical cross- section but due to higher diameter (988 µm ± 2) and smooth surface, showed one of the lowest efficiency in this category. Profile 3 (rectangular cross-section with round corners and smooth surface) collected the lowest amount of water (1109 ± 221 µg).

In **category B** profile 11, which has circular cross-section and v-shaped microgrooves, was the most efficient fog collector (1431 ± 120 µg) followed by profile 8 having similar cross-section but wavy microgrooves. It is to be noted that profile 11 has a higher diameter than profile 8 (see **Table 8.1**). The depth of the grooves of profile 11 is larger than profile 8 (**Table 8.2**); that clarifies the difference of their efficiency. Profile 13 (parallelogrammatic cross-section and smooth surface) collected the lowest amount of water (949 ± 148 µg). Profiles 9 (triangular cross-section) and 10 (polygonal cross-section) collected higher amount of water (1168 ± 104 and 1128 ± 57 µg, respectively) than profile 12 (hexagonal cross-section) (1010 ± 113 µg) due to their lower diameter (**Table 8.1**) compared to profile 12. Profile 14 having hook-shaped edges on both sides improved the water collection (1134 ± 85 µg). The hooks possibly improved the capture of fog droplets.

Water collection efficiency is also related to a fast directed movement of the deposited water on the fiber surfaces. Time required for the first droplet to move to the bottom and the onset of dripping of water drops on the single fiber of each profile was recorded and the data are shown in **Figure 8.5a–b**. In **category A** (profile1–7), profile 2 and 5 took about the same time (38 ± 8 and 41 ± 2 s, respectively) for the 1st droplet to move to the bottom while a large difference occurred in their onset of dripping (98 ± 10 and 151 ± 8 s correspond to profile 2 and 5, respectively). Profile 2, which was proved to be the most efficient in fog collection, took shorter time (38 ± 8 s) for the 1st droplet to move to the bottom than profile 7 (62 ± 8 s), the second most efficient, but both took about the same time for their onset of dripping (98 ± 10 and 94 ± 6 sec, respectively). This is because of the smaller diameter/width of profile 7 (~317 µm) than profile 2 (~570 µm). Similar results can be seen in **category B** too. It took 61 ± 9 and 31 ± 1 s for profile 8 and 11,

respectively for the 1st droplet to move to the bottom. They both have microgrooves on their surfaces. They took longer time (171 ± 23 and 159 ± 10 s for profile 8 and 11, respectively) than profile 2 (98 ± 10 s) for the onset of dripping.

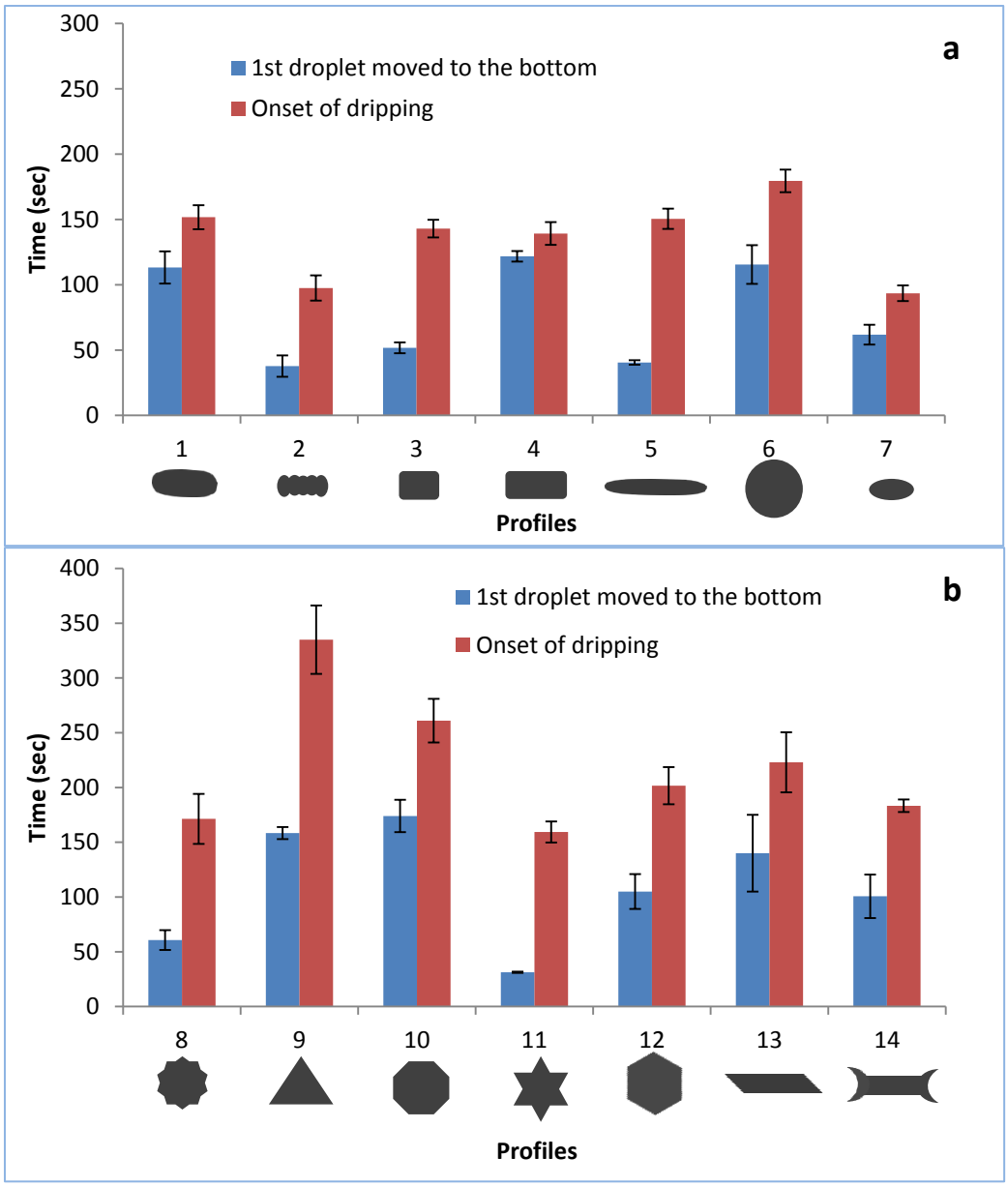

Figure 8.5: Time required for the first droplet to move to the bottom, and onset of dripping of water drops on a single fiber of each profile of (a) category A (profile 1-7) and (b) category B (profile 8-14).

However, profile 11 remained prominent on both cases due to the larger depth of the grooves than profile 8 (**Table 8.2**). Other profiles of this **category B** took much longer time

as shown in **Figure 8.5b**. A channel in each side of profile 14 improved the transport compared to profiles 9, 10, 12 and 13.

8.2.4. Fog droplet behavior on different fiber profiles

Fog droplet behavior on the surfaces of all the sample profiles was analyzed. The common event observed for the single fiber samples, except profile 2, 8 and 11, was the deposition of tiny fog droplets followed by the enlargement by the coalescence of the neighboring fog droplets. Then adjacent droplets merged and a water drop with an elongated shape was formed. The fusion of water droplets caused a slight down movement along the fiber. In the resulting gaps, small water drops were formed again. This process was repeated within the collection phase until the fiber surface was covered with a maximum number of large water droplets. A large droplet, while slipping downward, collected all the droplets on its way down. This caused free space for new droplets to form, though the time for the process, i.e., movement of droplets and their onset of dripping varied depending upon their cross-section profile and diameter as shown in **Figure 8.5**.

However, a difference with the above described phenomenon was observed on the microgrooved fiber profiles (2, 8 & 11), where water film formation on their surfaces and faster onset of dripping were found. Nevertheless, fog droplet behavior and/water dripping on the surfaces of sample profiles, e.g., profile 2, profile 4 and profile 7 is described and compared in **Figure 8.6a–x**. Profiles 2 and 7 were chosen because of their higher efficiency. Profile 4 was chosen as one of the lowest efficient samples.

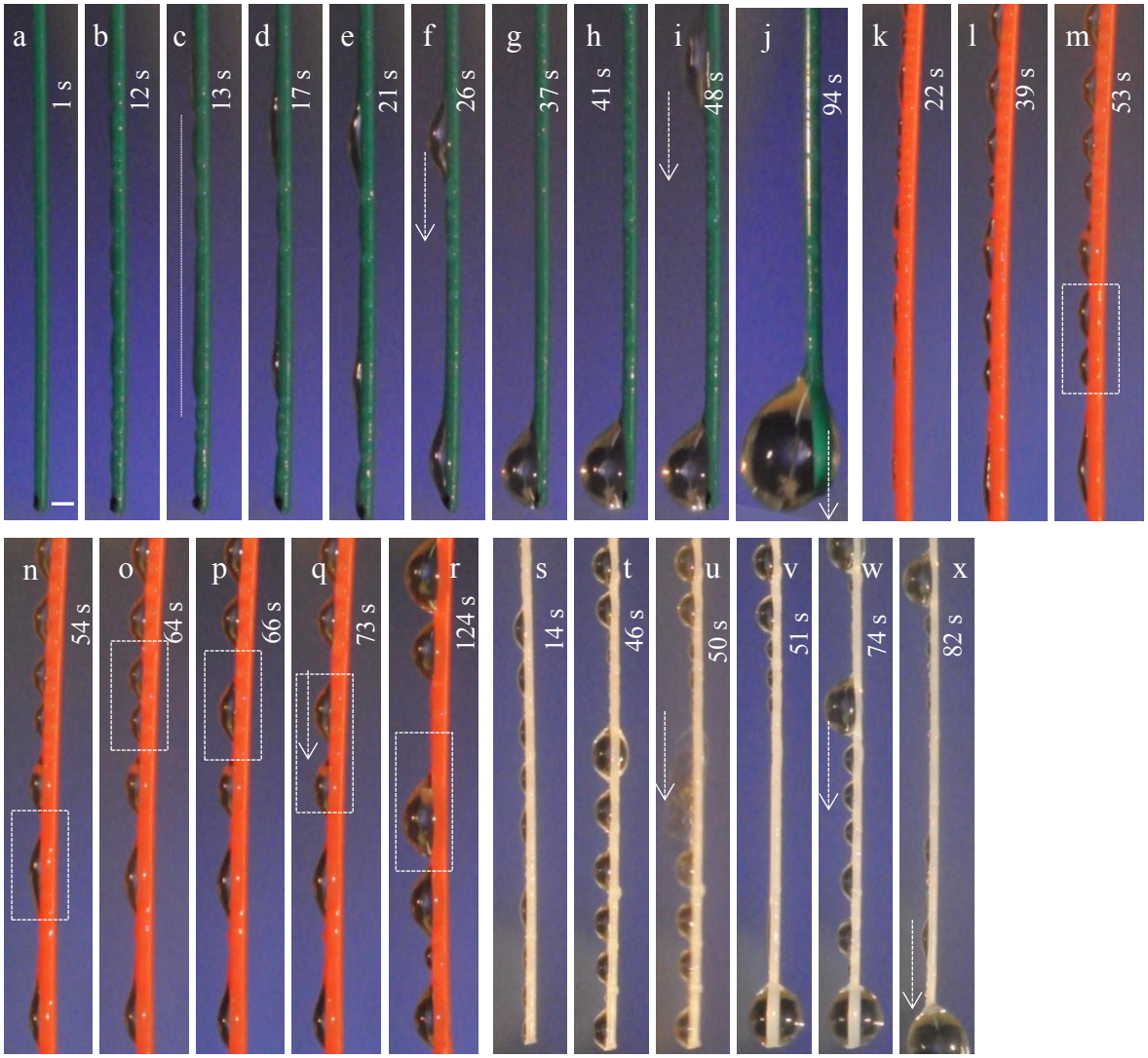

Figure 8.6: Fog deposition and movement on the surfaces of different fiber profiles: (a–i) profile 2, (k–r) profile 4 and (s–x) profile 7. Scale bar 500 µm. Microgrooves on profile 2 improved film formation shown by the dotted line in (c). Arrows in (f) shows the downward movement of droplets following the film. Figures (g–h) show the increase of size of the droplet at the bottom by the movement of water through the film, droplet is about to fall down (j). Rectangular marks in (m–r) show the fusion of neighboring droplets. Fusion of neighboring droplets (s–w) and downward movement of droplets is indicated by arrows in figures u, w, x. Time scales (sec) can be seen on respective images.

Profile 2 (rectangular cross-section profile with round edges, microgrooved surface)

Tiny droplets were observed to fuse with neighboring droplets, resulting in the formation of elongated drops only after 12 s (**Figure 8.6a–b**). Subsequently, elongated droplets on the surface formed an apparent film (**Figure 8.6c**). Two elongated droplets on two points of the film were seen to increase in size (**Figure 8.6d**), resulting in the downward movement (**Figure 8.6e–f**). All of a sudden one of the droplets appeared at the bottom of the fiber (**Figure 8.6f**) in about 38±8 s. The droplet was not seen all through the way from its first position to the bottom during the water transport rather a film. Therefore, it is assumed that there were already water filaments on the grooves that facilitated the film formation. It should be noted that the two droplets of same age can appear in different sizes because of the different size distribution of the fog droplets (2–50 µm) from the fog generator. The water from the second droplet was transported via the film and finally the second droplet joined the first droplet (**Figure 8.6g**) already moved to the bottom. The increase of the size of the combined droplet at the bottom over time (37 s – 41 s in **Figure 8.6g,h**), proved the transport of water via the film on the surface of the fibers. Another droplet (**Figure 8.6i**) elsewhere in the middle of the fiber was large enough about to move to the bottom. Finally, when the 2nd drop accumulated with the droplet at the bottom, it was about to fall down (**Figure 8.6j**) and at 107 s the droplet dripped, while an average for the onset of dripping was 98 ± 10 s (**Figure 8.4**).

Profile 4 (rectangular cross-section profile with round corners, smooth surface)

In addition to the deposition of lots of tiny droplets, elongated droplets were formed (**Figure 8.6k–l**). However, even after 40 s significant fusion of droplets was not observed

(**Figure 8.6l**). After 53 s, two large neighboring droplets only in one point fused together (**Figure 8.6m–n**). The droplets were then too far away to fuse together (**Figure 8.6n–q**). However, over time other neighboring droplets fused (**Figure 8.6o–r**) and increased in size also by the deposition of new droplets. The droplets started moving downwards gradually and when large enough at the middle of the fiber (**Figure 8.6r**) a droplet moved to the bottom resulting in a hanging droplet. The cycle continued until the hanging droplet is large enough to drip.

Similar results of droplet behavior were observed on all the smooth fiber profiles having diameter/width of more than 430 µm but due to different cross-sections and diameters/widths, their fog-collection efficiency varied.

Profile 7 (oval cross-section, smooth surface)

On the smooth surfaces of the oval cross-section profile of the fiber, half circle shaped droplets were observed. They were increasing by fusing with the neighboring droplets (**Figure 8.6s–t**). At around 66s a droplet moved to the bottom all on a sudden collecting other tiny droplets on its way down (**Figure 8.6u**). New droplets deposition continued, followed by the accumulation and movement of new droplets to the bottom to cause dripping (**Figure 8.6v–x**). However, no film formation was observed on the surface of profile 7 but probably the oval cross-section and smaller diameter helped improve the transport. The increase of the surface area of the edges due to smaller diameter may improve better fog droplet deposition. Relatively smaller droplets moved downwards along the fibers collecting all the drops on its way down because of the smaller diameter

of the fibers. Moreover, the diameter of the 1st droplet at the bottom was measured over time from 51 – 74 s; but the increase was negligible (**Figure 8.6v,w**).

8.2.5. Transport or drainage of the deposited fog water

The ratio of dripped water to total collected water signifies the transport or drainage of the deposited water. It indicates how much water drained from the fibers to the collector under the sample. Based on the analysis, the results (**Figure 8.7a–b**) showed that in each category separately, the profiles with microgrooved surfaces (Profiles 2, 8 and 11)

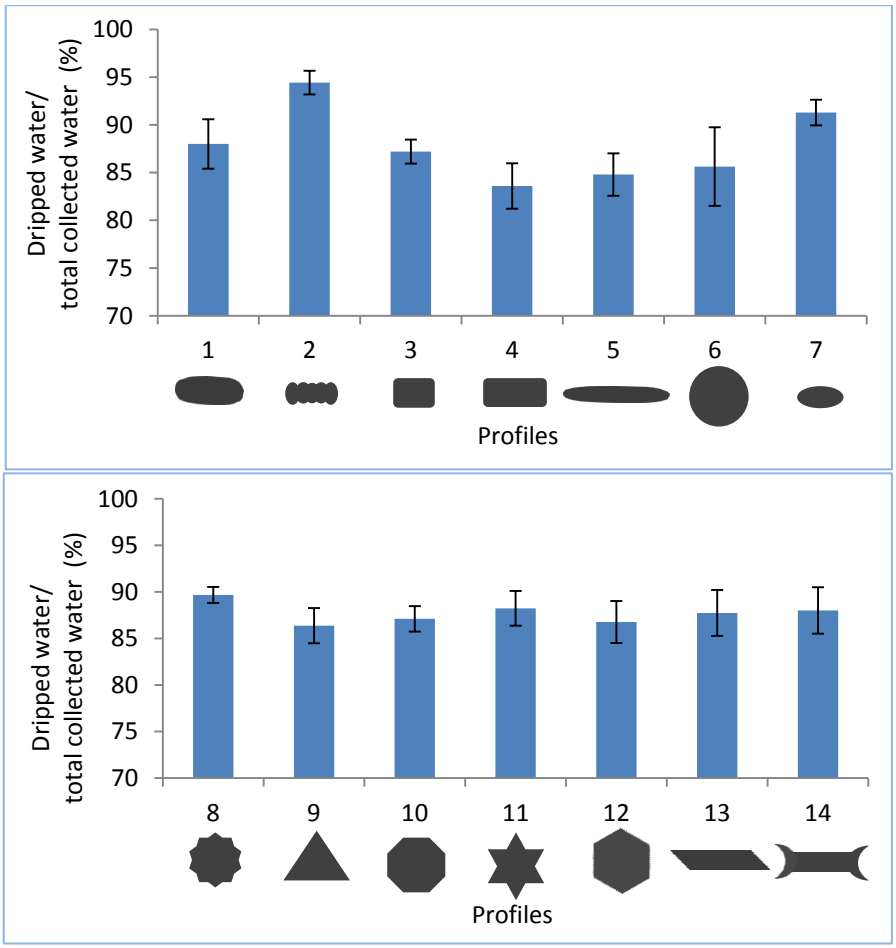

Figure 8.7: Ratio of dripped water to total collected water by different fiber profiles calculated over 30 min; (a) **category A** (profile 1–7) and (b) **category B** (profile 8–14).

showed higher transport efficiency than other samples with smooth surfaces. However, profile 7 having oval cross-section and the lowest diameter showed better transport efficiency than the rest of the samples except profile 2; even though its surface is smooth. Furthermore, the size and volume of the drop, dripping down from the fibers of profile 2 was larger than that of profile 7 (**Figure 8.6j,x**). Therefore, both parameters, i.e., lower diameter and microgrooves on the fiber surface played important role in water transport.

8.2.6. Simulation

A simulation was conducted in cooperation with Prof. Dr. Albert Baars and Leon Danter, Bremen University of Applied Sciences, Germany to validate the droplet behavior on the surface of a microgrooved fiber. Experimental microgrooved surfaces with the characteristics based on the fiber profile 2 shown in **Table 8.2** were generated by the use of the software. Due to the highest fog collection efficiency among the samples the dimensions of profile 2 were used in the simulation.

The behavior of the droplet from an initial state to the preliminary spreading in the grooves at time 16.6 x 10^{-4} s is displayed in **Figure 8.8a–f.** At the beginning a droplet was located on the top of a ridge (**Figure 8.8a**). With time the droplet started to wet the grooved surface and spread into the two neighboring grooves (**Figure 8.8b**). After 1.8 x 10^{-4} s the droplet split up into two parts. During the splitting a few tiny droplets detached from the main volume (**Figure 8.8c**). Most of them reunited or left the numerical domain, while one tiny drop can still be seen in the left view in **Figure 8.8c** (marked by an arrow). After the split the droplet reunited and moved around the ridge (**Figure 8.8d**). The droplet volume tended to fill the grooves rather than rested on the ridge. Therefore, the droplet

spread over the two adjacent grooves (**Figure 8.8e**). Finally, the droplet moved into a single groove (**Figure 8.8f**).

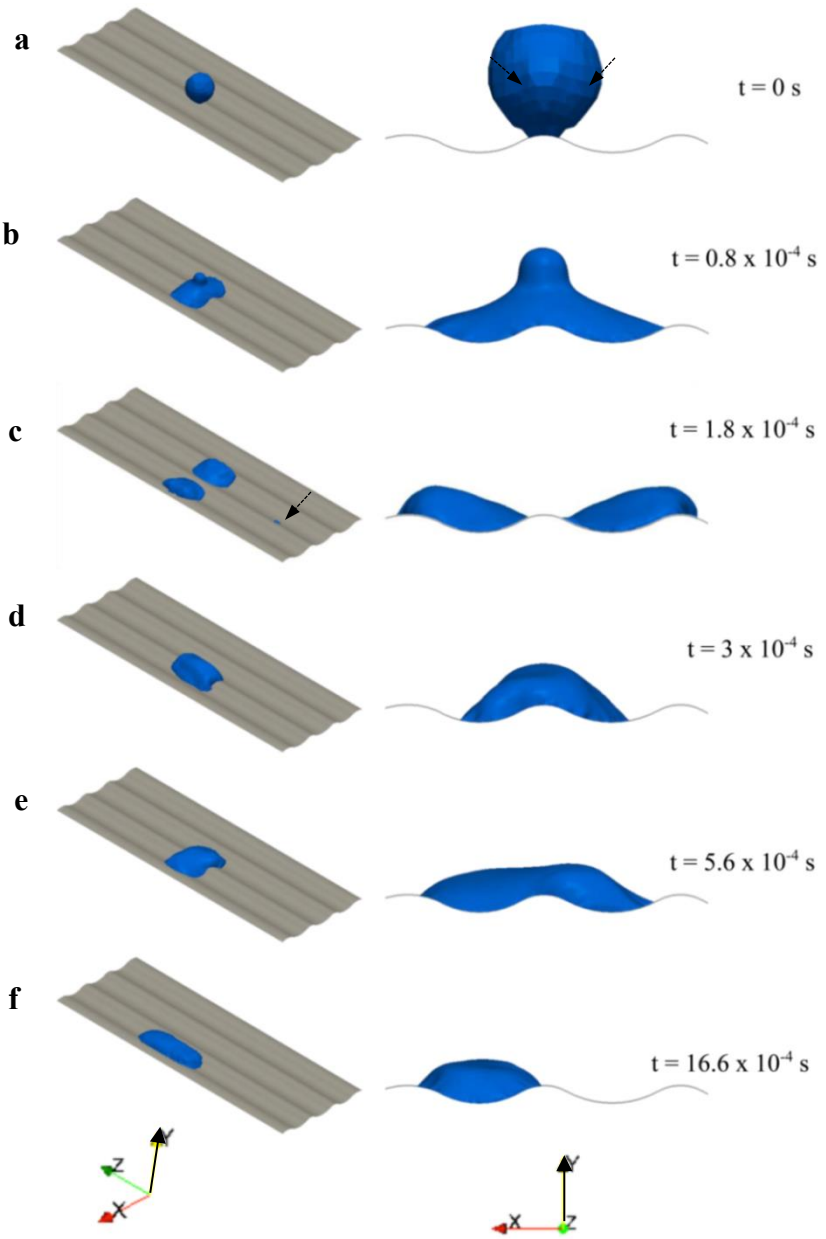

Figure 8.8: Droplet behavior in simulation is shown at different times *t*. Water and grooved surface are shown in blue and gray, respectively. On the left side an isometric view of the entire numerical domain is given. Right side presents a view along the direction of gravity (z axis). From this angle the infinitesimal thin grooved surface is invisible. Time unit is in second and coordinate systems for both views are given at the bottom. Pixelated, i.e., unsmooth surface of water droplet (a) is marked with arrows.

8.3. Discussion

Different cross-section profiles of fibers, their diameter and surface structures influence their fog-collection efficiency. Microgrooved hydrophilic fiber surface along with smaller diameter (~320 µm) of the fiber is the most favorable. Directional delivery of collected fog droplets by the microgrooves and a thinner boundary layer of the surfaces caused by the surface asperities (Vogel 1994) enhance the fog-collection efficiency. Although the fibers are three-dimensional, due to their very low thickness multi-fiber samples are imagined as two-dimensional. Thus, here the sideways of the fibers are referred as edges. A reduction of fiber diameter, keeping the effective surface area of samples same, increases frequencies of free flow spaces as well as edges of multi-fiber samples but decreases the flow resistance to the fog flow. An increase of surface area of edges of the fibers helps deposit more droplets as observed in plant samples in **Chapter 6**. Thus, smaller diameter of the fibers improves fog collection.

A fast or effective water transport on microgrooved hydrophilic fiber surface (θ_{adv} = 78° ± 2, θ_{rec} = 45° ± 3) results from the difference in energy barriers in different directions of the grooves (Johnson and Dettre 1964; Kannan and Sivakumar 2008a). Provided that, all the samples have same material properties but due to microgrooves on the surface of some fiber profiles their contact angle hysteresis should reduce as observed earlier for microgrooved copper wires in **Chapter 5**. Consequently, the microgrooved fibers demonstrated higher transport efficiency compared to others (**Figure 8.7a–b**). In a microgrooved hydrophilic surface the energy barrier is lower in the direction parallel to the grooves than that in the direction vertical to the grooves. Therefore, deposited fog

droplets, after coalescence with neighboring droplets tend to elongate. Tiny droplets impinged on the fiber surface in between two larger droplets must be entering into the grooves. Later on, the elongated water droplet move parallel to the grooves and fuse with another elongated droplet. The elongated droplets gather enough momentum to travel till the end resulting in the formation of a film on the grooved surface (Chen *et al* 2005; Kannan and Sivakumar 2008b; Kusumaatmaja *et al* 2008; Kannan *et al* 2011). Smooth hydrophilic surface or hydrophobic surface of the fibers causes clogging on the multi-fiber samples, where there are lots of droplets adhered (Park *et al* 2013; Azad *et al* 2015b). In contrast, data in this study showed that a water film formation on the microgrooved surface of fiber profile 2 can overcome the clogging effect.

The numerical simulation (**Figure 8.8a–f**) also validates the film formation on a microgrooved surface. Due to the coarse basic mesh (here the term 'mesh' is related to simulation) at the initial state the surface of the droplet appears pixelated, i.e., unsmooth surface water droplet at time, t=0 s in **Figure 8.8a**. With time, mesh refinement sets in and leads to smoothing of the surface. Up to time $t = 16.6 \times 10^{-4}$ s a quite dynamic behavior of the droplet can be observed which is determined by alternative conversion of kinetic energy into potential surface energy by dissipation, resulting in a slow-down of the process. At the end, a single droplet remains inside a single groove with an elongated shape, which is superior to that of the initial droplet. The phenomena results from the hydrophilic property of the microgrooved surface. The influence of gravity on the shape can be assumed negligible due to small Bond number of $Bo = {\rho_l g d^2}/{\sigma}$ =1.36×10^{-3}<<1.

The observations indicate the intent of the system to minimize the surface energy.

Therefore, it is assumed that further droplets settle in the grooves too. With decreasing distance of adjacent droplets, they coalesce and form liquid filaments in the grooves to minimize surface energy. With growing cross-section area of the filaments a unification of adjacent filaments leads to a water film on the grooved surface. This is confirmed by the experimental data of the microgrooved surface of profile 2 in **Figure 8.6a–j**.

The negligible increase of the diameter of the droplet, hanging at the bottom of the fiber of profile 7 (**Figure 8.6v–w**), confirms that there was no film formation on the fiber. Moreover, the roll off of smaller droplets (compared to those of profile 2) from the fibers of relatively smaller diameter (~317 µm) proves their better efficiency than other profiles except profile 2. Profile 7 has the smallest diameter among the fiber samples and reached 80% of the efficiency of profile 2. It can be assumed that profile 2 with a smaller diameter equivalent to profile 7 (~317 µm) or to optimum diameter (~340 µm) could show much better efficiency than with its current diameter.

Even though multi-fiber samples had equivalent shade coefficients (ratio of the free flow area to total surface area for fog deposition) their flow resistance to the fog carrying air might vary due to uneven distribution of the free flow space (de Dios Rivera 2011; Holmes *et al* 2015). However, in that case, the consideration of two points can signify the findings:

1. Profile 7 that has the lowest diameter (~317 µm), which is close to the optimum diameter (~340 µm of a round profile) (Park *et al* 2013), collected a lower amount of water than profile 2 (diameter ~570 µm) with microgrooves.

2. The consistency of a higher fog-collection efficiency of fiber profiles with microgrooved surface (even if with a larger diameter) compared to other fiber profiles with smooth surface.

Furthermore, this is the only possibility to compare the influence of different fiber diameters on fog collection keeping the total area of the samples equivalent.

8.4. Conclusion

The influence of cross-section profiles and surface structures of the fibers on fog droplet behavior on their surfaces, and their fog collection were analyzed for optimizing fog collecting meshes. Our study confirms that any fiber with smooth surface would capture a very low amount of fog droplets due to the thicker boundary layer. It is demonstrated that microgrooved surface of the fibers increases the deposition efficiency, supported by a thinner boundary layer (Vogel 1994). Directional transport of the surface enhances the drainage efficiency, followed by the improvement of the total fog-collection efficiency. Therefore, a combination of round profile (or rectangular cross-section profile with round edges, e.g., profile 2) with microgrooved hydrophilic-superhydrophilic surface and the optimum diameter (~340 μm) (Park *et al* 2013) can optimize the collection efficiency. In addition, although the multi-fiber samples had equivalent effective surface areas, the variation of their diameter may influence the results. Therefore, further testing of above described ideal fiber profiles and surface structures arranged in multi-fiber samples should follow.

9. Proposed design of optimized biomimetic fog collectors

A design for highly efficient fog collectors has been proposed in **Figure 9.1**. Highly wettable (θ_{adv} = 16° ± 2.7 and θ_{rec} = 9° ± 2.6) as discussed in **Chapter 6** for DH awn of *Hordeum* or superhydrophilic barbed fibers are vertically oriented with a constant gap in between. The gap may be similar to the width of the fiber or less. The horizontal fibers are only for support and they are placed as far apart as possible so that the transport is not hampered. It would be better if the horizontal fibers can be placed on the backsides of the vertical barbed fibers resulting in a challenge of engineering optimization. The dimension can be chosen as discussed for the model sample in **Chapter 6** and/or optimized by further research.

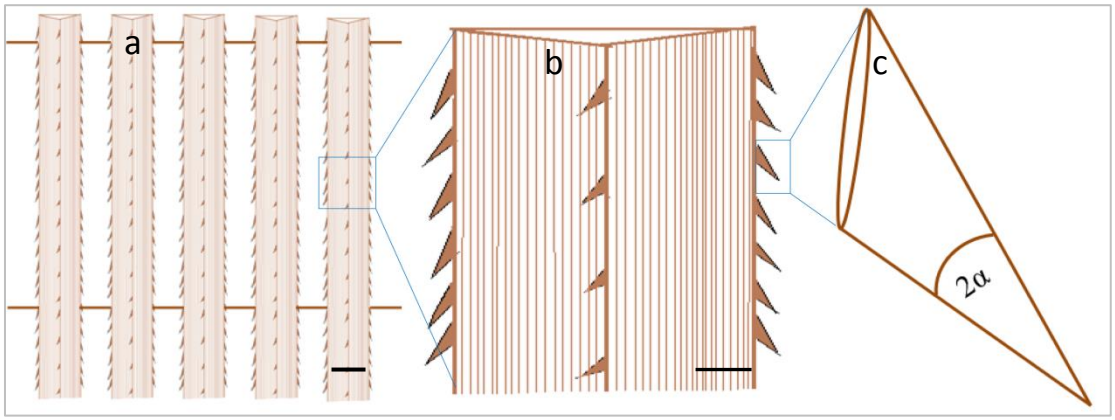

Figure 9.1: (a) Schematic of the proposed design of a fog collector: microgrooved barbed fibers are aligned vertically parallel to each other with a constant gap (similar to the width of the fiber or less) in between; scale bar 500 µm, (b) a magnified part of a barbed fiber with microgrooves from top to bottom; scale bar 150 µm, (c) a single barb with an apex angle 2α. Published in Azad *et al* 2015a.

Summary

Azad, M.A.K. (2016). ***Fog Collection on Plant Surfaces and Biomimetic Applications.*** **Doctoral thesis, Faculty of Mathematics and Natural Sciences, Rheinische Friedrich-Wilhelms-University of Bonn.**

Shortages of fresh water affect around one billion people world-wide; mostly in arid and semi-arid climates. Fog, in certain regions, may be an important source of water that is often overlooked. Inspired by the distinctive fog-collection mechanisms of certain plants surviving in these climatic conditions, biomimetic fog collectors are an innovation that could enable us to alleviate the water shortages. The influence of leaf shape, surface microstructure and hierarchical architecture, and wettability of plant and biomimetic samples on their fog-collection efficiency is analyzed.

A pinnate leaf shape shows higher efficiency compared to perforate or simple leaf shapes as a result of a lower flow resistance of the fog droplets transported by air, as well as sufficient space on the surfaces for their deposition. Pinnate and perforate leaf shapes were prepared by experimental modification of simple leaves. Directed channels on the surfaces and a drip tip at the lower edge of leaf samples improve the transport of water. Adhesion of a thick water layer at the bottom edges of the samples without the drip tip results in the saturation of the surfaces and a lower efficiency.

Microstructured surfaces show two to three times higher efficiency over smooth surfaces. A continuous fog droplet deposition, an effective water transport to the target and a very efficient fog collection is found in dry hydrophilized *Hordeum vulgare* (barley) awn with hierarchical architecture. A unique fog-collection ability is demonstrated by the structured trichomes of *Ptilotus manglesii*. Polymer fibers with microgrooved surface demonstrates a higher water transport (drainage efficiency) than different other fiber profiles with smooth surface, resulting in the increase of total fog collection. Numerical simulation supports the findings.

Superhydrophilic surface property plays a major role to enhance the deposition efficiency as well as transport of water droplet, i.e., superhydrophilic meshes collect twice as much fog as hydrophobic meshes and five times as much fog as hydrophilic meshes. Therefore, fibers with a combination of optimized diameter and microgrooved superhydrophilic surface can enhance the efficiency.

In conclusion, a new fiber design with a hierarchical architecture and superhydrophilic surface is proposed to develop optimized meshes for fog collection.

Zusammenfassung

Azad, M.A.K. (2016). ***Fog Collection on Plant Surfaces and Biomimetic Applications.*** **Dissertation, Mathematisch-Naturwissenschaftliche Fakultät, Rheinische Friedrich-Wilhelms-Universität Bonn.**

Weltweit leiden rund eine Milliarde Menschen unter Frischwassermangel; vor allem in den ariden und semiariden Klimaten/Gebieten der Erde. Dabei kann Nebel, was oft übersehen wird, in bestimmten Regionen als eine wichtige Quelle für Wasser angesehen werden. Nebel-Sammelmechanismen, welche für einige, unter solchen klimatischen Bedingungen vorkommende, Pflanzen charakteristisch sind, können dabei eine Inspiration für biomimetische Nebelkollektoren darstellen. Diese sind eine Innovation, die es uns ermöglichen könnte die Wasserknappheit zu lindern. In dieser Studie werden die Einflüsse unterschiedlicher Blattformen, der Oberflächenmikrostruktur und hierarchischer Architektur, sowie der Benetzbarkeit von pflanzlichen und biomimetischen Proben auf ihre Nebelsammeleffizienz hin analysiert.

Versuche mit unterschiedlich modifizierten Blattformen zeigen eine höhere Effizienz bei einer gefiederten Form im Vergleich zu einfachen oder perforierten Blattformen. Dies ist auf einen geringeren Strömungswiderstand, für die Nebeltröpfchen transportierende Luft, und die Größe, der zur Anlagerung geeigneten, Oberfläche zurückzuführen. Gerichtete Rillen auf den Oberflächen und eine Träufelspitze an der unteren Spitze der Blattproben verbessern den Abtransport von Wasser ebenfalls. Proben ohne diese Träufelspitze sammeln Wasser an der unteren Spitze, was zur Sättigung der Oberfläche und einer geringeren Effizienz führt.

Mikrostrukturierte Oberflächen weisen eine zwei- bis dreimal höhere Effizienz als glatte Oberflächen auf. Eine trockene hydrophilisierte Granne von *Hordeum vulgare* (Gerste) hat eine hierarchische Architektur und weißt eine kontinuierliche Nebeltröpfchen Abscheidung, einen wirksamen Wassertransport und eine sehr effiziente Nebelsammlung auf. Eine einzigartige Nebelsammelfähigkeit durch strukturierte Trichome wird auch

durch *Ptilotus manglesii* demonstriert. Polymerfasern mit mikrogerillter Oberfläche zeigen einen höheren Abtransport des Wassers (Entwässerungseffizienz) als verschiedene andere Faserprofile mit glatten Oberflächen, was zu einer Erhöhung der Effizienz führt. Numerische Simulationen unterstützen die Ergebnisse.

Superhydrophile Oberflächeneigenschaften spielen eine wichtige Rolle, um die Abscheidungseffizienz zu verbessern sowie den Transport von Wassertropfen. Superhydrophile Netze beispielweise sammeln doppelt so viel Nebel wie hydrophobe Netze und fünfmal so viel Nebel wie hydrophile Netze. Daher können Fasern mit einer Kombination aus optimiertem Durchmesser und mikrogerillter superhydrophiler Oberfläche die Effizienz verbessern.

Abschließend wird ein neues Faserdesign mit einer hierarchischen Architektur und superhydrophilen Oberflächenchemie vorgeschlagen, um optimierte Netze für die Nebelsammlung zu entwickeln.

Bibliography

Abdul-Wahab, S.A., Al-Damkhi, A.M., Al-Hinai, H., Al-Najar, K.A. and Al-Kalbani, M.S. (2010). Total fog and rainwater collection in the Dhofar region of the Sultanate of Oman during the monsoon season. *Water International,* 35: 100-109

Andrews, H.G., Eccles, E.A., Schofield, W.C.E. and Badyal, J.P.S. (2011). Three-dimensional hierarchical structures for fog harvesting. *Langmuir,* 27: 3798-3802

Azad, M.A.K., Barthlott, W. and Koch, K. (2015a). Hierarchical plant surface architecture as an inspiration for biomimetic fog collectors. *Langmuir,* 31: 13172-13179

Azad, M.A.K., Ellerbrok, D., Barthlott, W. and Koch, K. (2015b). Fog collecting biomimetic surfaces: Influence of microstructure and wettability. *Bioinspiration & Biomimetics,* 10: 016004

Bai, H., Ju, J., Sun, R., Chen, Y., Zheng, Y. and Jiang, L. (2011). Controlled fabrication and water collection ability of bioinspired artificial spider silks. *Advanced Materials,* 23: 3708-3711

Bai, H., Ju, J., Zheng, Y. and Jiang, L. (2012). Functional fibers with unique wettability inspired by spider silks. *Advanced Materials,* 24: 2786-2791

Bai, H., Tian, X., Zheng, Y., Ju, J., Zhao, Y. and Jiang, L. (2010). Direction controlled driving of tiny water drops on bioinspired artificial spider silks. *Advance Matererials,* 22: 5521-5525

Barthlott, W. and Capesius, I. (1974). Contribution to the cuticular water absorption of some xerophytes. *Zeitschrift Fur Pflanzenphysiologie,* 72: 443-455

Barthlott, W. and Neinhuis, C. (1997). Purity of the sacred lotus, or escape from contamination in biological surfaces. *Planta,* 202: 1-8

Benzing, D.H. (1987). Vascular epiphytism: Taxonomic participation and adaptive diversity. *Annals of the Missouri Botanical Garden,* 74: 183-204

Benzing, D.H., Givnish, T.J. and Bermudes, D. (1985). Absorptive trichomes in Brocchinia reducta (Bromeliaceae) and their evolutionary and systematic significance. *Systematic Botany,* 10: 81-91

Benzing, D.H., Henderson, K., Kessel, B. and Sulak, J. (1976). Absorptive Capacities of Bromeliad Trichomes. *American Journal of Botany,* 63: 1009-1014

Beysens, D., Broggini, F., Milimouk-Melnytchouk, I., Ouazzani, J. and Tixier, N. (2013). New architectural forms to enhance dew collection. *Chemical Engineering Transactions,* 34: 79-84

Beysens, D., Clus, O., Mileta, M., Milimouk, I., Muselli, M. and Nikolayev, V.S. (2007). Collecting dew as a water source on small islands: The dew equipment for water project in Bisevo (Croatia). *Energy,* 32: 1032-1037

Beysens, D., Milimouk, I., Nikolayev, V., Muselli, M. and Marcillat, J. (2003). Using radiative cooling to condense atmospheric vapor: a study to improve water yield. *Journal of Hydrology,* 276: 1-11

Bhushan, B. and Jung, Y.C. (2007). Wetting study of patterned surfaces for superhydrophobicity. *Ultramicroscopy,* 107: 1033-1041

Bhushan, B. and Jung, Y.C. (2008). Wetting, adhesion and friction of superhydrophobic and hydrophilic leaves and fabricated micro/nanopatterned surfaces. *Journal of Physics: Condensed Matter,* 20: 225010

Birajdar, M.S. and Lee, J. (2015). Nanoscale bumps and dents on nanofibers enabling sonication-responsive wetting and improved moisture collection. *Macromolecular Materials Engineering,* 300: 1108-1115

Bliznyuk, O., Veligura, V., Kooij, E.S., Zandvliet, H.J.W. and Poelsema, B. (2011). Metastable droplets on shallow-grooved hydrophobic surfaces. *Physical Review E,* 83: 041607

Burgess, S.S.O. and Dawson, T.E. (2004). The contribution of fog to the water relations of Sequoia sempervirens (D. Don): Foliar uptake and prevention of dehydration. *Plant Cell and Environment,* 27: 1023-1034

Bussmann, M., Chandra, S. and Mostaghimi, J. (2000). Modeling the splash of a droplet impacting a solid surface. *Physics of Fluids (1994-present),* 12: 3121-3132

Cao, M., Ju, J., Li, K., Dou, S., Liu, K. and Jiang, L. (2014). Facile and large-scale fabrication of a cactus-inspired continuous fog collector. *Advanced Functional Materials,* 24: 3235-3240

Cao, M., Xiao, J., Yu, C., Li, K. and Jiang, L. (2015). Hydrophobic/hydrophilic cooperative Janus system for enhancement of fog collection. *Small,* 11: 4379-4384

Cassie, A.B.D. and Baxter, S. (1944). Wettability of porous surfaces. *Transactions of the Faraday Society,* 40: 546-551

Cereceda, P., Villegas, L., Osses, P. and Schemenauer, R. (1998). 'Evaluation of the use of fog water for regeneration of arid ecosystems. Proceedings of the First International Conference on Fog and Fog Collection.'

Chen, Y., He, B., Lee, J. and Patankar, N.A. (2005). Anisotropy in the wetting of rough surfaces. *Journal of Colloid and Interface Science,* 281: 458-464

Chen, Y., Wang, L., Xue, Y., Jiang, L. and Zheng, Y. (2013). Bioinspired tilt-angle fabricated structure gradient fibers: micro-drops fast transport in a long-distance. *Science Report,* 3: 2927

Chhatre, S.S. (2012). Designing liquid repellent surfaces for fabrics, feathers and fog. Massachusetts Institute of Technology

Chung, J.Y., Youngblood, J.P. and Stafford, C.M. (2007). Anisotropic wetting on tunable micro-wrinkled surfaces. *Soft Matter,* 3: 1163-1169

Comanns, P., Effertz, C., Hischen, F., Staudt, K., Bohme, W. and Baumgartner, W. (2011). Moisture harvesting and water transport through specialized micro-structures on the integument of lizards. *Beilstein Journal of Nanotechnology,* 2: 204-214

Davis, R.W. and Tauss, C. (2011). A new and rare species of Ptilotus (Amaranthaceae) from a suburban wetland of the eastern Swan Coastal Plain, Western Australia. *Nuytsia,* 21: 97-102

Dawson, T.E. (1998). Fog in the California redwood forest: ecosystem inputs and use by plants. *Oecologia,* 117: 476-485

de Dios Rivera, J. (2011). Aerodynamic collection efficiency of fog water collectors. *Atmospheric Research,* 102: 335-342

Dong, H., Wang, N., Wang, L., Bai, H., Wu, J., Zheng, Y., Zhao, Y. and Jiang, L. (2012). Bioinspired electrospun knotted microfibers for fog harvesting. *Chemphyschem,* 13: 1153-1156

Dower, S. (2002). Clouds on tap: water supply. *SA Waterbulletin,* 28: 15-17

Ebner, M., Miranda, T. and Roth-Nebelsick, A. (2011). Efficient fog harvesting by Stipagrostis sabulicola (Namib dune bushman grass). *Journal of Arid Environments,* 75: 524-531

Edelmann, H.G., Neinhuis, C., Jarvis, M., Evans, B., Fischer, E. and Barthlott, W. (1998). Ultrastructure and chemistry of the cell wall of the moss Rhaccocarpus purpurascens (Rhaccocarpaceae): a puzzling architecture among plants. *Planta,* 206: 315-321

Ekern, P.C. (1964). Direct interception of cloud water on Lanaihale, Hawaii. *Soil Science Society of America Journal,* 28: 419-421

Ensikat, H., Ditsche-Kuru, P., Barthlott, W., Méndez-Vilas, A. and Díaz, J. (2010). Scanning electron microscopy of plant surfaces: simple but sophisticated methods for preparation and examination. *Microscopy: Science, technology, applications and education,* 1: 248-255

Escobar, C., Lopez, A., Aristizabal, H. and Molina, J. (2010). 'Operational fog collection and its role in environmental education and social reintegration: A case study in Colombia. 5th International Conference on Fog, Fog Collection and Dew.'

Estrela, M.J., Valiente, J.A., Corell, D., Fuentes, D. and Valdecantos, A. (2009). Prospective use of collected fog water in the restoration of degraded burned areas under dry Mediterranean conditions. *Agricultural and Forest Meteorology,* 149: 1896-1906

Estrela, M.J., Valiente, J.A., Corell, D. and Millán, M.M. (2008). Fog collection in the western Mediterranean basin (Valencia region, Spain). *Atmospheric Research,* 87: 324-337

Extrand, C.W. (2002). Model for contact angles and hysteresis on rough and ultraphobic surfaces. *Langmuir,* 18: 7991-7999

Food and Agricultural Organization, United Nations Conventions to Combat Desertification, Mountain Partnerships, Swiss Agency for Development and Corporation and Centre for Development and Environment (2011). Highlands and drylands: mountains, a source of resilience in arid regions. Rome

Fessehaye, M., Abdul-Wahab, S.A., Savage, M.J., Kohler, T., Gherezghiher, T. and Hurni, H. (2014). Fog-water collection for community use. *Renewable and Sustainable Energy Reviews,* 29: 52-62

Gandhidasan, P. and Abualhamayel, H.I. (2007). Fog collection as a source of fresh water supply in the Kingdom of Saudi Arabia. *Water and Environment Journal,* 21: 19-25

Gao, L. and McCarthy, T.J. (2006). Contact angle hysteresis explained. *Langmuir,* 22: 6234-6237

Garrod, R.P., Harris, L.G., Schofield, W.C.E., McGettrick, J., Ward, L.J., Teare, D.O.H. and Badyal, J.P.S. (2007). Mimicking a Stenocara Beetle's Back for Microcondensation Using Plasmachemical Patterned Superhydrophobic−Superhydrophilic Surfaces. *Langmuir,* 23: 689-693

Gennes, P.-G., Brochard-Wyart, F. and Quéré, D. (2004). *Capillarity and wetting phenomena : drops, bubbles, pearls, waves.* (New York: Springer) 33-34

Goodman, J. (1985). The collection of fog drip. *Water Resources Research,* 21: 392-394

Hamilton, W.J. and Seely, M.K. (1976). Fog Basking by Namib Desert Beetle, Onymacris-Unguicularis. *Nature,* 262: 284-285

Hammer, T., Davis, R. and Thiele, K. (2015). A molecular framework phylogeny for Ptilotus (Amaranthaceae): Evidence for the rapid diversification of an arid Australian genus. *Taxon,* 64: 272-285

Henderson, B. and Falk, D. (2001). 'Fog water collection in ecuador: An appropriate technology for the rural poor. Proceedings of the 2nd International Conference on Fog and Fog Collection.'

Heng, X., Xiang, M., Lu, Z. and Luo, C. (2014). Branched ZnO Wire Structures for Water Collection Inspired by Cacti. *ACS Appl. Mater. Interfaces,* 6: 8032-8041

Holmes, R., Rivera, J.d.D. and de la Jara, E. (2015). Large fog collectors: New strategies for collection efficiency and structural response to wind pressure. *Atmospheric Research,* 151: 236-249

Hou, Y., Chen, Y., Xue, Y., Zheng, Y. and Jiang, L. (2012). Water collection behavior and hanging ability of bioinspired fiber. *Langmuir,* 28: 4737-4743

Hou, Y., Gao, L., Feng, S., Chen, Y., Xue, Y., Jiang, L. and Zheng, Y. (2013). Temperature-triggered directional motion of tiny water droplets on bioinspired fibers in humidity. *Chemical Communications,* 49: 5253-5255

Hutchinson, J. (1919). The Rain Tree of Hierro, Canary Islands. (Oreodaphne foetens.). *Bulletin of Miscellaneous Information (Royal Gardens, Kew),* 1919: 153-164

Johnson, R.E. and Dettre, R.H. (1964). Contact angle hysteresis. I. Study of an idealized rough surface. *Advanced Chemical Series,* 43: 1964-2393

Ju, J., Bai, H., Zheng, Y., Zhao, T., Fang, R. and Jiang, L. (2012). A multi-structural and multi-functional integrated fog collection system in cactus. *Nature Communications,* 3: 1247

Ju, J., Xiao, K., Yao, X., Bai, H. and Jiang, L. (2013). Bioinspired conical copper wire with gradient wettability for continuous and efficient fog collection. *Advanced Materials,* 25: 5937-5942

Ju, J., Yao, X., Yang, S., Wang, L., Sun, R., He, Y. and Jiang, L. (2014). Cactus stem inspired cone-arrayed surfaces for efficient fog collection. *Advanced Functional Materials,* 24: 6933-6938

Jung, Y.C. and Bhushan, B. (2006). Contact angle, adhesion and friction properties of micro-and nanopatterned polymers for superhydrophobicity. *Nanotechnology,* 17: 4970

Jung, Y.C. and Bhushan, B. (2008). Wetting behaviour during evaporation and condensation of water microdroplets on superhydrophobic patterned surfaces. *Journal of Microscopy-Oxford,* 229: 127-140

Kannan, R. and Sivakumar, D. (2008a). Drop impact process on a hydrophobic grooved surface. *Colloids and Surfaces A: Physicochemical and Engineering Aspects,* 317: 694-704

Kannan, R. and Sivakumar, D. (2008b). Impact of liquid drops on a rough surface comprising microgrooves. *Experiments in Fluids,* 44: 927-938

Kannan, R., Vaikuntanathan, V. and Sivakumar, D. (2011). Dynamic contact angle beating from drops impacting onto solid surfaces exhibiting anisotropic wetting. *Colloids and Surfaces A: Physicochemical and Engineering Aspects,* 386: 36-44

Klemm, O., Schemenauer, R.S., Lummerich, A., Cereceda, P., Marzol, V., Corell, D., van Heerden, J., Reinhard, D., Gherezghiher, T., Olivier, J., Osses, P., Sarsour, J., Frost, E., Estrela, M.J., Valiente, J.A. and Fessehaye, G.M. (2012). Fog as a fresh-water resource: Overview and perspectives. *Ambio,* 41: 221-234

Koch, K. and Barthlott, W. (2009). Superhydrophobic and superhydrophilic plant surfaces: an inspiration for biomimetic materials. *Philosophical Transactions of the Royal Society A: Mathematical, Physical and Engineering Sciences,* 367: 1487-1509

Koch, K., Bhushan, B. and Barthlott, W. (2008a). Diversity of structure, morphology and wetting of plant surfaces. *Soft Matter,* 4: 1943-1963

Koch, K., Blecher, I.C., Koenig, G., Kehraus, S. and Barthlott, W. (2009). The superhydrophilic and superoleophilic leaf surface of Ruellia devosiana (Acanthaceae): a biological model for spreading of water and oil on surfaces. *Functional Plant Biology,* 36: 339-350

Koch, K., Schulte, A.J., Fischer, A., Gorb, S.N. and Barthlott, W. (2008b). A fast, precise and low-cost replication technique for nano- and high-aspect-ratio structures of biological and artificial surfaces. *Bioinspiration & Biomimetics,* 3: 046002

Koračin, D., Dorman, C.E., Lewis, J.M., Hudson, J.G., Wilcox, E.M. and Torregrosa, A. (2014). Marine fog: A review. *Atmospheric Research,* 143: 142-175

Kusumaatmaja, H., Vrancken, R.J., Bastiaansen, C.W.M. and Yeomans, J.M. (2008). Anisotropic drop morphologies on corrugated surfaces. *Langmuir,* 24: 7299-7308

Lakes, R. (1993). Materials with structural hierarchy. *Nature,* 361: 511-515

Lam, C.N.C., Wu, R., Li, D., Hair, M.L. and Neumann, A.W. (2002). Study of the advancing and receding contact angles: liquid sorption as a cause of contact angle hysteresis. *Advances in Colloid and Interface Science,* 96: 169-191

Larrain, H., Velásquez, F., Cereceda, P., Espejo, R., Pinto, R., Osses, P. and Schemenauer, R.S. (2002). Fog measurements at the site "Falda Verde" north of Chañaral compared with other fog stations of Chile. *Atmospheric Research,* 64: 273-284

Lee, A., Moon, M.W., Lim, H., Kim, W.D. and Kim, H.Y. (2012). Water harvest via dewing. *Langmuir,* 28: 10183-91

Lekouch, I., Mileta, M., Muselli, M., Milimouk-Melnytchouk, I., Sojat, V., Kabbachi, B. and Beysens, D. (2010). Comparative chemical analysis of dew and rain water. *Atmospheric Research,* 95: 224-234

Lekouch, I., Muselli, M., Kabbachi, B., Ouazzani, J., Melnytchouk-Milimouk, I. and Beysens, D. (2011). Dew, fog, and rain as supplementary sources of water in south-western Morocco. *Energy,* 36: 2257-2265

Limm, E.B., Simonin, K.A., Bothman, A.G. and Dawson, T.E. (2009). Foliar water uptake: a common water acquisition strategy for plants of the redwood forest. *Oecologia,* 161: 449-459

Liu, L., Jacobi, A.M. and Chvedov, D. (2009). A surface embossing technique to create micro-grooves on an aluminum fin stock for drainage enhancement. *Journal of Micromechanics and Microengineering,* 19: 035026

Lorenceau, E. and Quéré, D. (2004). Drops on a conical wire. *Journal of Fluid Mechanics,* 510: 29-45

Lummerich, A. and Tiedemann, K.J. (2011). Fog water harvesting on the verge of economic competitiveness. *Erdkunde,* 65: 305-306

Lüttge, U. (2011). *Vascular plants as epiphytes: Evolution and ecophysiology.* (London: Springer)

MacQuarrie, K., Pokhrel, A., Shrestha, Y., Osses, P., Schemenauer, R., Vitez, F., Kowalchuk, K. and Taylor, R. (2001). 'R. 2001. Results from a high elevation fog water supply project in Nepal. Proceedings of the 2nd International Conference on Fog and Fog Collection.'

Malik, F.T., Clement, R.M., Gethin, D.T., Krawszik, W. and Parker, A.R. (2014). Nature's moisture harvesters: a comparative review. *Bioinspiration & Biomimetics,* 9: 031002

Marloth, R. (1903). Results of experiments on Table Mountain for ascertaining the amount of moisture deposited from the south-east clouds. *Transactions of the South African Philosophical Society,* 14: 403–408

Marloth, R. (1905). Results of further experiments on Table Mountain for ascertaining the amount of moisture deposited from the southeast clouds. *Transactions of the South African Philosophical Society,* 16: 97-105

Martorell, C. and Ezcurra, E. (2002). Rosette scrub occurrence and fog availability in arid mountains of Mexico. *Journal of Vegetation Science,* 13: 651-662

Martorell, C. and Ezcurra, E. (2007). The narrow-leaf syndrome: a functional and evolutionary approach to the form of fog-harvesting rosette plants. *Oecologia,* 151: 561-573

Mileta, M. and Likso, Z. (2010). 'Fog water collection with SFC on the mountain Velebit (Croatia) during the period 2000–2009. Proceedings of the 5th International Conference on Fog, Fog Collection and Dew.'

Molina, J.M. and Escobar, C.M. (2008). Fog collection variability in the Andean mountain range of Southern Colombia. *Die Erde,* 139: 127-140

Mtuleni, V., Henschel, J. and Seely, M.K. (1998). 'Evaluation of fogharvesting potential in Namibia. Proceedings of the First International Conference on Fog and Fog Collection.'

Muselli, M., Beysens, D., Marcillat, J., Milimouk, I., Nilsson, T. and Louche, A. (2002). Dew water collector for potable water in Ajaccio (Corsica Island, France). *Atmospheric Research,* 64: 297-312

Nagel, J. (1962). Fog precipitation measurements on Africa's south-west coast. *Notos,* 11: 51-60

Nagel, J.F. (1956). Fog Precipitation on Table Mountain. *Quarterly Journal of the Royal Meteorological Society,* 82: 452-460

Neinhuis, C. and Barthlott, W. (1997). Characterization and Distribution of Water-repellent, Self-cleaning Plant Surfaces. *Annals of Botany,* 79: 667-677

Nelson, R.A., (2003). Air wells, fog fences & dew ponds. Methods for Recovery of Atmospheric Humidity, http://www.rexresearch.com/airwells/airwells.htm.

Nørgaard, T. and Dacke, M. (2010). Fog-basking behaviour and water collection efficiency in Namib Desert Darkling beetles. *Frontiers in Zoology,* 7: 23

Nørgaard, T., Ebner, M. and Dacke, M. (2012). Animal or plant: Which Is the better fog water collector? *PLoS One,* 7: e34603

Nosonovsky, M. and Bhushan, B. (2008a). Biologically inspired surfaces: Broadening the scope of roughness. *Advanced Functional Materials,* 18: 843-855

Nosonovsky, M. and Bhushan, B. (2008b). Roughness-induced superhydrophobicity: a way to design non-adhesive surfaces. *Journal of Physics: Condensed Matter,* 20: 225009

Olivier, J. (2004). Fog-water harvesting along the West Coast of South Africa: A feasibility study. *Water Sa,* 28: 349-360

Olivier, J. and de Rautenbach, C.J. (2002). The implementation of fog water collection systems in South Africa. *Atmospheric Research,* 64: 227-238

Osses, P., Schemenauer, R.S. and Leibbrand, M. (2004). 'Fog collection evaluation in the Sadaa Governorate, Yemen. Proceedings of the Third International Conference on Fog, Fog Collection and Dew.'

Park, K.-C., Chhatre, S.S., Srinivasan, S., Cohen, R.E. and McKinley, G.H. (2013). Optimal design of permeable fiber network structures for fog harvesting. *Langmuir,* 29: 13269-13277

Park, K.C., Chhatre, S.S., McKinley, G.H. and Cohen, R.E., (2014). Liquid collecting permeable structures. Patent Application Nr. US 2014/0190352A1,

Petterssen, S. (1936). On the Causes and the Forecasting of the California Fog. *Journal of the Aeronautical Sciences,* 3: 305-309

Porembski, S. (1994). Opuntia invicta, eine nebelabsorbierende Cactaceae aus Baja California (Mexiko). *Beiträge zur Biologie der Pflanzen,* 68: 73-79

Prinz, D. and Wolfer, S. (1998). 'Opportunities to ease water scarcity (water conservation techniques and approaches; added values and limits). Proceedings of the international conference on world water resources at the beginning of the 21st century.'

Rauh, W., Schill, R., Ehler, N. and Barthlott, W. (1973). Some remarks on the water supply of bromeliads. *Journal of Bromeliad Society,* 23: 89-109

Rawlings, A.E., Bramble, J.P. and Staniland, S.S. (2012). Innovation through imitation: biomimetic, bioinspired and biokleptic research. *Soft Matter,* 8: 6675-6679

Renvoisé, P., Bush, J., Prakash, M. and Quéré, D. (2009). Drop propulsion in tapered tubes. *EPL (Europhysics Letters),* 86: 64003

Roach, P., Shirtcliffe, N.J. and Newton, M.I. (2008). Progess in superhydrophobic surface development. *Soft Matter,* 4: 224-240

Roth-Nebelsick, A., Ebner, M., Miranda, T., Gottschalk, V., Voigt, D., Gorb, S., Stegmaier, T., Sarsour, J., Linke, M. and Konrad, W. (2012). Leaf surface structures enable the endemic Namib desert grass Stipagrostis sabulicola to irrigate itself with fog water. *Journal of the Royal Society Interface,* 9: 1965-1974

Rundel, P.W. (1982). Water uptake by organs other than roots in Lange, O.L., Nobel, P.S., Osmond, C.B., Ziegler, H. (Eds.) Physiological Plant Ecology II (Springer: Berlin, Heidelberg) 111-134

Sarsour, J., Stegmaier, T., Linke, M. and Planck, H. (2010). 'Bionic development of textile materials for harvesting water from fog. 5th International Conference on Fog, Fog Collection and Dew.'

Schemenauer, R. and Cereceda, P. (1988). 'The collection of fog water in Chile for use in coastal villages. VIth IWRA (International Water Resources Association) World Congress.'

Schemenauer, R.S. and Cereceda, P. (1991). Fog-Water Collection in Arid Coastal Locations. *Ambio,* 20: 303-308

Schemenauer, R.S. and Cereceda, P. (1992). Monsoon cloudwater chemistry on the Arabian Peninsula. *Atmospheric Environment. Part A. General Topics,* 26: 1583-1587

Schemenauer, R.S. and Cereceda, P. (1994a). Fog collection's role in water planning for developing countries. *Natural Resources Forum,* 18: 91-100

Schemenauer, R.S. and Cereceda, P. (1994b). A proposed standard fog collector for use in high-elevation regions. *Journal of Applied Meteorology,* 33: 1313-1322

Schemenauer, R.S., Fuenzalida, H. and Cereceda, P. (1988). A neglected water resource: The Camanchaca of South America. *Bulletin of the American Meteorological Society,* 69: 138-147

Schemenauer, R.S. and Joe, P.I. (1989). The collection efficiency of a massive fog collector. *Atmospheric Research,* 24: 53-69

Schemenauer, R.S., Osses, P., Lara, F., Zywina, C. and Cereceda, P. (2001). 'Fog collection in the Dominican Republic. Proceedings of the 2nd International Conference on Fog and Fog Collection.'

Schemenauer, R.S., Rosato, M. and Carter, V. (2007). 'Fog collection projects in Tojquia and La Ventosa, Guatemala. Proceedings of the 4th International Conference on Fog, Fog Collection and Dew.'

Schill, R. and Barthlott, W. (1973). Kakteendornen als wasserabsorbierende Organe. *Naturwissenschaften,* 60: 202-203

Seely, M.K. (1979). Irregular fog as a water source for desert dune beetles. *Oecologia,* 42: 213-227

Shanyengana, E.S., Sanderson, R.D., Seely, M.K. and Schemenauer, R.S. (2003). Testing greenhouse shade nets in collection of fog for water supply. *Journal of Water Supply Research and Technology-Aqua,* 52: 237-241

Shirtcliffe, N.J., McHale, G. and Newton, M.I. (2009). Learning from superhydrophobic plants: The use of hydrophilic areas on superhydrophobic surfaces for droplet control. *Langmuir,* 25: 14121-14128

Simonin, K.A., Santiago, L.S. and Dawson, T.E. (2009). Fog interception by Sequoia sempervirens (D. Don) crowns decouples physiology from soil water deficit. *Plant Cell Environ,* 32: 882-892

Sommers, A.D. and Jacobi, A.M. (2006). Creating micro-scale surface topology to achieve anisotropic wettability on an aluminum surface. *Journal of Micromechanics and Microengineering,* 16: 1571-1578

Stabentheiner, E., Pfeifhofer, H.W., Peters, J., Jiménez, M.S., Morales, D. and Grill, D. (2004). Different surface characteristics of primary and secondary needles of Pinus canariensis. *Flora - Morphology, Distribution, Functional Ecology of Plants,* 199: 90-99

Stanton, D.E. and Horn, H.S. (2013). Epiphytes as “filter-drinkers”: life-form changes across a fog gradient. *The Bryologist,* 116: 34-42

Suga, K., Matsumura, Y., Ashitaka, Y., Tominaga, S. and Kaneda, M. (2010). Effects of wall permeability on turbulence. *International Journal of Heat and Fluid Flow,* 31: 974-984

Sun, T., Feng, L., Gao, X. and Jiang, L. (2005). Bioinspired surfaces with special wettability. *Accounts of Chemical Research,* 38: 644-652

Taylor, G.I. (1917). The formation of fog and mist. *Quarterly Journal of the Royal Meteorological Society,* 43: 241-268

Thickett, S.C., Neto, C. and Harris, A.T. (2011). Biomimetic surface coatings for atmospheric water capture prepared by dewetting of polymer films. *Advanced Materials,* 23: 3718-3722

United Nnations Conventions to Combat Desertification (UNCCD) (2014). Desertification: The invisible frontline. Bonn

United Nations Educational, Scientific and Cultural Organization (UNESCO) (2012). 'Managing water under uncertainty and risk' in 'The United Nations World Water Development Report'. Paris

Van Damme, P. (1991). Plant ecology of the Namib desert. *Afrika Focus,* 7: 355-400

Van Heerden, J., Olivier, J. and Van Schalkwyk, L. (2010). 'Fog sater systems in South Africa: An update. 5th International Conference on Fog, Fog Collection and Dew.'

Vogel, S. (1994). *Life in moving fluids: the physical biology of flow.* (Princeton: Princeton University Press)

Vogel, S. and Müller-Doblies, U. (2011). Desert geophytes under dew and fog: The "curly-whirlies" of Namaqualand (South Africa). *Flora,* 206: 3-31

Vogelmann, H.W., Siccama, T., Leedy, D. and Ovitt, D.C. (1968). Precipitation from fog moisture in the Green Mountains of Vermont. *Ecology,* 49: 1205-1207

Wenzel, R.N. (1936). Resistance of solid surfaces to wetting by water. *Industrial & Engineering Chemistry,* 28: 988-994

Westbeld, A., Klemm, O., Griessbaum, F., Strater, E., Larrain, H., Osses, P. and Cereceda, P. (2009). Fog deposition to a Tillandsia carpet in the Atacama Desert. *Annales Geophysicae,* 27: 3571-3576

White, B., Sarkar, A. and Kietzig, A.-M. (2013). Fog-harvesting inspired by the Stenocara beetle—An analysis of drop collection and removal from biomimetic samples with wetting contrast. *Applied Surface Science,* 284: 826-836

World Health Organization (WHO) and United Nations Children's Fund (UNICEF) (2013). Progress on sanitation and drinking water, 2013 update. Geneva

Wilhelmi, H. and Barthlott, W. (1997). Mikromorphologie der Epicuticularwachse und die Systematik der Gymnospermen. *Trop. subtrop. Pflanzenwelt,* 96: 1-49

Xia, D., Johnson, L.M. and López, G.P. (2012). Anisotropic wetting surfaces with one-dimesional and directional structures: Fabrication approaches, wetting properties and potential applications. *Advanced Materials,* 24: 1287-1302

Xue, Y., Wang, T., Shi, W., Sun, L. and Zheng, Y. (2014). Water collection abilities of green bristlegrass bristle. *RSC Advances,* 4: 40837-40840

Yan, Y.Y., Gao, N. and Barthlott, W. (2011). Mimicking natural superhydrophobic surfaces and grasping the wetting process: A review on recent progress in preparing superhydrophobic surfaces. *Advances in Colloid and Interface Science,* 169: 80-105

Yang, H., Zhu, H., Hendrix, M.M.R.M., Lousberg, N.J.H.G.M., de With, G., Esteves, A.C.C. and Xin, J.H. (2013). Temperature-triggered collection and release of water fromfogs by a sponge-like cotton fabric. *Advanced Materials,* 25: 1150-1154

Yang, S., Ju, J., Qiu, Y., He, Y., Wang, X., Dou, S., Liu, K. and Jiang, L. (2014). Peanut leaf inspired multifunctional surfaces. *Small,* 10: 294-299

Young, T. (1805). An essay on the cohesion of fluids. *Philosophical Transactions of the Royal Society of London,* 95: 65-87

Yuan, Y. and Lee, T.R. (2013). Contact angle and wetting properties in Bracco, G., Holst, B. (Eds.) Surface Science Techniques (Springer: Berlin, Heidelberg) 3-34

Zhang, X., Shi, F., Niu, J., Jiang, Y. and Wang, Z. (2008). Superhydrophobic surfaces: From structural control to functional application. *Journal of Materials Chemistry,* 18: 621-633

Zheng, Y.M., Bai, H., Huang, Z.B., Tian, X.L., Nie, F.Q., Zhao, Y., Zhai, J. and Jiang, L. (2010). Directional water collection on wetted spider silk. *Nature,* 463: 640-643

List of Figures

List of Tables

Appendix

All relevant data are provided digitally in a compact disc (CD) at the end of this thesis.

Acknowledgement

This research work was carried out in the Bionics and Biodiversity working group at Nees Institute for Biodiversity of Plants, Rheinische Friedrich-Wilhelms-University of Bonn under the Graduate program (*DFG Graduiertenkolleg 1572*) "Bionics-Interaction across Boundaries to the Environment" funded by German Research Foundation (DFG). I acknowledge DFG as well as DAAD (German Academic Exchange Service) for their financial support. I would like to acknowledge some people without whom it would be difficult for me to complete the work. First of all, I must thank my supervisor Prof. Wilhelm Barthlott for giving me the opportunity to work in this very interesting topic in his bionics research group. He was always by my side to encourage and to discuss about new ideas and the new findings. His review critics on the manuscripts and presentation helped improve the quality. His passion to scientific works, innovation and management is worth watching and learning; and I learned a lot. Thank you so much for inviting us to enjoy the barbeque, and fresh and tasty berries and apricots from your garden. I cannot thank enough to my co-supervisor, Prof. Kerstin Koch who used to extend her helping hands with her expertise, ideas, suggestions, discussions and above all the technical cooperation and the access to her laboratory at any time. I am thankful to the associate students, Dorothee Ellerbrok and Tobias Krause, whom I supervised for their Bachelor theses. I would like to express my gratitude to Leon Danter and Prof. Albert Baars (Bremen University of Applied Sciences) for the simulation to validate a part of the results of this work. One man, who was always there to clarify the administrative things as well as geographical and climatological topics nicely, was none other than Dr. Daud Rafiqpoor;

I am grateful to him. I am grateful to the staffs of the Botanical Gardens of Bonn (BG Bonn) for cultivating and supplying the plant materials, I needed. I appreciate the staffs of the electronic laboratory at Institute for Cellular and Molecular Botany (IZMB), University of Bonn for their assistance in sample preparation and experimental setup. My sincere thanks go to Prof. Georg Noga for allowing me to work in his laboratory with ESEM. Many thanks Dr. Hunsche and Mr. Knut for your assistance. I appreciate Gabriela Wyss and Urs Eggli and other staffs for the guided visit and the hospitality in the world's largest succulent plant collection in *Sukkulenten-Sammlung* in Zurich, Switzerland and providing me some samples for investigation. I would not miss the opportunity to remember late Wolfgang Roden (Technical Assistant) for your help in the very beginning of my work in Bonn. Thank you so much Hans-Jurgen Ensikat and Axel Hinnemann (Rhine-Waal University of Applied Sciences) for the technical assistances for SEM and AFM analysis; and thanks Axel once again for being a very good friend. Mrs. Hohmann and Mrs. Busch, these two secretaries at our institute are too good to explain in words. Thanks Matthias and Birte for the fruitful discussions and useful suggestions during the group meetings. I should thank Robin, Eva and Maggie for their feedbacks during different discussions and above all a nice time together. I improved my German with their help. I cordially thank Danica Christensen for proofreading the texts of some manuscripts. I am thankful to other colleagues of Nees Institute. I greatly thank all the colleagues of the Graduate School of Bionics from University of Bonn, Technical University of Aachen (RWTH Aachen) and Juelich Research Centre (Forschungszentrum Jülich) for their friendly chatting and inspiring discussion in the autumn school programs. Nothing would be enough to thank my lovely wife who was hugely loving and supportive to me all the time.

I appreciate the Bangladeshi community here in Germany for arranging different programs and having an enjoyable time together. I would like to remember and thank my family members for their constant support, love and blessings.

Publications

Journal articles

Azad, M. A. K., Barthlott, W., and Koch, K., (**2015**), Hierarchical surface architecture of plants as an inspiration for biomimetic fog collectors. *Langmuir* 31 (48): 13172–13179 (ACS publications).

Azad, M. A. K., Ellerbrok, D., Barthlott, W., and Koch, K., (**2015**), Biomimetic fog collecting surfaces: Influence of microstructure and wettability. *Bioinspiration and Biomimetics* 10: 016004 (IOP publishing).

In preparation

Azad, M. A. K., Krause, T., Danter, L., Baars, A., Koch, K., and Barthlott, W., (), Fog collecting biomimetic meshes: Droplet behavior and collection efficiency influenced by cross-section profiles and surface structures of fibers.

Azad, M. A. K., Barthlott, W., and Koch, K., (), Trichomes of *Ptilotus manglesii*: An integrated system for an efficient water droplet transport and fog collection.

Azad, M. A. K., Koch, K., and Barthlott, W., (), Fog collection on plant surfaces: Influence of leaf shape modification and directed water transport on the surfaces.

Conference contributions

Azad, M. A. K., Barthlott, W., and Koch, K., (**2014**), Fog collecting structures based on plant surface architectures: Barbed structure a key factor to enhance the collection efficiency. Patente aus der Natur: Bionic Congress 2014

Azad, M. A. K., Ellerbrok, D., Barthlott, W., and Koch, K., (**2014**), Influence of microstructure and wettability of the surfaces on fog collection. Material Science and Engineering Conference 2014

Barthlott, W., Böhnlein, B., **Azad, M. A. K.**, Schulte, A.-J., and Mail, M., (**2014**), Learning from plant biodiversity: Self-cleaning, drug reduction and other functionalities. International BION (Biodiversity Network Bonn) Conference 2014

Azad, M. A. K., Hinnemann, A., Koch, K., Lucassen, R., Shirtcliffe, N.J., and Fahmi, A., (**2013**), Characterization of fabricated cost effective antibacterial nanofibers based on hybrid materials by electrospinning. Euro BioMAT 2013

Erklärung

Hiermit versichere ich, das die vorliegende Dissertation selbständig angefertigt und die benutzen Quellen vollständing angegeben habe. Sie wurde an keiner anderen Hochschule als Dissertation eingereicht und wurde auch nicht an einer anderen Stelle veröffentlicht. Für die Erstellung der vorgelegten Arbeit wurde keine Hilfe von Vermittlungs- bzw. Beratungsdiensten in Anspruch genommen.

Bonn Januar 2016

Md. Abul Kalam Azad